CZECH TECHNICAL UNIVERSITY IN PRAGUE

FACULTY OF NUCLEAR SCIENCES AND PHYSICAL ENGINEERING

DOCTORAL THESIS

Searching for Lightweight Dark Matter in the NOvA Near Detector

Prague 2019

Filip Jediný

Bibliografický záznam

Autor	Ing. Filip Jediný České vysoké učení technické v Praze Fakulta jaderná a fyzikálně inženýrská Katedra dozimetrie a aplikace ionizujícího záření
Název práce	Hledání Lehké temné hmoty v Blízkém detektoru NOvA
Studijní program	Aplikace přírodních věd
Studijní obor	Jaderné inženýrství
Školitel	RNDr. Jan Smolík, Ph.D. České vysoké učení technické v Praze Fakulta jaderná a fyzikálně inženýrská Katedra dozimetrie a aplikace ionizujícího záření
Školitel specialista	RNDr. Jaroslav Zálešák, Ph.D. Fyzikální ústav Akademie věd České republiky Sekce fyziky elementárních částic
Akademický rok	2018/2019
Počet stran	144
Klíčová slova	Hledání temné hmoty, Lehká temná hmota, skrytý sektor, temný sektor, vektorový portál, temný foton, neutrino, pružný rozptyl, NOvA, Fermilab, strojové učení

Bibliographic Entry

Author	Ing. Filip Jediný Czech Technical University in Prague Faculty of Nuclear Sciences and Physical Engineering Department of Dosimetry and Application of Ionizing Radiation
Title of Dissertation	Searching for Lightweight Dark Matter in the NOvA Near Detector
Degree program	Applications of Natural Sciences
Field of study	Nuclear Engineering
Supervisor	RNDr. Jan Smolík, Ph.D. Czech Technical University in Prague Faculty of Nuclear Sciences and Physical Engineering Department of Dosimetry and Application of Ionizing Radiation
Supervisor specialist	RNDr. Jaroslav Zálešák, Ph.D. Institute of Physics of the Czech Academy of Sciences Division of Elementary Particle Physics
Academic Year	2018/2019
Number of Pages	144
Keywords	Search for Dark Matter, Lightweight Dark Matter, Hidden sector, Dark sector, Vector portal, dark photon, neutrino, elastic scattering, NOvA, Fermilab, machine learning

Abstract

Beyond the Standard Model ideas include lightweight (sub-GeV) Dark Matter candidates (DM) produced through a vector particle mediator belonging to Dark Sector. In this thesis, I postulate that they could be produced within the NuMI beam at Fermilab. The NOvA neutrino experiment has recorded ~10^{21} protons on target (POT), which correspond to millions of neutrino interaction events in its low-Z, 300-ton, off-axis Near Detector (ND). Among these neutrinos, I search for EM-shower signatures from DM candidates scattering within the detector in a model independent approach. First half of the thesis contains introduction to the DM field and simple Dark Sector model, describes the beam production, the NOvA near detector and the reconstruction tools and deep machine learning techniques to identify particle signatures. In the second half, I simulate a $m_\chi = 30\,\mathrm{MeV}$ example and perform a blind DM scattering analysis in the channel extending to 15 GeV of kinetic energy. On 1.1×10^{20} POT dataset, I observe no excess of signal above simulation accountable for DM scattering and calculate the 90% C.L. upper limit of annihilation constant *Y* for such LDM model to be $1.59\pm0.28\times10^{-12}$.

Abstrakt

Hypotézy fyziky za Standardním modelem částic zahrnují lehkou (pod ~GeV) temnou hmotu (DM), vznikající pomocí zprostředkující vektorové částice náležící k temnému sektoru částic. V této práci postuluji jejich předpokládanou produkci v NuMI svazku ve Fermilabu. Neutrinový experiment NOvA nabral data z ~10^{21} srážek protonů s terčíkem (POT), odpovídajícím řádově milionům neutrinových interakcí v nízkohustotním 300tunovém Blízkém detektoru, postaveném mimo osu svazku. Nezávisle na daném DM modelu mezi těmito neutriny hledám signály od DM částic rozptylujících se elektromagneticky uvnitř detektoru. První polovina práce obsahuje úvod do tématu temné hmoty, popis jednoduchého modelu Temného sektoru, produkce svazku, Blízkého detektoru NOvA a technik k rekonstrukci a identifikaci částic a signálů pomocí umělé inteligence. V druhé části vyhodnocuji DM rozptyl na $m_\chi = 30\,\mathrm{MeV}$ příkladě v kanále dosahujícím 15 GeV kinetické energie pomocí slepé analýzy. V naměřených datech odpovídajících $1{,}1\times10^{20}$ POT nepozoruji oproti simulacím výskyt signálu vysvětlitelný rozptylem DM, což odpovídá horní hranici anihilační konstanty *Y* takového modelu $1{,}59\pm0{,}28\times10^{-12}$ s 90% intervalem spolehlivosti.

Acknowledgements

This thesis would not come into existence without an enormous multitude of help and support from people with who I was lucky to work with or who simply stood by me during my doctoral studies. It is impossible to thank everyone who ought to be thanked, but I would like to express my gratitude to few of those who deserve the most.

First, I would like to express my gratitude to my dear friend and colleague Athanasios Hatzikoutelis, who I enjoyed working with on the DCS systems and instrumentation of the NOvA detectors in my first years at NOvA and transitioned to LDM. Athans, thank you for bringing my attention to the dark matter search in the first place and continuing to work with me throughout the years, I am still learning new things from the vast skillset and wisdom you were so generous to share with me.

Jan Smolík, my supervisor, thank you for the unprecedented support and always doing your best to help me. You many times showed me the right direction through your straightforward insight, you are an inspiration for never losing your bright, calm, and cheerful attitude.

Gavin Davies, besides being a great friend, thank you for helping me with my coding struggles. You are the spirit of the collaboration and the core of all the NOvA analysis and we should worship you and your skills.

Biao Wang and Sergey Kotelnikov, thank you for the great help with the analysis and finding time to share your thoughts and intel about LDM and NOvAsoft.

Jaroslav Zálešák, thank you for sharing the years at Fermilab with me and for your never-changing philosophy. Kamil Augsten, thank you for giving me all the insight when (and after) I first came to the US. Tomáš Nosek, thank you for inspirational discussions at the lab and beyond, and bringing fresh air into my days.

There are many other important individuals who made all this possible, let me thank everyone in a broader, collective way.

In the broadest way possible, I would like to thank the Universe not only for providing mankind with such great mysteries to pursue, but also for bringing me

opportunities and possibilities to be able to do what I like and care for the most in my life. If one would call this luck, I consider myself very lucky.

Tomáš, Tomáš, Tomáš, Tomáš and all other colleagues from my department at FNSPE CTU in Prague, thank you for making me feel like home and taking me as part of the "family" despite me being vacant from the office most of the time. Also, all other staff and members of my alma mater, you were always ready to offer a helping hand and did a great job. To members of the Czech NOvA group from Charles University and Academy of Sciences, thank you for all the years of exciting co-working on the research at Fermilab.

People from the NOvA Collaboration, but more importantly the Young NOvA, and the exotics analysis group, thank you for making my work possible, bearable and enjoyable, without you, I would not be able to neither start nor conclude my research.

To all my other friends, work colleagues, family members and loved ones, I am grateful for you always encouraging me to finish my graduate studies and for understanding in the times I was absent on one or the other side of the Atlantic.

Michal Kusmierczak, my dear cousin, thanks for all the positive distractions and for proofreading this thesis.

Renata and Petr, my beloved parents. Thank you for never stopping believing in me and always being the most awesome parents, one could possibly imagine. Seeing you being proud of me fills me with joy and was of the greatest motivation, I dedicate this dissertation to you.

Dedication

To my family.

Preface

I am submitting this dissertation, titled "Searching for Lightweight Dark Matter in the NOvA Near Detector", to be defended as my Ph.D. thesis for Nuclear Engineering doctoral degree in Applications of Natural Sciences study program at the Faculty of Nuclear Sciences and Physical Engineering, Czech Technical University in Prague.

I have started my studies in 2012, transitioning from rare bound meson research at CERN to neutrino physics and joining the NOvA Collaboration. In first years, besides gaining more knowledge about neutrino oscillation physics, I was working on the detector construction and commissioning at Fermilab and Ash River and became a Detector Control Systems expert and co-author of NOvA publications. To acquire authorship, all collaborators are required to bring a significant effort to the project (analysis or service work for the experiment) and contribute to data taking (serving shifts in the NOvA Control Room) for extended period of time.

Although NOvA is a mid-sized collaboration (more than 250 members), its narrow and specific list of physics goals allows it to yield significantly less publications than similar accelerator based, but multi-purposed international collaborations. This further emphasizes the attractivity of alternative searches on the same detector and data already in place, with zero or negligible investments and significant scientific impact, such as my Lightweight Dark Matter (LDM) search. NOvA has currently published around 20 heavy-impact scientific papers. I have also actively contributed to the presentation of NOvA results towards the scientific community during my countless trips to Fermilab (near Chicago, IL) and other places in the USA and international conferences around the globe, as well as popularization for general public, namely via talks and publications, in the Czech Republic. Attached List of Publications summarizes the output from these activities.

In 2015, I have also joined the newly formed DUNE Collaboration, which is a next generation accelerator-based neutrino and new physics experiment, also using beam coming from Fermilab. The DUNE detectors and facility construction has already started and after the conclusion of NOvA oscillation program, DUNE will

take over around year 2025. DUNE started producing first publications, which I am also a co-author of.

In later years of my doctoral program, I have focused on search for exotic particles in the NOvA Near Detector (ND), which I have proposed in my dissertation study in 2016, defining the topic of my dissertation to be "Searching for Lightweight Dark Matter in the NOvA Near Detector", and presenting it at many major international particle physics conferences, through talks, posters and proceedings. In this thesis I present my findings.

After introduction in the first chapter, Chapter 2 describes the history of DM, current state of the DM field and some basic introduction into LDM theory. It is very hard not to oversimplify these topics and the purpose of this chapter is to put my research into some context and get the reader familiar with the DM landscape and terminology, in no way it should be considered thorough and exhaustive historical and theoretical pursuit. The third and fourth chapters describe the accelerator beam, the NOvA detector technology and the tools and techniques used for event reconstruction and particle identification (PID) with some part specific only for LDM search.

My analysis is based on NOvA experimental apparatus and data, which are subject to a large international collaboration; most of the tools I used were developed by an enormous number of scientists and it would be not trivial to keep track of what is collective effort and what is my original work without losing an advantage of structured and readable text. Although I am strongly against using active voice in scientific work and publications, to help the reader keep track of my contributions, I write about common or general NOvA specifics in plural-active (we, our, us...), and in case I have carried out, modified or developed same part by myself, I use singular-active (I, me, my...). Also, please note that I omit the c^2 in the energy and mass units (mostly GeV and MeV instead of GeV/c^2 and MeV/c^2).

In Chapter 5 I describe my Monte Carlo (MC) simulation and how the simulated LDM particles of one specific model example behave in NOvA Near detector. Chapter 6 summarizes how exactly I have analyzed the LDM scattering on electrons. This is not a chronological and complete description, but rather logical and condensed report. Here, unless cited or stated otherwise, all work presented is done by myself, as well as most of the plots showed (unless there is a source

citation in the figure description). All my original plots containing NOvA data are marked as NOvA Preliminary, since the analysis is currently under review to publish a paper based on measured LDM upper limit.

Some tools and technicalities are omitted or considered "general" and not suitable for the scope of this work (like GRID computing, ROOT analysis, *svn* distributed SW management, neural network construction, data formats, libraries used etc.), as well as the obstructions and minor challenges encountered during the analysis. Similarly, description of all my other NOvA activities and service work is beyond the scope of this work and is summarized in my thesis study (1).

I sincerely hope you will enjoy your reading.

Filip Jediný

27th of September 2019 in Prague, Czech Republic

Update: 12th of June, 2020

Due to the circumstances appearing during 2020 and postponing my defense and based on suggestions from my thesis reviewers, I decided to withdraw the print from the defense procedure and update it and correct several things. Besides minor corrections and clarifications, this update mainly consists of shifting the mass range of LDM particles of interest (the model parameter sets based on most up to date globally known results) and rescaling the results from upper limit on scattering cross section to (upper limit of) the parameter *Y* (so called self-annihilation parameter, which is controlling both the production and the scattering rates) and further generalization, discussion, and interpretation of obtained results in a broader context.

Contact the author: filip.jediny@gmail.com

Contents

List of Figures

List of Tables

1 Introduction

Particle physics is undoubtably a frontier of discovery and the Standard Model (SM) of particles is an enormous success of particle physics of the 20th century, concluded with the experimental confirmation of the Higgs boson predicted in the SM. However, it is obvious that there must be some New Physics beyond the standard model (BSM), which will have to shed light on unexplained phenomena of our Universe.

The NOvA experiment measures oscillation parameters of beam neutrinos between its two second-generation neutrino detectors. Just the fact that neutrinos oscillate means they have mass, which, when discovered, was not in concordance with SM. But there are much bigger mysteries in nature, like matter-antimatter asymmetry, the Dark Energy or Dark Matter.

To explore the parameters of the neutrino mixing, mankind has built spectacular instruments – enormous detectors and mighty particle beams. NOvA is one of the top accelerator-based neutrino experiments currently running, using 700kW muon-neutrino beam, 14kiloton Far detector (FD) and 300ton Near Detector (ND) underground at Fermilab. NOvA has already recorded more than 2×10^{21} POT and we have published several papers with neutrino oscillation results (2) (3) (4) (5) (6) (7) (8).

The outstanding resolution and the proximity to the beam also enable us to reinterpret the NOvA ND as a beam dump experiment, looking for exotic particles very rarely interacting in the detector mass. That is a rather novel point of view on an experiment already in place and setting limits on its sensitivity has a strong scientific impact and is very important for projecting 3rd generation experiments as DUNE (9) or SHiP (10).

This thesis describes analysis of the Lightweight Dark Matter (LDM) channel bellow few GeV of mass in a model independent way, comparing the data with the mainstream NOvA analysis simulation and custom LDM-signal Monte Carlo simulation. This kind of BSM analysis belongs to "Exotics" analysis group and is set to explore the possibilities of using currently-at-hand tools to constrain the sensitivity level of our NOvA Near Detector.

1.1 Objectives

As mentioned in the Preface, the basic physics case of this research is "**utilizing existing neutrino facility for Dark matter search**".

An undefined, but broadly accepted term Lightweight Dark Matter (sometimes Light Dark Matter, or sub-GeV DM) covers the masses below ~GeV scale down to around MeV. In my work, I focus on a minimal Dark sector (or Hidden Sector) model, or rather family of models, of Vector portal DM containing one neutral "dark gauge boson" *V* and one pair of DM particles χ (11).

Each of these neutral vector portal models is characterized by the masses of such particles m_χ, m_V, the kinetic mixing parameter ϵ, and the gauge coupling parameter α_D. The physics case is the beam production of the mediator *V* and its prompt decay into a pair of $\chi + \chi$. The χ particles continue into the Near detector, where they can scatter of nuclei and electrons of the detector material. The electron scattering, as a very clean leptonic process, is the interaction channel of interest of this search (12).

The production rates scale with ϵ^2 and the cross section of χ DM particles scattering off electrons in the detector is dependent on $\epsilon^2\alpha_D$, so the total number of observed scattered electrons in the detector then strongly depends on ϵ^4. By rescaling ϵ to

$$Y = \epsilon^2 \alpha_D \left(\frac{m_\chi}{m_V}\right)^4, \tag{1}$$

we get an important cosmological "self-annihilation" parameter, which also enables us to compare the result across several models and experiments, which is vital in broad BSM fields (13), (14).

The principal goal of this thesis is to cover a new area of $Y \times m_\chi$ phase-space, where NOvA has the largest potential for DM observation. In case of zero observation, the upper **limits of *Y*** for given parameter set of m_χ, m_V can be calculated. Such dedicated NOvA analysis has not yet been carried out and the result would have a significant scientific impact.

The whole DM field is recently gaining more and more momentum and both the theoretical and experimental landscapes are changing at a rapid pace, so the specific parameter set for my DM hypothesis was gradually evolving during my research. In my analysis, I reflect the most up-to-date results from different experiments and observations and fix the $\alpha_D = 0.5$ and $3m_\chi = m_V$ and operate within the range of m_χ masses 7 MeV - 500 MeV (14).

1.2 Roadmap

To achieve such goal, several fundamental analytic tasks need to be performed, while following basic standards of experimental particle physics. To simplify, I am testing a hypothesis of DM set of fixed parameters against already measured NOvA data. On a chosen model example with fixed values of parameters ϵ, α_D, m_χ, m_V , I can perform the whole analysis chain and within the mass region of 7-500 MeV, I can then generalize the results.

For initial study, I need to make a Monte Carlo simulation of particles with given characteristics and investigate their behavior in the detector. Based on the findings, I define and optimize a set of selection criteria (cuts) and validate them in a control region, which is not signal dominated. The cuts are eventually applied on real data in signal region without further tweaking (this is so called blinded analysis).

In case of disproving the hypothesis, I am then able to calculate the upper limit of parameter Y (rescaled mixing constant ϵ) in frequentist approach. With fixed ratio of dark photon and dark scalar pair masses and assuming model-independence of search in chosen channel, I can also recalculate the Y upper limit for different masses and plot its dependence on m_χ.

1.3 Outline

Although NOvA is a neutrino experiment and most NOvA publications and theses include overviews of neutrino theory and history to some extent, the physics and discoveries in neutrino oscillation field are omitted in following text. Instead, a condensed description of Dark matter landscape and history is believed to be more beneficial to the reader, together with some introduction to Dark matter particle theory.

Other chapters describe the measuring apparatus – the NOvA experiment, the NuMI beam as the most intensive neutrino beam in the world, the NOvA detector design with emphasis on ND, and the simulation used in the analysis, following the "*ν+e*" analysis flow with the LDM specifications added, and showcases the LDM search through a Neutral-Current-like scattering on an electron in the detector material. Reconstruction and particle identification with emphasis on electron clustering, as I am essentially looking for electromagnetic (EM) showers (resulting in single prongs in Near detector) caused by the scattered electron, is described in Chapter 4.

In Chapter 5, I describe my simulation process to obtain LDM beam and EM showers from LDM scattering inside the detector. The actual LDM "search" is conducted in Chapter 6. The reconstructed beam neutrino interactions and other neutrino events are the background in LDM search and understanding these events properly is the core of this research. The uncertainties of the analysis are also evaluated. The work is concluded with so called "box opening" procedure and representation and discussing of the results.

In the last chapter I comment on the impact of the result and give some ideas and possibilities for the extension of this analysis.

2 Lightweight Dark Matter

We believe only around 5 % of the Universe is made of matter as we know it. The cosmological measurements, more and more compelling in recent years (15), have proved that some form of matter, undetectable by our instruments and senses, causes the majority of the gravitational forces holding the galaxies and galaxy clusters together. The fact that this Dark Matter, otherwise neutral under all SM charges (electromagnetic, weak and strong), takes up almost quarter of our Universe (the remaining 68 % is believed to be the Dark Energy) and still we haven't been able to explain or detect it, has been driving physicist to create new ideas and models of DM as well as experiments to detect the DM particles for the first time.

2.1 Dark Matter history

Analogically to the "atomistic" philosophy proposed by Democritus (or arguably even earlier in India), some hints of ideas of Dark matter might be found in Greek philosophy (Epicurus or Philolaus (16)). Modern history of DM although starts in the 20th century, when astronomers realized that the visible part of galaxy clusters cannot make up to the mass required to create gravity strong enough to hold them together. This was later connected to the galaxy rotation problem and a new field of science was created when particle physicists joined the astrophysicists in a quest to explain these discrepancies.

2.1.1 Nomenclature

Given the level of our current knowledge, calling the Dark matter "dark" might be misleading. Dark bodies absorb light, which is the exact opposite of one of the main DM properties. Also, common language adjectives evolved in "normal matter" world so it is fundamentally not possible to define a straightforward name for a substance falling out of the reach of our senses and macro-world experience. But it is important to realize that the term Dark matter have been used for over one century now and that originally it was indeed used for some dark, non-luminous matter adding up to the total mass of the galaxies.

The first mention of "dark" bodies in our universe was derived from Newtons universal law of gravity, when John Michell and later Pierre Simon Laplace postulated black holes at the end of 18th century (16). Based on precise

observations, Friedrich Bessel predicted existence of "invisible" star, influencing a luminous star only by its gravity pull. More dark astronomical objects were discovered based solely on their gravitational pull and at the end of the 19th century, after astronomical photography was put into practice and discovery of gaseous nature of nebular masses, the questions of dark, absorbing areas between stars were attempted to be solved through calculations and simulations.

In a response to Kelvins dynamical estimation based on gas theory (or virial theorem taken from thermodynamics), Henri Poincaré used the term Dark Matter for the first time in 1906 (17). The reality of a portion of the universe being made of some dark matter started to be broadly accepted and scientists started to focus more on where is this matter located and what might it be made from – suggesting non-luminous gas, microscopic dust, meteorites, planets, faint or dead stars. After Fritz Zwicky and Sinclair Smith proved the existence of dark matter through red shift of galaxy clusters and Kent Ford, Vera Rubin and many others studied the rotations of galaxies (read further bellow), the definition of dark matter further broadened, with possible subatomic particle candidates, with rise of pioneering astro-particle science discipline. It took more than half a century to rule out all of the macroscopic possibilities and shift the meaning to the elementary particles realm.

After the rise of particle astrophysics and cosmology, many models of DM were proposed, but known SM particles would be gradually ruled out. One of the main candidates or candidate group was Weak Interacting massive Particles, WIMP, and again, the meaning of this term had changed over the time. Originally it was, similar to DM in its early years, a general name for particle candidates like neutrinos, but today WIMP is a specific group of DM candidates which we haven't been able to directly detect yet.

Since all possible explanations using common, known matter were ruled out, it was clear that DM has to be in the form of some non-baryonic matter and indeed "Non-baryonic matter" was the most accurate name for DM for a longer period of time, however, it doesn't comprise all the special properties of DM we are now aware of and therefore "Dark Matter" is still heavily used in both scientific and popular literature, usually with a specific type of particle added to clarify it.

History proved that some ideas and models were indeed correct, but the discovered amount of excess mass was not enough to account for the whole DM gravitational effect (i.e. free cold or hot hydrogen, neutrinos, some MACHO candidates). It is also entirely possible, that the DM effects we observe might be a sum of larger number of unknown particles or phenomena, which would make the creation of some elegant terminology even more challenging.

2.1.2 Astronomical observations

As mentioned earlier, first astronomical observations were based on gravitational pull of dark stars or dark planets. With astronomical photography, more precise measurements brought more data to be compared with calculations.

First quantitative models of our Galaxy were published by Jacobus Kapteyn and improved by his student Jan Oort, but their calculations disfavored existence of dark matter in larger quantities, comparing the "stellar mass" with "nebulous or meteoric matter" (18).

The most famous and heavily cited research was carried out by Fritz Zwicky, who studied the mass and velocity of galaxy clusters based on the red shift calculations proposed by Hubble and Humason and the virial theorem (19). He described a large discrepancy in relative velocities of individual galaxies in the Coma Cluster and in 1937 published an estimation of mass/light ratio to be around 500, suggesting a majority of cluster to be made of dark matter (20). Similar estimate was calculated by Sinclair Smith on the Virgo Cluster at the same time (16).

The discrepancy between Hubble's and Zwicky's and Smith's estimates draw a lot of attention and several explanations were proposed, more or less conservative (low luminosity surroundings of galaxies, free gas or invalidity of the virial theorem (16)). More precise calculations on the universe dynamics and precise X-ray emission measurement ruled out both the non-equilibrium theorem and the intracluster free gas (21).

Parallel to the cluster observations, astronomers were measuring the rotational curves of galaxies. This research also showed large discrepancies in mass/light ratios and was accelerated by the invention of radio astronomy after World war II. After Kent Ford developed a tube spectrograph in 1960s, he worked with Vera

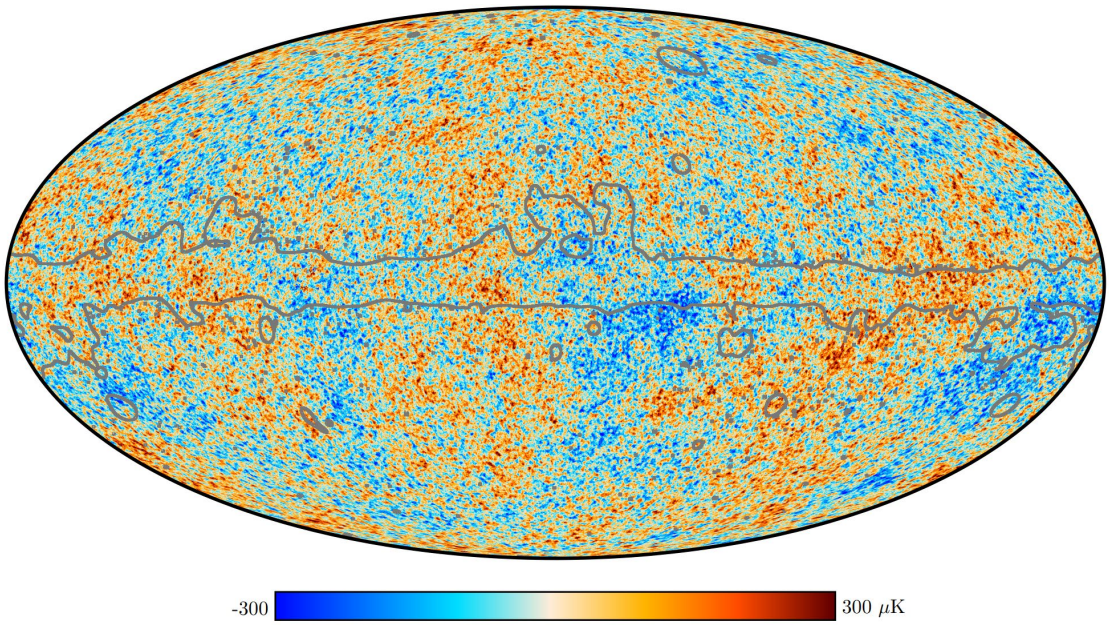

Figure 1: The map of the CMB temperature anisotropies, extracted using the SMICA method. The gray outline shows the extent of the confidence mask. Taken in July 2018 by ESA's Planck satellite (171).

Rubin and in 1970 published precise results on the galaxy rotation curves, which stayed flat further from the core of galaxy than expected, suggesting that additional invisible mass is needed to stabilize the galaxies (22).

This was believed to be of stellar origin (intermediate or dark stars) or later also of gaseous galaxy coronas, black holes or other baryonic structures like massive astrophysical compact halo objects (MACHO).

The belief that DM is made of MACHOs survived till the end of 20th century. The existence of such objects could be proved through the gravitational microlensing and indeed the first result from MACHO collaboration in 1993 aligned with the baryonic paradigm (23), but more data from MACHO and EROS observations finally disproved this model (24) (25). Alternatively, after the cosmic microwave background discovery in 1965, precision measurement started being made and constraints on cosmological baryon density were set and satellite experiments like WMAP (26) and Planck (27) eventually ruled out most of the MACHOs.

Besides baryonic and non-baryonic DM models, a significant effort was made in Modified Newtonian Dynamics (MOND), which proposed a simple change in how gravitational force works and denied the existence of DM (28) (29) (30). Although

some predictions of this compelling proposal matched to the rotations of galaxies, the apparatus and extensions behind this model were getting very complicated (31). In 2006, the lensing (i.e. mass) and x-ray spectra of two colliding galaxy clusters ("Bullet Cluster", Figure 2) showed a discrepancy between spatial distributions of baryons and "general mass" (32). The bullet cluster is believed to be a direct proof of non-baryonic DM existence and also heavily rules out MOND (although some complicated modifications to accommodate the Bullet Cluster discrepancy were later proposed).

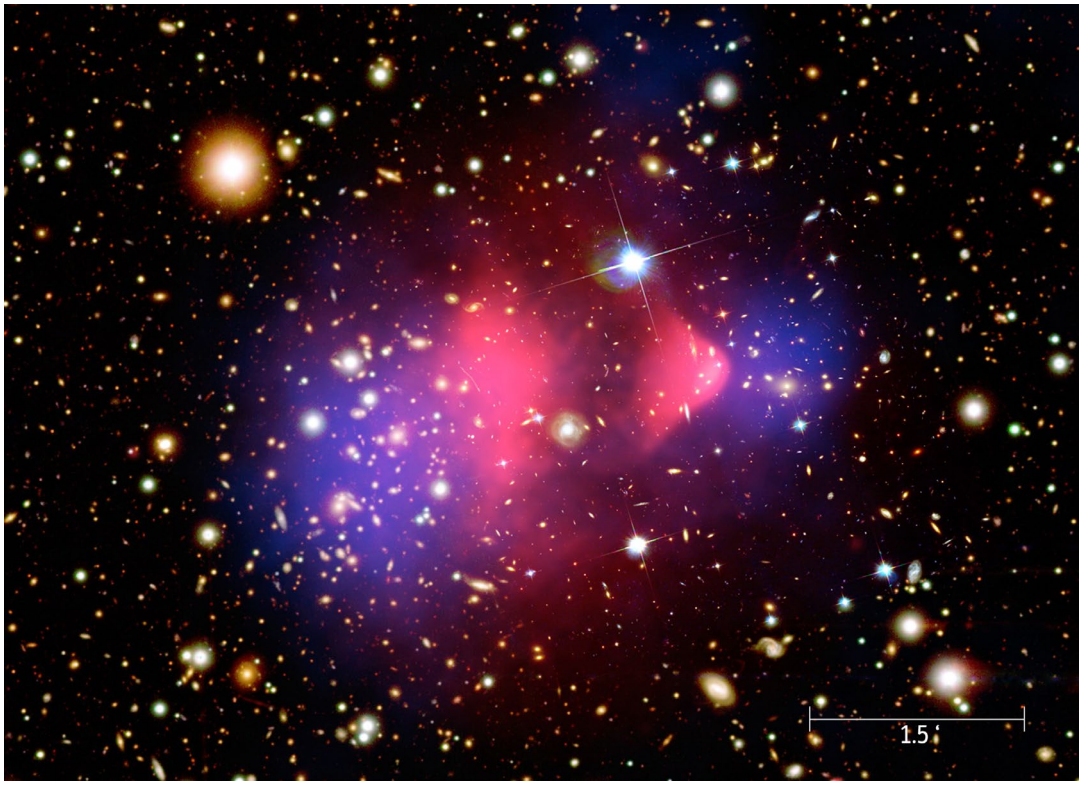

Figure 2: Galaxy cluster 1E 0657-56 - the Bullet Cluster. This image is an overlay of visible spectrum from Magellan and Hubble telescopes, X-ray spectrum from Chandra (pink) and mass distribution based on gravitational lensing (blue). Scale on the right in megaparsecs (169).

2.1.3 Particle-astrophysics

In 1983, Fermilab founded the Theoretical astrophysics group. This can be seen as a natural result of particle physicists and astrophysicists needing to work closer together. This created the "Cosmic Frontier" and paved the way to precision cosmology and particle-astrophysics. In the second half of 20th century, the particle DM paradigm was gaining more and more popularity among scientists

and eventually took the role of generally accepted theorem for DM origins. Today, the Cosmic Frontier is one of the pillars of elementary research, as is stated in the P5 report (the US long-term strategic plan for particle physics) (33).

First particle candidate which could account for the missing mass was the neutrino. The cosmologists were able to calculate limits of neutrino mass and also later realized this type of a weakly interacting particle is a good candidate for dark matter (34) (35). Although neutrinos as DM were later ruled out through numerical simulations, it was a pioneering idea for DM made of non-baryonic particles and set the foundations for a whole group of possible weakly interacting massive particles outside the SM.

Supersymmetric particles were also studied in terms of cosmology and later on started to be considered as DM candidates (36). Supersymmetry is a very attractive framework by itself, with many predictions and consequences, but four supersymmetric neutralinos could also "close" the Universe in terms of missing mass and are considered one of the most studied DM candidates (16) (37) (38).

A global broken symmetry was introduced to dynamically scale the Θ parameter in quantum chromodynamics (QCD) but also implied a new boson – axion (Peccei-Quinn (39) (40) (41)). Strong constraints on axion mass and interaction rates also made it an interesting DM candidate (42). Besides direct thermal axion production mechanisms (43), proposed field misalignment production (44) suggests that in case of Peccei-Quinn symmetry breaking before the inflation, we might find ourselves in an anthropic tuned current universe which had enough time to develop from a local low-density region (45) (46) (47).

2.1.4 Current status and outlook

The astrophysical and cosmological evidence of DM existence is undeniable, yet we don't know anything about its constituents, their cosmological origin or way of interaction. Even though the presence of DM in Universe is now broadly accepted and believed to come from some kind of new particle(s) BSM, alternative ideas still haven't been completely ruled out (i.e. MACHOs up to $M_{\odot}$). The scope of the unknown properties of DM makes the research program very broad and challenging to manage. Currently, the astrophysical program (based purely on gravitational effects) coexists with "particle-DM detection" frontier. The variety of

possible explanations of DM is vast, therefore, the experimental program also has to be very diverse and cover numerous models.

In 2014, the above mentioned "P5 report" (33) solidified this tendency, defining the particle physics goals for the US scientific agencies for the coming years and proclaiming the importance of broad DM-search program at every scale and on all possible platforms. Many of the DM scenarios are covered by the large-scale DM experiments (like the WIMP, gravitino, or sterile neutrino), but others, like ALPs, Asymmetric DM and Hidden Sector DM, have a large and well-motivated parameter space reachable through different small-scale experiments. Reinterpreting NOvA as an accelerator beam-dump DM detection apparatus perfectly fits into this search program portfolio.

Many of currently known DM limits came from re-analyzing of data already measured by differently purposed experiments in the past. An ever-growing population of first-generation DM experiments collected tremendous amounts of data and published physics results. More optimistically, the discovery potential of this field attracts more and more physicists and therefore novel detection techniques are now more frequently appearing.

There are also many discrepancies between the SM predictions and experimental results, like the muon magnetic moment (48), the proton radius (49) or the ^{8}Be decay anomaly (50). Many of these anomalies already drawn attention of DM researches and more synergies are yet to come, i.e. with nuclear, atomic and condensed matter physicists.

In the near future, the satellite Cosmic Microwave Background (CMB, see Figure 1) and gravitational observations will continue, with apparatuses capable of measuring gravitational microlensing effects under the solar-mass scale. Furthermore, a completely new avenue of cosmic measurements was uncovered through the detection of gravitational waves by the LIGO experiment (51).

The DM detection projects of the second generation (G2) are already underway (52) and many large-scale direct or indirect detection experiments have secured financing for construction in coming years. Complementary to these big projects, a DM program now turned into an integral part of all viable small scale or accelerator-based experiments

2.2 Experimental landscape

Since particle physicists became interested in the DM problem in the second half of 20th century, they proposed a number of experimental setups capable of detecting hypothetical DM particles. In last 30 years, experimentalists were carrying out these challenging projects, ruling out a large variety of DM models. There are several detection principles (direct, indirect, thermal, collider, beam dump, missing mass, visible mediator) and there is a few dozen DM dedicated experiments currently running and many other DM programs in experiments focused on other types of physics, in which we can also include the LDM search in NOvA. Other efforts also assign some SM experimental discrepancies to the DM existence and many experiments now use DM to explain the anomalies in their data. Here we briefly describe the mainstream DM-detection efforts.

2.2.1 Axion telescopes

There are several experiments based on a special behavior of axions and axion-like particles. One of the detection principles for catching axions is called "light shining through a wall". Photons passing through a strong magnetic field can change to axions, which would pass through a non-transparent material like thick metal wall (experiments ALPS (53), BFRS (54), OSQAR (55)). Alternatively, a magnetic field in a vacuum can be changed (polarized) by passing light source, i.e. laser shining through a cavity (PVLAS experiment in Italy (56)).

Most of the axion detectors use a common property of axion models – when passing through a strong static magnetic field, an axion can be converted to a monochromatic microwave photon (Primakoff effect). This photon can be detected in a cavity which is tuned to its energy. The leading experiments searching for axions are ADMX (57), CAST (58), HAYSTACK (59) and ORGAN (60). Axions could be also detected in direct recoil detectors like XENON100, CDMS, EDELWEISS, XMASS (see below) (61).

2.2.2 Direct DM scattering

When a DM particle hits the detector material, it can scatter off its nuclei or electrons and deposit energy. Pioneering direct detection experiments trying to detect such events were using cryogenic superconducting colloid detectors (62). By energy deposited by the elastic DM particle collision, cold microscopic grain was transitioned above the superconducting state which resulted in measurable

collapse of the magnetic field. Similar approach was used in the first-generation DM detectors, searching for a signal from DM particle scattering coherently with nuclei through spin-independent couplings (or alternatively with much lower yield through spin-dependent couplings) in low-background germanium ionization detectors. These measurements set the first limit on DM cross sections, but they quickly reached the background limits (63). One of the ways of challenging the background limits is to measure in two channels in cryogenic crystals – ionization (or scintillation) and heat – to distinguish nuclear recoils from gamma and beta events (experiments CDMS (64), EDELWEISS (65), CRESST (66)). Another elegant way of pushing the background limits was to observe seasonal fluctuations of the otherwise not distinguishable backgrounds over a long period of time to correlate with the Earth orbiting the Sun and Sun travelling through the DM halo. This technique is employed in DAMA (DAMA/LIBRA in Gran Sasso) experiment, which claims its results are consistent with DM observation (67), interestingly however, similar experiments with different detector materials like XENON100 and CoGeNT disprove this measurement (68) (69).

To gain further sensitivities for DM experiments, larger projects were proposed (like i.e. the 1-ton cryogenic EURECA (70)), but solid-state detectors are too expensive to scale to larger sizes. Instead, liquid noble gas detection was implemented, which also uses a pair of scintillation/heat channels. Good examples of experiments using liquid xenon are XENON100 (71), DEAP (72), PandaX (73), ArDM (74), WARP (75), LUX or LZ (52) (planned).

2.2.3 Indirect detection

Competitive to direct detection are experiments using indirect measurements of DM annihilation or decay products. Pioneering indirect DM searches were looking for excess of gamma-rays from (preliminary) heavy stable lepton (76), but later the focus shifted to looking for excess of antiprotons and positrons from high density DM areas like dwarf Milky way satellite galaxies. Most of the annihilation gamma-ray signals from satellite detectors like EGRET or Fermi (FGST) are today assigned to the normal galactic activity and known sources (77) (78) (79). Similarly, antiproton spectra from PAMELA, CAPRICE, AMS and BESS experiments can be mostly assigned to known sources (80) (81) (82). More challenging to explain were measurements of positron spectrum from the same satellites, although baryonic

activity interpretations (namely pulsars) are already proposed as sources of these events (83).

According to some models, DM particles can be gravitationally bound to the Sun (or Earth) and become trapped in its core after losing enough energy through elastic scattering on normal matter (84) (85) (86). Experiments like IMB, FREJUS, AMANDA or Super-Kamiokande started looking for events like light electron- or muon-neutrinos scattering in the detectors (87), with currently most sensitive ANTARES and IceCube (88). The NOvA Far detector also has good resolution to see such events and a search for upward-going muons coming from DM annihilation in the Sun is currently underway (89).

2.2.4 Accelerator DM

According to many models, DM can be produced in particle accelerators, when intensive particle beams either collide or hit a solid target, "collider DM" therefore can only work if some kind of interaction between the SM and DM particles exists. Same as a neutrino in most collider experiments at the Energy frontier (33), the DM particle of interest leaves the detector without interaction and the only way to access the reaction is through a missing-momentum analysis. Most notably, the ATLAS, CMS and LHCb detectors at the LHC at CERN are leading the efforts in this direction, with 13TeV proton-proton beam collisions and prospect for the high luminosity upgrade, projected to take place in year 2026.

The simplest mechanism of the DM-SM interactions is through portal models, in which either the Higgs boson or *Z* boson mediate a feeble coupling of DM to SM particle (the *Z* portal search at LEP was also well motivated). If the mediator is also new (invisible) particle, the models get more complex and challenging. Other WIMP or SUSY models can be also constrained in these detectors at different levels of complexity (simplified neutralinos or cascade decays of SUSY particles).

If a signal at the LHC detectors is measured, mostly in some "mono-X" jet channel (interactions in which a QCD or other SM particle, like photon or Higgs or *Z* bosons, is created among the DM), it doesn't necessarily mean that DM particle was discovered, as the missing momentum can only point out some neutral, stable particle leaving the detector (90) (91).

If any of the considered portal models are valid, independently of how and where the DM will be discovered, we will be able to create DM beams and further probe DM properties.

2.3 Physics motivation

Dark matter BSM physics models are well motivated with the above mentioned global broken symmetries (Chapter 2.1.3) and concepts like the elusive Axion (~meV) and other Axion-like-particles (ALPs) which do not bind their masses (~MeV) with the Weak scale coupling (92). There also exist ideas of Dark or Heavy Photons, whose decay may be a source of Dark Matter in a Dark Sector and Heavy Neutrinos that may complete the puzzle of the CP violation in the lepton sector.

The direct detection experiments and searches with colliders mentioned in Chapter 2.2 have put very stringent constraints on candidates with masses over 10 GeV. This limit drives the ideas which claim that BSM Physics may come from what is referred to as "Hidden Sectors" (HS, sometimes also called "Dark sector"), phase spaces which contain an arrangement of lightweight "dark" or "hidden" states. These states have no charge under the SM. There have been some compelling arguments from several well motivated models (93) on the production of mediating states that represent a weak (here as feeble, rare, not as the weak interaction) coupling of these HS to the SM.

The impact of any discovery of such HS candidates will not only define the High Energy Physics research for this century but will also give us either the first ever dynamic coupling case with ALPs, or a view into nature's intentions, in the case of HS, where there are no reasons to have any anthropic-motivated fine tuning of parameters (Chapter 2.1.3).

2.3.1 Theory background

During the continuing searches for DM candidates, various ideas and techniques for looking for the signatures of such states coming from the galaxy or Earth-bound sources have been developed (94). The accelerator technology advancements of the past 20 years which brought the era of the Intensity Frontier in High Energy Physics experimentation (95) (96) (97) may also have given us such sources of New Physics candidates. The most intense of these beams are used to conduct neutrino experiments (94) (95). A series of models (12) (11) (98) (99) have

been developed describing that the Lightweight Dark Matter (LDM) could be potentially produced from these high intensity beams of ~10^{15} protons or electrons per second striking targets made of carbon, mercury or other high-Z material. The currently largest operating accelerator-based neutrino experiment is NOvA at Fermilab, described in Chapter 3.

In order for the HS particles to be reachable through a beam-dump setup, they have to include at least one mediator which can couple to the SM. That can be a scalar ϕ, a pseudoscalar a, a fermion *N* or a vector particle *V*. The way in which the mediator couples to the SM is restricted by the SM symmetries and the dominant interactions are the SM gauge singlet operators:

$$\mathcal{L}_V \supset -\frac{\epsilon}{2cos\theta_W} B_{\mu\upsilon} F'^{\mu\upsilon}, \tag{2}$$

$$\mathcal{L}_\phi \supset (\mu\phi + \lambda\phi^2) H^\dagger H, \tag{3}$$

$$\mathcal{L}_N \supset y_n L H N, \tag{4}$$

$$\mathcal{L}_a \supset \frac{a}{f_a} F_{\mu\upsilon} \tilde{F}^{\mu\upsilon}, \tag{5}$$

where $H^{(\dagger)}$ is a SM Higgs doublet, *L* is a lepton doublet, $B_{\mu\upsilon}$ is a hypercharge field strength tensor, $F^{\mu\upsilon}$ is the photon field strength tensor, θ_W is weak mixing angle, and $F'^{\mu\upsilon}$ is a dark vector boson field strength. These are the most important portals to the Hidden Sector. Among the prevailing theoretical models (92) (93), the one with the lowest dimension is called "Neutral Vector Portal" (12) (11) (100), which will serve here as my benchmark model for LDM search. It introduces a minimal kinetically mixed vector field mediator (often also called dark photon) V, with Lagrangian

$$\mathcal{L}_V = -\frac{1}{4} F'^{\mu\upsilon} F'_{\mu\upsilon} + \frac{1}{2} \frac{\epsilon}{cos\theta_W} B^{\mu\upsilon} F'_{\mu\upsilon} - \frac{1}{2} m_V^2 V^\mu V_\mu \,, \tag{6}$$

with dark photon field strength $F'_{\mu\upsilon}$ and SM hypercharge field strength $B_{\mu\upsilon}$, dark photon mass m_V and free kinetic mixing parameter ϵ. If we simply extend this sector with a DM candidate which couples to the dark photon *V* through dark-sector new interactions, the dark photon then serves as a mediator between the DM particle (fermion χ or scalar boson ϕ with dark sector fine structure constant

α_D) and electromagnetic field in SM matter – i.e. detector material in our laboratory (98) (99).

Figure 3 shows an example of two possible channels of production at a proton beam-dump using the method of the Vector Portals with the creation of a mediator particle *V* that decays into a pair of Dark Matter particles $(\chi, \chi^\dagger)$ that belong to a Dark or Hidden Sector of New Physics BSM. That is the source interaction we look for in the NOvA ND LDM search.

2.3.2 LDM interactions

When a high luminosity beam falls on a target material (beam-dump), besides the SM particle products, which eventually become the neutrino beam, there may also be produced vector particles *V* at a much lower branching ratio. Cosmological constraints from (12) (11) (98) (99) estimate a sub-GeV mass mediator *V* production cross section of ~40μb and slowly declining for higher mediator masses. This dark photon particle, according to the model, is the mediator state between the SM natural world we inhabit and a simple Hidden Sector of nature that contains at least one pair of DM particles that can be scalars or fermions.

The first two diagrams in Figure 3 represent the two most viable mechanisms for vector mediator creation from leading order hadron processes. In the direct production scenario

$$q + q \longrightarrow V \longrightarrow \chi + \chi^\dagger , \tag{7}$$

the quark from the protons of the beam and the quark from a proton or neutron from the nuclei of the NuMI carbon target interact with $s^{1/2}$ = 15GeV available energy at the center of mass, with the LDM production cross section:

$$\sigma\left(p + p(n) \longrightarrow V \longrightarrow \chi + \chi^\dagger\right) = \sigma(pp(n) \longrightarrow V) \times \mathrm{Br}\left(V \longrightarrow \chi\chi^\dagger\right), \tag{8}$$

Or as a differential function of energy and angle to the beam:

$$\frac{d\sigma\left(pp(n) \longrightarrow V \longrightarrow \chi\chi^\dagger\right)}{dE_\chi d\cos\theta} = \frac{\delta(x, \cos\theta)}{\delta\left(E_\chi, \cos\theta\right)} \cdot \frac{d\sigma(pp(n) \longrightarrow V)}{dx} \cdot \mathrm{Br}\left(V \longrightarrow \chi\chi^\dagger\right) \cdot g(\cos\theta), \tag{9}$$

Where g is the LDM angular distribution and *x* is the quark momentum fraction.

In the indirect process (Figure 3 middle), the proton on proton (or neutron) interaction produces mesons ϕ as secondary particles which promptly decay, potentially into a minute fraction of LDM through the same mediator mechanism of the Vector Portal. This case is less helicity-suppressed than the direct production and is favored in lower energies, is also reachable in Fermilab's Booster neutrino beam experiments like LSND (101) (102) and MiniBooNE (103) (104) as well as the JPARC complex feeding the T2K experiment (105). For NuMI beam, the mesons (ϕ) under investigation are mainly π^0 with some additional contribution from η. The total number of DM particles χ from decays of such mesons is

$$N_\chi = 2N_{POT}\, N_{\phi/POT}\, Br\left(\phi \rightarrow \chi\chi^\dagger\right), \tag{10}$$

where, for our scenario of parameters and masses, and only for on-shell production of *V* lighter than m_ϕ, the narrow width approximation yields a simple branching ratio formula (13)

$$Br\left(\phi \rightarrow \chi\chi^\dagger\right) = Br(\phi \rightarrow \gamma\gamma) \times 2\epsilon^2 \left(1 - \frac{m_V^2}{m_\phi^2}\right)^3 \times Br\left(V \rightarrow \chi\chi^\dagger\right). \tag{11}$$

Here we slightly underestimate the flux, as we ignore kinematically suppressed addition from secondary and tertiary mesons produced in target and also the off-shell three-body decays of mesons, which are more significant for higher energies. The $N_{\phi/POT}$ for pion is ~1 and for η ~1/30, the choice of very small $\epsilon = 10^{-4} - 10^{-5}$ results in the Dark Photon exclusively decaying into a pair of DM, i.e. $Br\left(V \rightarrow \chi\chi^\dagger\right) = 1$, and, eventually for meson decay modes, $Br(\pi^0 \rightarrow \gamma\gamma) = 1$ and $Br(\eta \rightarrow \gamma\gamma) = 0.39$.

With a nominal beam intensity of 6×10^{20} POT per year, $10^{10} - 10^{12}$ DM particles would be produced through such decays at NuMI beam. Note the rate scales only with mediator mass and mixing parameter ϵ and is independent of m_χ , α_D .

For off-shell production (three body decay of meson) a non-trivial formula for branching ratio does depend on all four HS model parameters (13):

$$Br\left(\phi \rightarrow \gamma\chi\chi^\dagger\right) = \frac{1}{\Gamma_\phi} \times \frac{\epsilon^2\alpha_D}{2m_\phi} \int d\Phi_{\phi\rightarrow\gamma V} d\Phi_{V\rightarrow\chi\chi} \frac{ds}{2\pi} \langle \left|\hat{A}_{\phi\rightarrow\gamma\chi\chi^\dagger}\right|^2 \rangle \tag{12}$$

Bottom diagram on Figure 3 represents the reverse process where one of the LDM particles interacts with a nuclear target of a neutrino detector material. It may elastically scatter on a nucleon or an atomic electron and the LDM interacts very weakly (i.e. very low cross section) with one of them through the portal again but with the mediator coupling with a space photon to provide the actual interaction and energy transfer to the nucleon (N) or the atomic electron (e). Unlike neutrinos, for which the ratio of scattering cross sections on nucleus and on electron is ≈10^4, the χ - electron scattering is the dominant process (if $m_V \ll \Lambda_{QCD}$). The elastic electron scattering cross section as function of masses and energies of incoming LDM particle and recoiling electron with *C* as the SM-HS coupling constant (106):

$$\frac{d\sigma_{\chi-e}}{dE_e} = C \cdot \frac{2m_e E_\chi^2 - \left(2m_e E_\chi + m_\chi^2\right)(E_e - m_e)}{\left(E_e^2 - m_\chi^2\right) \cdot (m_V^2 + 2m_e E_e - 2m_e^2)^2} \tag{13}$$

and $C = 4\pi\epsilon^2\alpha^2$, where ϵ is HS kinetic mixing parameter and α is HS gauge coupling parameter.

This kind of scattering on electron is a two-body collision with scattering angle θ_e following

$$\cos\theta_e = \frac{E_\chi + m_e}{E_\chi}\sqrt{\frac{E_e}{E_e + 2m_e}}\,, \tag{14}$$

where m_e is the scattered electron mass, E_e is the scattered electron kinetic energy and E_χ is the beam DM (or incoming beam neutrino) energy. This is a purely leptonic process, which gives us one more advantage by removing uncertainties from nuclear effect and other reconstruction challenges. For high incoming particle energies of several GeV and very small angle limit, eq. 14 can be approximated as $E_e\theta^2 < 2m_e$. This kinematic property of the scattered electron (small $E_e\theta^2$ or $T\theta^2$) shows the "forwardness" or boost in the beam direction and can be later used as an important signal selection criterion in the data analysis.

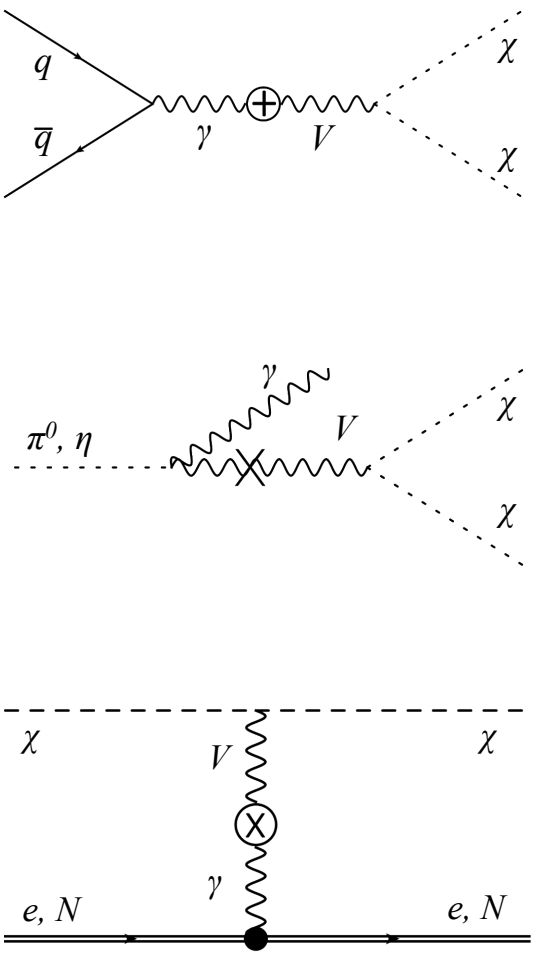

Figure 3: Example of a New Physics LDM candidate (χ) production and scattering. Leading order processes are direct (top) and indirect (mid) production through a Neutral Vector Portal V. (Bottom) χ particle interacting through the reverse process of Vector Portal (V) mediating to SM member like a nucleon or atomic electron.

3 The NOvA experiment

NOvA is a long-baseline accelerator-based neutrino oscillation experiment. NOvA, of course, is an acronym for NuMI off-axis ν_e appearance experiment and the correct abbreviation would be NOνA, but a recent consensus changed the Greek ν [nu] letter to common lower "v" to make the citing, indexing and online searching easier for the scientific community.

NOvA uses the upgraded NuMI beam from Fermi National Accelerator Laboratory (Fermilab) and measures electron-neutrino appearance and muon-neutrino disappearance between its near detector and far detector 810 km away in Ash River, Minnesota. Goals of the experiment include measurements of θ_{13} parameter ($sin^2\ 2\theta_{13}$), mass hierarchy (order of the neutrino masses) and the CP violating phase δ. The NOvA collaboration has already published appearance and disappearance results on data from the first 4 years of running, as well as some non-oscillation physics papers.

The remarkable performance of NOvA detectors, the outstanding energy and spatial resolution, predetermines a non-trivial portion of other physics topics to be also measured on this apparatus. All these non-oscillation physics cases are organized into the "Exotics group", which operates parallel to the two main analysis groups "Nue" and "Numu" (for ν_e and ν_μ).

Neutrinos require enormous detectors with extremely powerful particle sources and NOvA was designed and built to maximize both these features. With the most powerful beam, large mass and proximity to the target, NOvA Near Detector can be reinterpreted as a Beam Dump experiment, which in this case could yield limits on the bellow-GeV Dark Matter candidates' sensitivity in a model independent way. For consistency, the analysis is based on the official NOvA tools, using regular data from first years of running in neutrino mode. The main parts of the experimental apparatus (namely the accelerator beam and the scintillation detector) are briefly described in this section.

3.1 NuMI Beam

Fermi National Accelerator Laboratory (Fermilab) is US premier research center and runs one of the largest accelerator complexes in the world. After the Tevatron shutdown, the lab's focus moved to so called Intensity Frontier. This was

commenced in 2005 with the construction of NuMI beamline – Neutrinos at the Main Injector, initially used for the MINOS experiment. The beam is made by colliding 120GeV protons with a graphite target (other materials were also considered and might be used as target). The NuMI was upgraded several times, currently, after the slip-stacking upgrade, delivering more than 700 kW of beam power. That makes it the most intensive beam in the world. "The NuMI Neutrino Beam" technical paper (107) is an excellent resource for very detailed information about the beam we use.

3.1.1 Accelerator complex

Current accelerator program at Fermilab can provide the experiments with three different particle beams. The Booster Neutrino Beam (BNB), the Neutrinos at the Main Injector beam (NuMI) and a muon beam for experiments Muon g-2 and Mu2e. Also, low intensity, high purity test beams can be delivered to the test beam facility.

The accelerator cascade (Figure 4) starts with a source of gaseous hydrogen where H^- ions are extracted and accelerated to 400 MeV in the linear accelerator (Linac), before being injected into the Booster ring, a synchrotron with 75.47m radius. Here the electrons are stripped, and the protons are accelerated to 8 GeV. The beam in the Booster is bunched at 53 MHz to produce batches of 4 to 5 $\times 10^{12}$ protons. The BNB beam is created when these low energy protons hit a solid target. The protons also can be re-bunched to 150ns and at 2,5 MHz hit a solid tungsten "pencil target" to secondary pions decaying into a muon beam.

For NuMI beam, the protons from the Booster are instead injected into the Main Injector (MI) synchrotron using a slip-stacking method, where six successive batches are injected in a train followed by six more in a different orbit, using the Recycler ring – the former storage ring from the Tevatron era. Once this twelve-batch group is loaded into the MI, it is accelerated to 120 GeV in the 528.3m radius synchrotron and then extracted to the NuMI beamline. The MI injection and acceleration cycle lasts 1.33 s and typically delivers 5 $\times 10^{12}$ protons on target (POT) in 10μs pulses called spills. POT is often used as the neutrino beam intensity unit (the number of neutrinos is roughly proportional to the number of primary protons, or secondary mesons). The nominal year exposure is projected to be 6 $\times 10^{20}$ POT.

Once the beam is extracted from the MI, it is directed downwards at an angle of 3° in the direction of the NuMI target and the on-axis MINOS/MINERvA detectors (and Soudan mine in north Minnesota) as is illustrated in Figure 4.

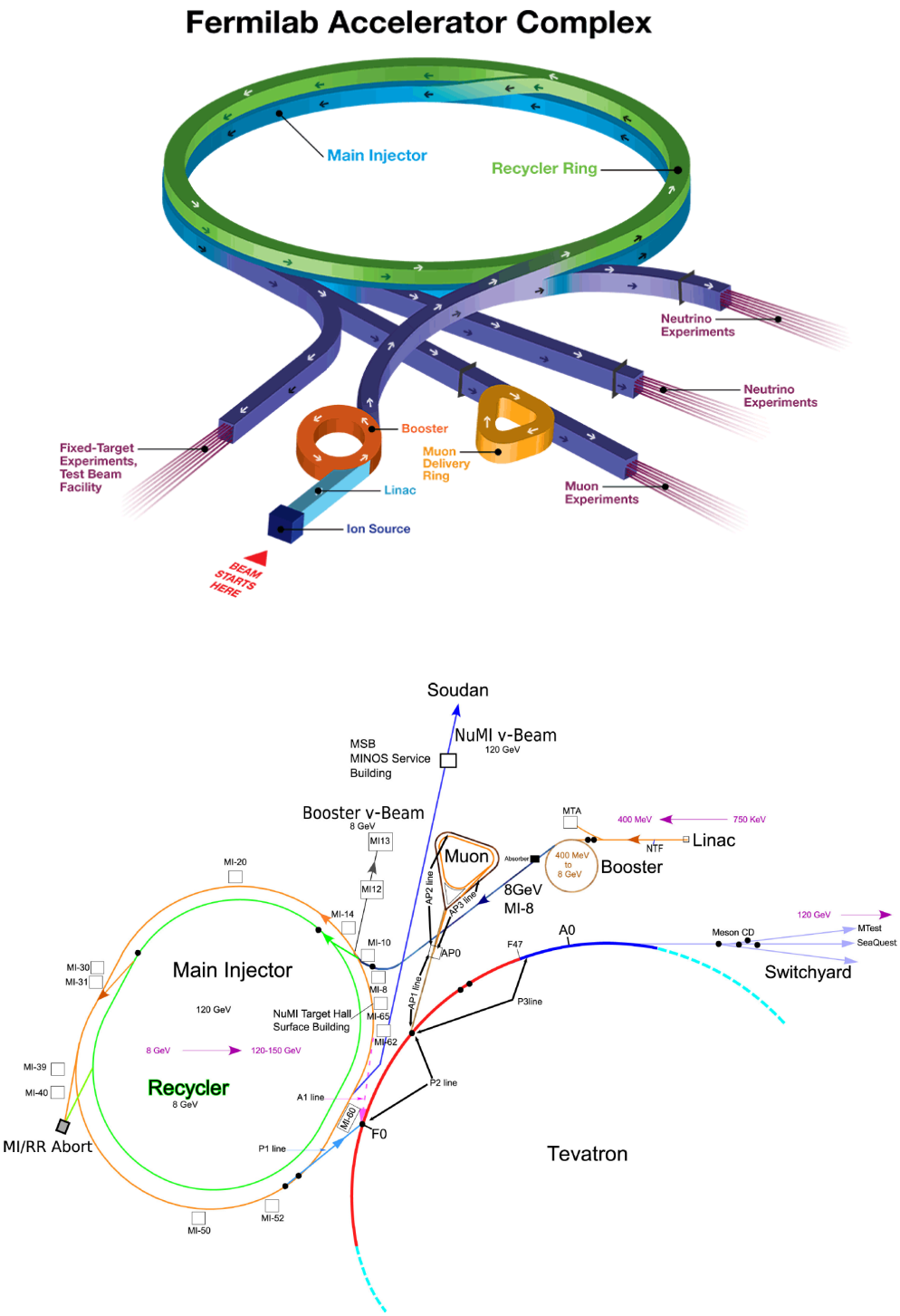

Figure 4: The outline of the upgraded accelerator complex at Fermilab and its schematic in a technical diagram (108).

3.1.2 Target, focusing and decay

The protons collide with a 1.2m graphite target producing a secondary meson beam of pions and kaons (the interaction length is ~60 cm). The NuMI Target (Figure 5 and Figure 8) is made of 50 segments called "fins", 24 mm thick, 7.4 mm wide and 63 mm tall, each separated by 0.5 mm from each other. The fins (the whole graphite stack) are encapsulated in anodized target pipe, through which two waterlines are constantly ran to provide sufficient cooling (108).

The target is located upstream of two parabolic magnetic focusing horns which are used to select the charge sign of the secondary mesons and to focus them in the direction of the detectors (109). The horns are 3 m long each ant they function as a lens with focal length proportional to the meson momentum. They operate in 1-ms pulse mode at 200 kA and must be cooled by water. Mesons that are focused by the parabolic magnetic field of the first horn pass unaffected through the second horn while poorly focused particles in the first horn move to a larger radius and may be focused by the second, which extends the momentum range of the beam.

The peak energy of the neutrino beam is determined by the relative position of the horns (Figure 7). The result of the magnetic horn selection is a predominantly neutrino or anti-neutrino beam (Figure 13 and Figure 12), depending on the polarity of the horns and focusing positive or negative pions and kaons (Figure 4). The positions of the horns can also be adjusted to change the produced neutrino beam energy profile. Most of the neutrinos in the NuMI beam are products of pion decays, because the kaon production cross sections are smaller and also the neutrinos from heavier kaon decays are less directional. The focusing system in Forward Horn Current configuration leads to almost pure muon-neutrino beam (FHC neutrino mode). The Reverse Horn Current focuses mostly muon-antineutrinos (RHC antineutrino mode).

A 675 m long and 2 m wide decay pipe filled with helium (pressurized to 0.9 atm) is placed downstream the horns. This length was chosen since it is the approximate decay length of a 10 GeV pion. The beam then passes through a water-cooled aluminum and steel hadron absorber and 240 meters of rock to remove any remaining muons, hadrons, and charged particles to leave a pure neutrino beam. The NuMI beamline is drawn in Figure 6.

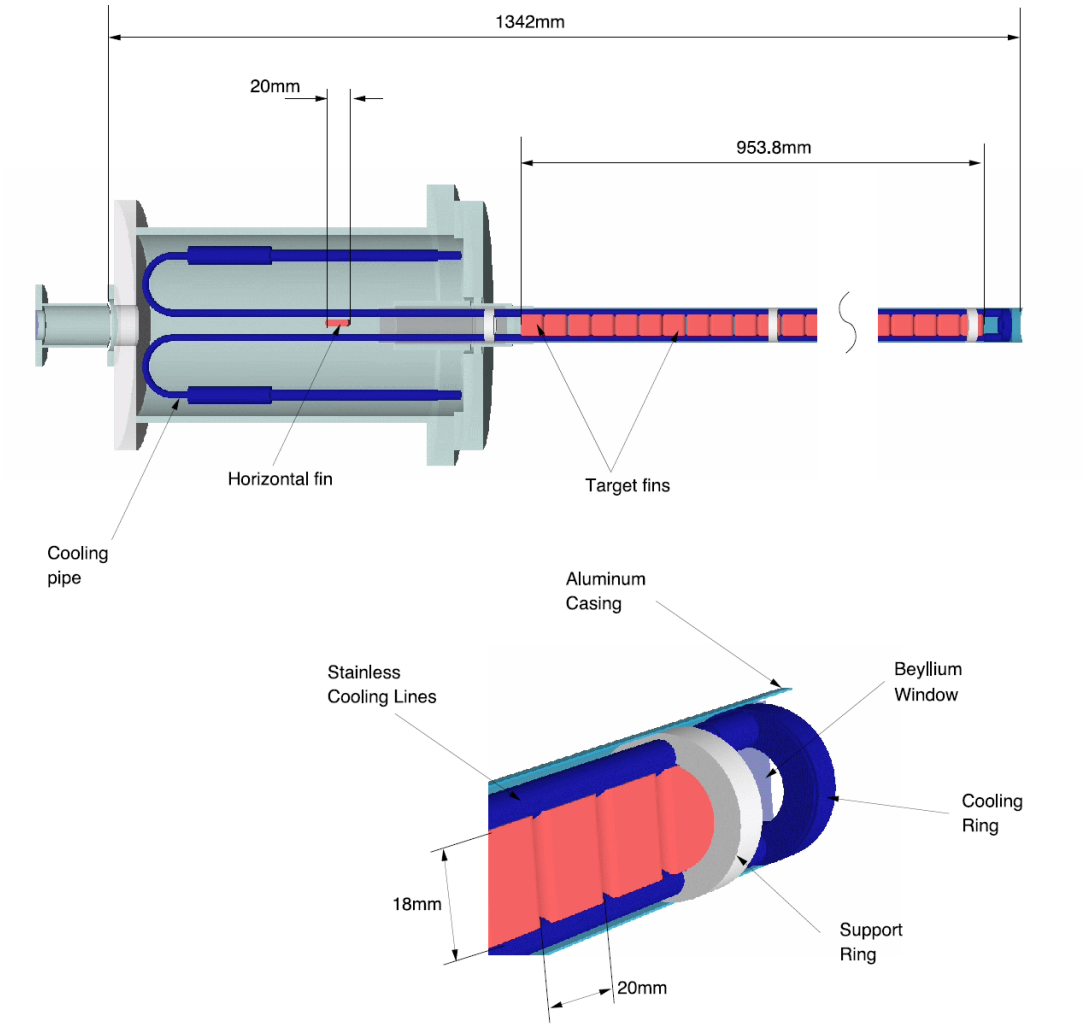

Figure 5: The NuMI target longitudinal cross section and detail of the Target Canister (107).

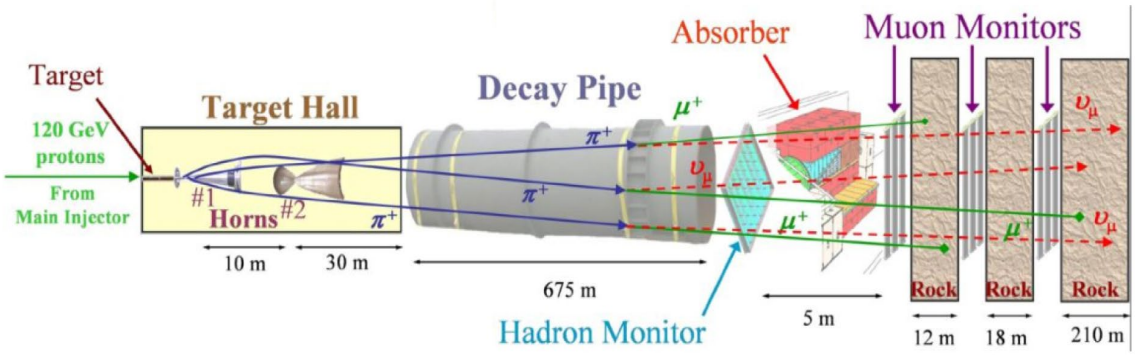

Figure 6: How to make a neutrino beam (1).

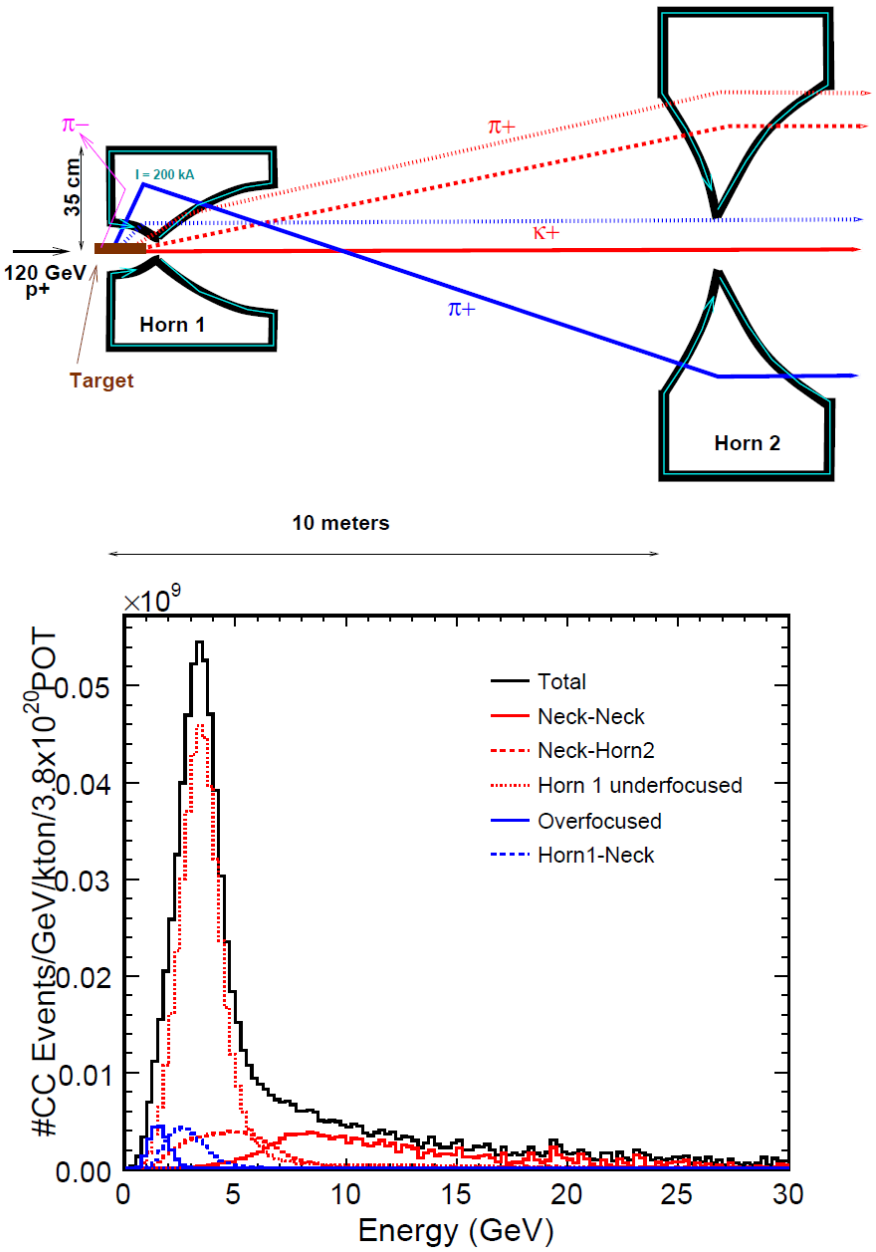

Figure 7: The NuMI magnetic focusing system – hadrons passing the two magnetic horns. The top diagram illustrates possible trajectories through the two NuMI horns. Hadrons that are underfocused or overfocused by the first horn are further focused by the second horn. The bottom graph illustrates the composition of the low energy NuMI spectrum from the different hadron trajectory classes through the horns (107).

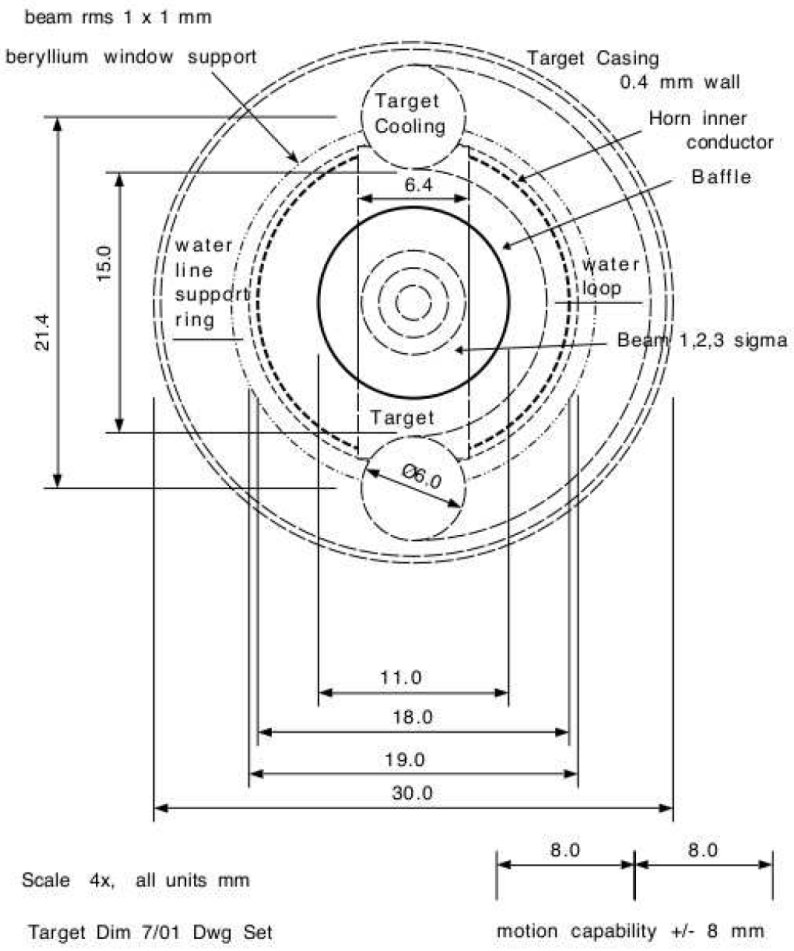

Figure 8: Beam's Eye View of the Baffle Inner Aperture. This figure shows what the proton beam sees as it travels through the NuMI baffle and hits the target. Superimposed on the diagram are the beam spot, the target fin, the horn neck, and the target cooling and support structure. All dimensions are in mm (107).

3.1.3 Beam performance

The NOvA detectors are located 0.84° off-axis from the NuMI beamline as opposed to the on-axis MINOS/MINERvA experiments. This choice was made due to the decay kinematics of pions and kaons in order to optimize sensitivity to the oscillation channel. In the rest frame, the mesons decay isotropically, producing mono-energetic neutrinos (Figure 9 and Figure 10). When boosted into the lab frame, the flux and energy of neutrinos produced from the meson decay in flight and measured at detector is relatively flat across a wide range of meson energies in small angles. For the selected detector angle of 0.84° the NuMI beam produces a relatively narrow flux peaked at 2 GeV with more events of that energy than

would be seen on-axis (see Figure 11 and Figure 12). This energy also maximizes the oscillation probability of electron-neutrino appearance in a muon-neutrino beam for our 810 km baseline. Moreover, the background for oscillation measurements coming from Neutral-current interactions is also considerably reduced by using the narrow off-axis beam, as well as ν_e contamination to the ν_μ flux.

After leaving the decay pipe, the beam travels mostly through the earth that protects the NOvA ND from all high energy hadronic products (including neutrons) much better than other current setups (105). The expected rate of neutrino-induced events in the ND is ~10^6 per year in the 0-3 GeV of neutrino kinetic energy and drops by two orders at 5-10 GeV and by two more in the region over 30 GeV. The model expectation for a viable LDM measurement is that the real event rate of χ - electron scattering drops off slower with kinetic energy and therefore, after the total data accumulation and the event type identification, the LDM signal to neutrino background will improve.

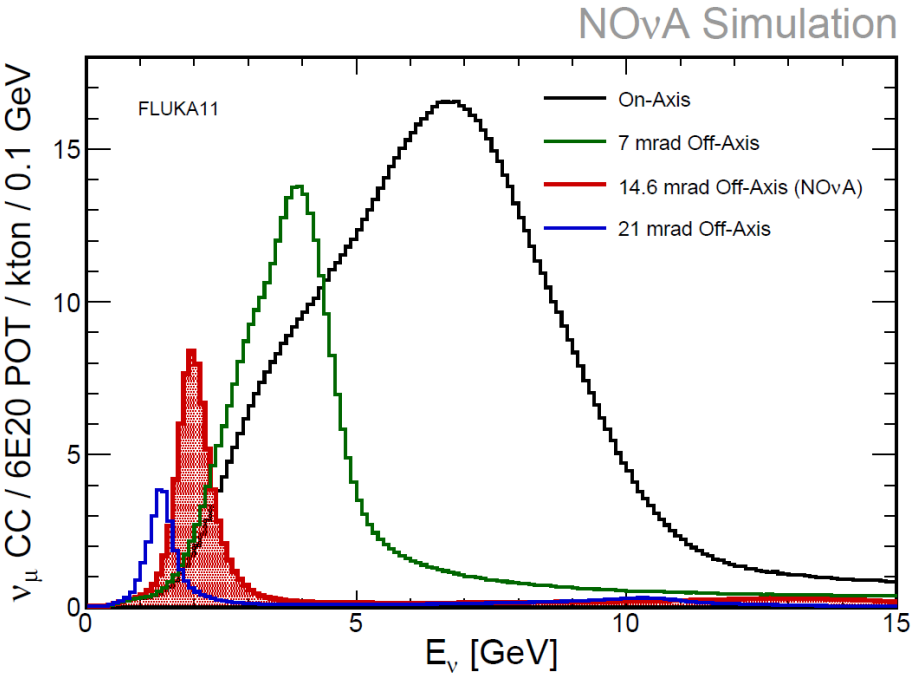

Figure 9: Simulated off-axis energy spectra with high energy tail suppressed.

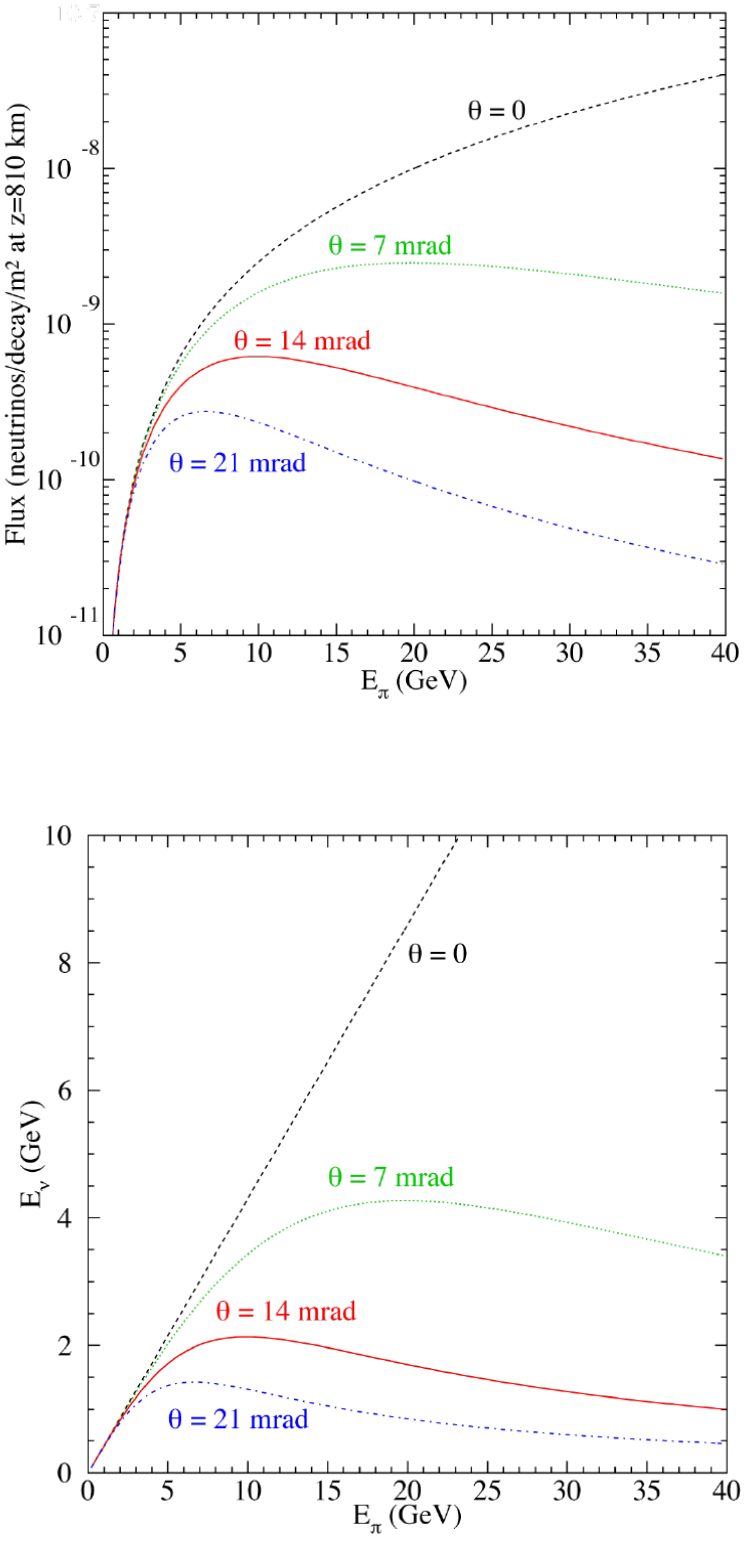

Figure 10: Neutrino flux and energy dependent on E_π and off-axis angle θ.

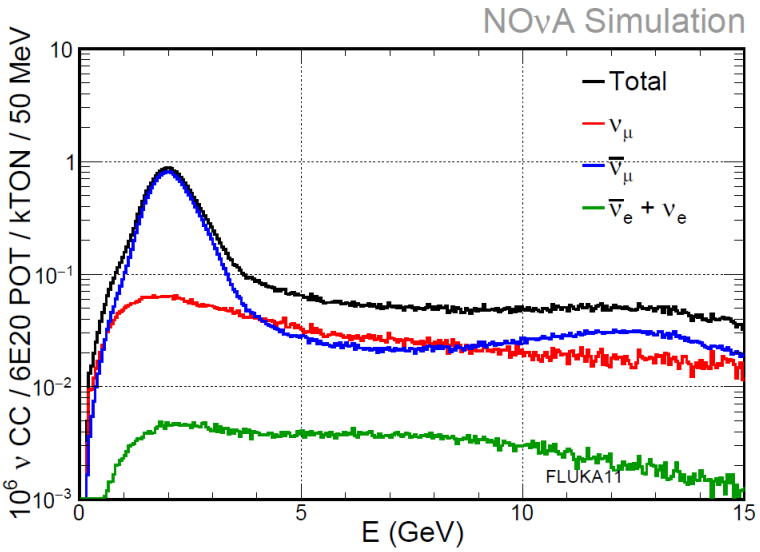

Event Rates	/ 6e20 POT	/ kton
Near Detector	(1-3)GeV	(0-120)GeV
Total	21.7	42.5
ν_μ	2.4	12.5
$\bar{\nu}_\mu$	19.2	28.9
$\nu_e+\bar{\nu}_e$	0.2	1.1
(1-3)GeV: $(\nu_e+\bar{\nu}_e)/\nu_\mu$	=	1%
(0-120)GeV: $(\nu_e+\bar{\nu}_e)/\nu_\mu$	=	3.8%

Figure 11: Simulated neutrino flux in reverse horn current (antineutrino) mode.

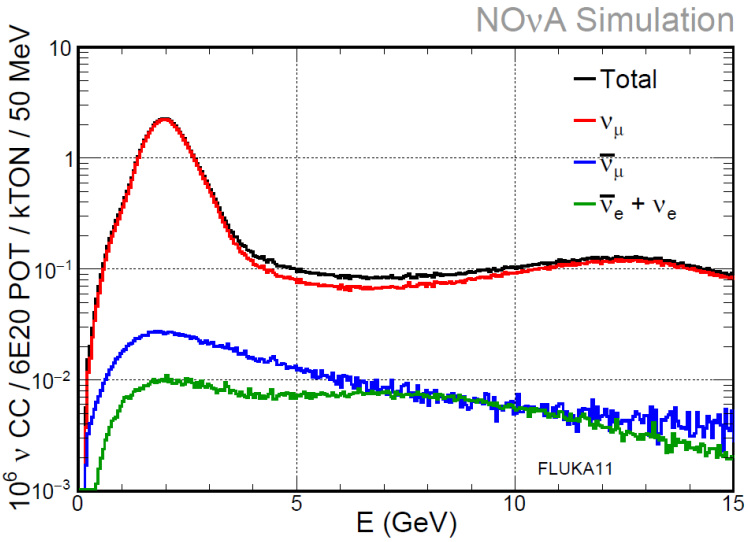

Event Rates	/ 6e20 POT	/ kton
Near Detector	(1-3)GeV	(0-120)GeV
Total	55.1	95.6
ν_μ	53.7	89.9
$\bar{\nu}_\mu$	1	3.7
$\nu_e+\bar{\nu}_e$	0.4	2.1
(1-3)GeV: $(\nu_e+\bar{\nu}_e)/\nu_\mu$	=	0.7%
(0-120)GeV: $(\nu_e+\bar{\nu}_e)/\nu_\mu$	=	2.3%

Figure 12: Simulated neutrino flux in NOvA ND in neutrino dominant mode.

3.1.4 Model examples of NuMI LDM production

Reinterpreting the NuMI source and the NOvA ND complex as a beam-dump experiment opens the door to searches of rare DM events without bias towards a particular model. For the popular example of the Vector Portal, the mass of a directly produced vector mediator particle *V* (Dark Photon) may take any value up to the maximum available of 15 GeV from the 120 GeV of the proton beam incident on the carbon target. I consider the simplest scenario of Dark Photon *V* decaying into a pair of identical LDM particles $\chi\chi^{\dagger}$. The studies with the NOvA ND on LDM masses (m_{χ}) can extend from few MeV up to 7.5 GeV.

Such large range of LDM masses cannot be accessed by direct detection experiments as they have a cut-off above 10 GeV (110) (111). It also cannot be studied by other current fixed target neutrino experiments with lower proton beam energy (99) (101) (103) (105). The low mass boundary on the other hand is set to be around 6.9 MeV, as that's the heaviest scenario excluded by results from experiment Planck (15). In contrary to charged mesons for neutrino production, the LDM flux is not affected by the configuration of magnetic focusing system (horns) described in Chapter 3.1.2, so the same signal channel can be used for both neutrino and antineutrino NOvA run with only the background changing.

In order to illustrate the NOvA ND sensitivity, I have simulated a subcategory of the above example of LDM using the PYTHIA framework (112). The initial samples were focusing on heavier *V* ($m_V = 1\ \mathrm{eV}$) decaying to an identical pair of χ of various masses. The spectra of signal events can be simply scaled based on the choice of mixing and coupling parameters ϵ, α_D. In later studies, I shifted to a fixed ratio of $3m_{\chi} = m_V$ and sampled mass cases of m_{χ}: 10 MeV to 500 MeV, where NOvA has the most competitive sensitivity (14). Eventually I chose one representative fixed model of $m_{\chi} = 30\ \mathrm{MeV}$, $m_V = 90\ \mathrm{MeV}$ for the hypothesis proofing in my analysis.

The angular and energy distributions of LDM particles leaving the target area can be seen in Figure 13 and Figure 14 for three mass cases (150 MeV, 300 MeV and 450 MeV), scaled to the distribution integral. This preserves the relative rate per unit of polar angle θ (i.e. away from the beam direction) for the different mass cases of LDM. It is safe to assume a uniform distribution around the azimuthal angle φ (i.e. around the direction of the beam). Superimposed on the plot is a

reproduction from (113). It corresponds to an analytical calculation of the 300 MeV mass case and is scaled here to the integral area, as the absolute normalization attempted in (113) is not relevant here. This reproduction is used as a validation of the simulation of this study against the detailed estimation from the Vector Portal model. The two angular distributions agree well in the range of small forward angles that are more interesting for the NOvA measurement. The effect strengthens the argument that further information can be drawn from the simulation of the behavior of LDM in the NOvA ND without more complicated analytical calculations that require stricter commitment to models in order for the calculations to be manageable. More details about such simulation are given in Chapter 5.

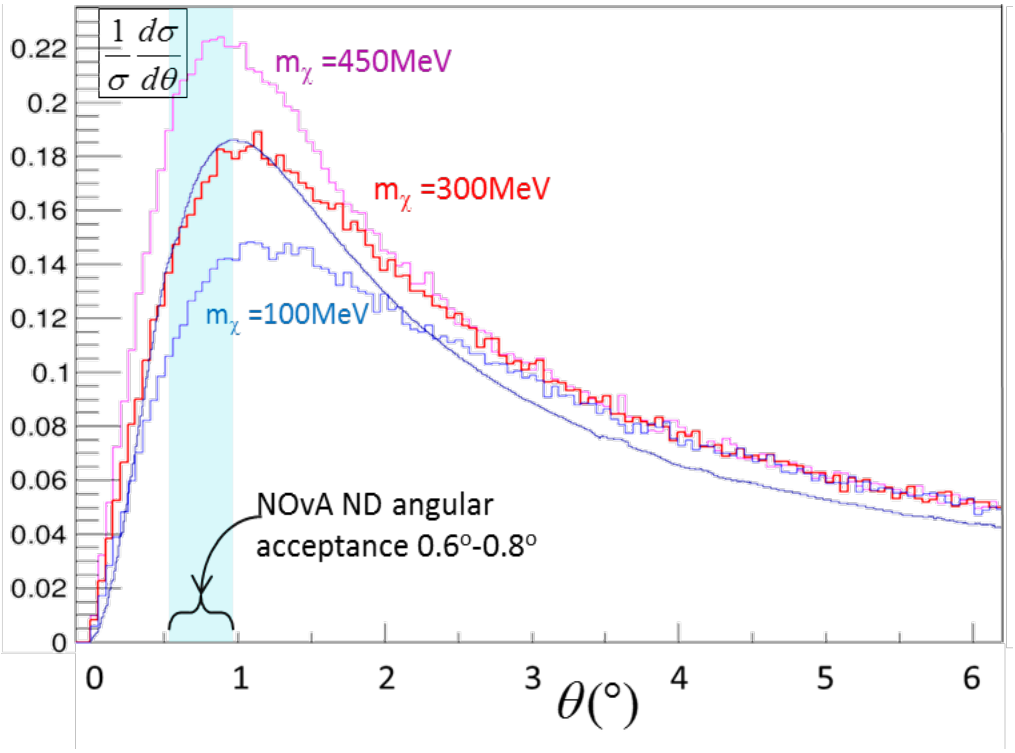

Figure 13: The target-LDM normalized angular distributions with 1GeV parent *V* mediator and several mass cases to compare with calculations from ref. (113). The *V* decay into χ was simulated using PYTHIA 8.244 and the simulation shows good agreement with the analytical prediction from ref. (113) and showcases the kinematic differences between various mass scenarios.

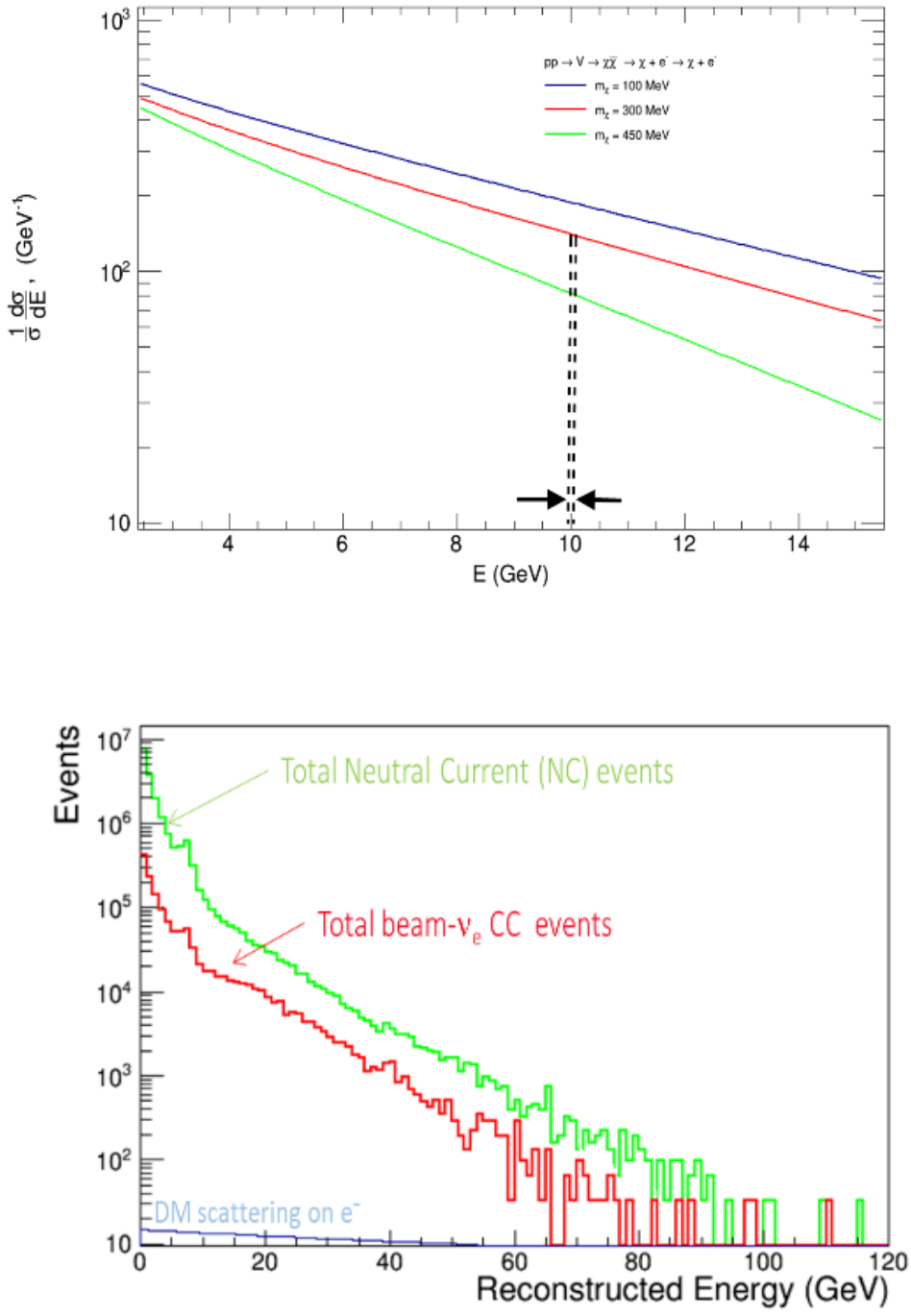

Figure 14: Calculated EM-shower energy spectra from LDM candidates scattered off an electron (top) from predictions in (113) and simulation of the two prominent neutrino interaction spectra resulting in EM-shower inside the NOvA ND (normalized to 1 year of running).

3.2 NOvA detectors

To minimize the systematic uncertainties in the neutrino oscillation analysis, the functional design of both Far and Near NOvA detectors is essentially identical. The detectors consist of long plastic tubes, filled with liquid scintillator and are read out by APDs in x/y views to form a 3D calorimeter. The Near Detector, close to the very intensive particle source, can be reinterpreted as a stand-alone beam dump experiment. Here we briefly describe components of the NOvA detectors; more detailed information can be found in the NOvA Technical Design Report (94).

3.2.1 PVC cells and modules

The NOvA detectors are composed of PVC modules extruded to form tube-like cells with rectangular cross-section (4 × 6 cm). A layer of cells forms one plane of the detector. The cells in adjacent planes are orthogonally rotated with respect to one another to allow for 3-D reconstruction of particle positions. There are 384 cells per plane in the FD, and 96 in ND (12 modules versus 3 modules).

Each cell is filled with the liquid scintillator and there is a loop of optical wavelength-shifting (WLS) fiber to catch the scintillation light (see Figure 15). The light from 32 such cells is read out by 32 pixels of an Avalanche Photo Diode chip. The cells inner dimensions are 3.6 cm and 5.6 cm. This defines the granularity of the NOvA detectors. A cell is 15.5 m long in the FD and 4 m long in the ND. These long fiber lengths mean that light attenuation is a significant effect in NOvA.

The structural elements of the NOvA detector and primary containment for the liquid scintillator are the PVC modules, almost 30% of the total NOvA detector mass. The high light-yield of NOvA is in part due to the reflectivity of the module material, which is boosted substantially by adding titanium dioxide (TiO_2) to the PVC. The reflectivity attained in this manner is about 90% at the peak wavelength of scintillator emission (430 nm).

The shape of the PVC extrusions is optimized for easy and reliable extrusion, minimum PVC stress and light reflectivity. The outer extrusion walls are 4.8 mm thick and the inner walls between cells are 3.3 mm thick. The outer wall of the modules and the cell corners are rounded for easier extrusion and less structural stress. The PVC extrusions were extruded in groups of 16 cells, later glued together to form a 32-cell module, sealed and strung with optical fiber. The two

fiber ends from each of the 32 cells are embedded into the grooves of the fiber raceways. The raceway routes the fiber ends to the optical connector that contains 32 holes through which the fiber ends are threaded. Each of the holes on the connector maps to a single channel on the APD. The top of the module is sealed with the manifold cover and the snout with the optical connector and a support for the APD and FEB. It also contains a port for filling the module with scintillator and another for ventilation.

The radiation length for an electromagnetic shower in liquid scintillator is 41 cm with a Moliere radius of 10.5 cm and the mean free path for photon conversion of 53 cm. The most competitive features of this design – the low-Z, fine-grained detector placed off-axis – are optimal for muon track and EM shower reconstruction, allowing typical electron showers in the signal region to traverse 10-80 planes and photons travel an order of 6 planes before converting.

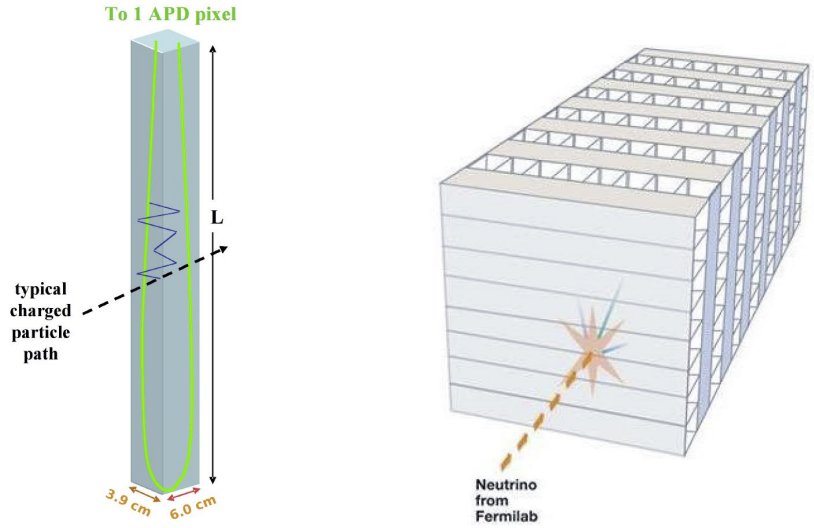

Figure 15: Schematic of a NOvA cell and the orthogonal cell arrangement.

3.2.2 Scintillator and fiber

The cells are filled with a liquid scintillator, a solution of 94.63% mineral oil, 5.23% pseudocumene (scintillator, 1,2,4- Trimethylbenzene), 0.14% PPO (WLS, 2,5-Diphenyloxazole), 0.0016% bis-MSB (WLS, 1,4-bis-(o-methyl-styryl-)-benzene), 0.001% Stadis-425 (anti-static), and 0.001% Vitamin E (anti-oxidant) (114). This mixture produces scintillation light in the near ultraviolet and shifts it to the

visible region of 380-450 nm. The liquid scintillator makes 65% of NOvA detectors total mass.

Within each cell a double-clad Kuraray WLS fiber is looped down the entire cell length in a U shape. The fiber absorbs light in the violet-blue range and emits in the blue-green (450-600 nm) range. The fiber is 0.7mm thin in order to withstand the end turn of 3cm bending radius. Both ends of the fiber are read out by a single pixel of the APD photodetector, this improves light collection efficiency.

3.2.3 APD

APDs are photo-sensitive avalanche diodes that are operated with a high reverse bias voltage. Under such conditions, the electron and hole pairs excited by photons are accelerated in the strong intrinsic electric field. As these highly energetic electrons move, they strike other electrons and cause them to be freed. These secondary electrons and holes are themselves accelerated and strike more electrons free and so on. This process is called impact-ionization and an avalanche of charge carriers in the diode leads to a significant amplification of the photocurrent.

APDs were favored over Photomultiplier Tubes (PMT) for light detection in NOvA because the quantum efficiency of APDs (85%) is about eight times higher than that for PMTs (10–20%) and is much flatter over the range of wavelengths of light that NOvA WLS fiber transmits (500-550 nm). The high quantum efficiency of APDs is a necessity for NOvA because it allows the observation of faint light signal from the end of 15 m long modules in the FD. The APDs used by NOvA are manufactured by Hamamatsu and have a custom design to accommodate two ends of the fiber loop per cell on a single pixel (Hamamatsu S11211 based on commercial S8550 APD). Each NOvA APD array consists of 32 pixels, where each 1×2mm pixel reads out a single cell.

For APDs to effectively detect signal from the far end in a 15 m long cell, the noise must be kept at low level. To minimize the dark current, APDs are operated at a temperature of -15 °C. Each APD carries its own thermoelectric cooler (TEC) to maintain this operational temperature. To remove heat from the TECs, a water-cooling system has been designed which circulates water chilled to 15 °C. The APD surface must be kept clean and dry for safe operation and to minimize surface currents. To achieve this, the surface of the APD is treated with parylene coating,

a transparent epoxy, and it is ventilated with dry-air to prevent humidity condensation.

The APDs are operated at high voltage close to 425 V, which produces a gain of about a 100. The operational conditions have been designed and demonstrated to produce a signal to noise ratio of 10:1 or better for majority of the APDs. The APDs run continuously without any external triggering. The signal received from each APD pixel is further amplified through individual integrated custom circuits. After amplification and pulse-shaping, the signal from eight cells is multiplexed into an ADC. The APD, and all the other components described here are mounted on a front-end board (FEB, seeFigure 16), digitizing the signal and providing voltage and cooling.

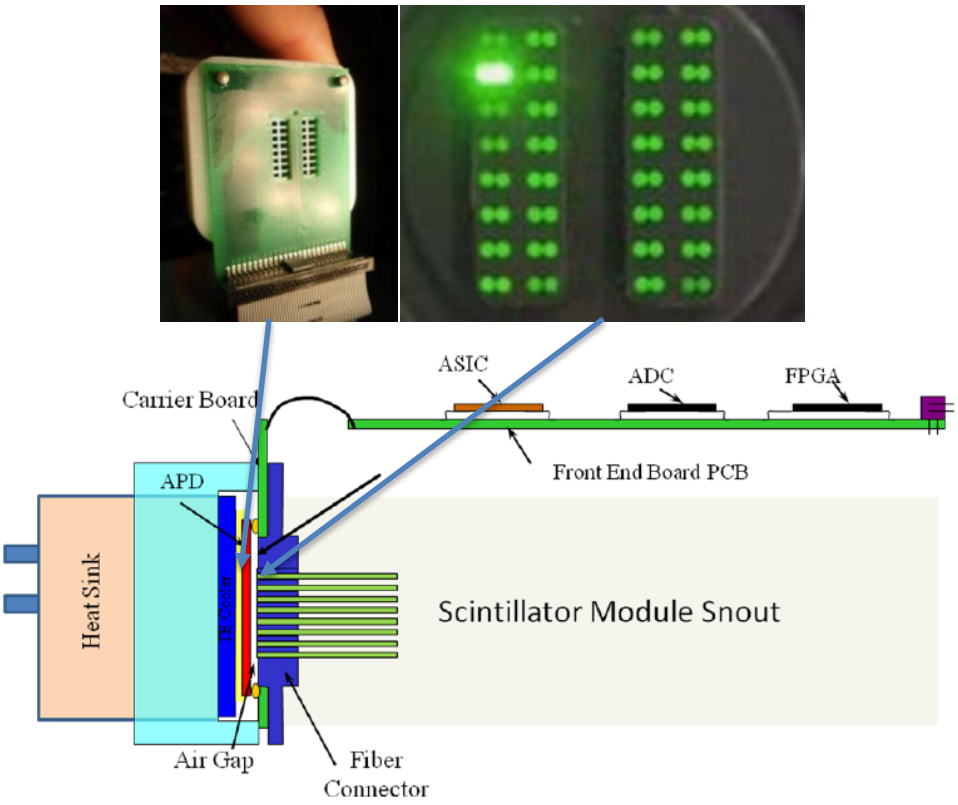

Figure 16: Schematic of APD with FEB and photos of APD and optical contact.

3.2.4 Far Detector

The NOvA Far Detector (FD) is truly a remarkable machine, but since the focus of this work is on ND, I only describe it very briefly.

The FD is located in Ash River, Minnesota, 810 kilometers from the NuMI target at Fermilab at an angle of 0.84° (14.6 milliradians) off the beam axis. The detector hall is located on the surface and uses a cosmic-ray shield made of concrete and loose barite rocks, shielding effectively 14 radiation lengths. The detector dimensions are 15.6 × 15.6 × 60 meters and it has 344 064 individual channels in 896 alternating planes and a total detector mass of 13 968 tons (115). The detector was constructed in 28 blocks, each consisting of 32 planes glued together. The electronics were instrumented in 64-plane sections called diblocks, with 12 Data Concentrator Modules (DCM) at each, containing 64 FEBs per DCM.

The detector was constructed and instrumented modularly in diblocks, which allowed data to be collected with a partial detector.

3.2.5 Near Detector

The NOvA Near Detector is located 100 meters underground at Fermilab, one kilometer downstream of the NuMI target. The kilometer of earth, which separates the NuMI target from the NOvA ND, protects it from any kind of products from the interactions at the target, besides the neutrinos and whatever other rarely-interacting LDM particles which may be produced. The detector is built using the same modules as the Far Detector but only 4.1 m in length. The detector is 15.9 meters long, divided into a 12.8m active region followed by a 3.1m muon catcher at the downstream end as shown in Figure 17. The Near Detector total weight is 290 t of which 130 t is scintillator, 78 t is the muon catcher steel and 82 tons are the PVC modules (116).

The active region consists of 192 planes, each 4.1× 4.1 m with three 32-cell modules (96 cells per layer). The active region electronics are instrumented in three 64 plane diblocks. Each diblock has two DCMs for the vertical planes and two for the horizontal planes. One DCM in each view is fully occupied with 64 FEBs and the other has 32 FEBs.

The muon catcher has 22 standard PVC planes and 10 steel plates interspersing with the scintillation planes in order to stop muons and to improve containment. The steel plates are recycled from the NOvA prototype detector (NDOS), each plate about 10 centimeters thick. The prototype had different dimensions and so the steel plates are 4.1 × 2.7 m, or two-thirds the height of the active region. The horizontal modules have the same dimensions as the active region with planes

consisting of two modules totaling 64 cells. The vertical modules are reduced to 2.7 meters in length with three modules per plane totaling 96 cells. The muon catcher region is a repeated sequence of horizontal plane, steel, vertical plane and uses one DCM for the vertical modules and one for the horizontal.

This attribute of the NOvA technology promotes ideas for new particle searches at the short baseline (i.e. between the NuMI source and the NOvA ND complex). Such searches study LDM signatures involving single electrons in the final state. Any LDM induced events would be very rare compared to the 6-order of magnitude more charger current (CC) neutrino interactions on nucleons, or the 4-orders of magnitude higher-rate NC interactions that are the dominant interactions within the NOvA ND.

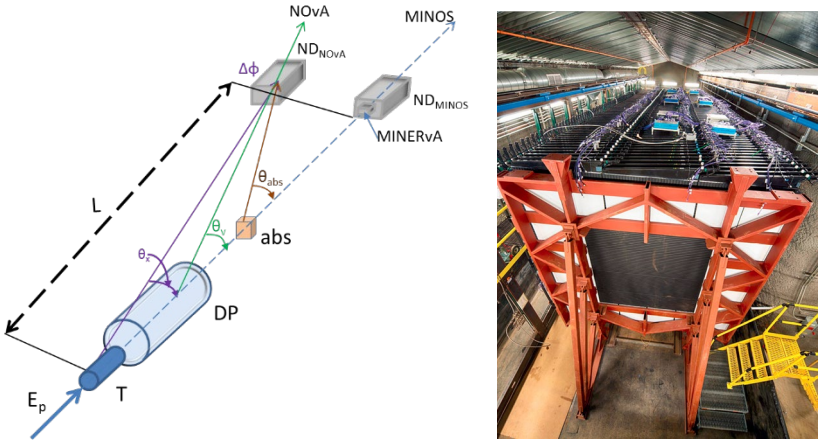

Figure 17: Schematic of the NOvA ND geometry and angular acceptance with the NuMI beam cascade and a picture of the ND underground.

3.2.6 Data Acquisition

A group of up to 64 FEBs send hits above threshold to a data concentrator module (DCM). The DCM collects hit information from its readout region and condenses the data in 50 microsecond blocks (microslice) that the DCM uses to build a larger 5 millisecond block (millislice). The DCMs transfer data to a buffer farm at a rate of 24 Mb/s in the form of millislices. All hits that are above threshold are digitized and stored in the buffer farm for up to 20 minutes before being erased from memory unless a trigger decision is made (Figure 18). Signals from the accelerator indicating the time of a beam spill arrive and start the readout of microslices from the buffer in the selected time range to create an event record that is saved for

permanent processing. While data is in the buffer it is processed through a series of fast algorithms that can trigger the recording of additional blocks of time that meet selection criteria. This data-driven trigger approach is used for exotic searches such as magnetic monopoles, supernova neutrinos and indirect dark matter. The DAQ is a very robust and complex system, its detailed description is beyond the scope of this study and can be seen in (117).

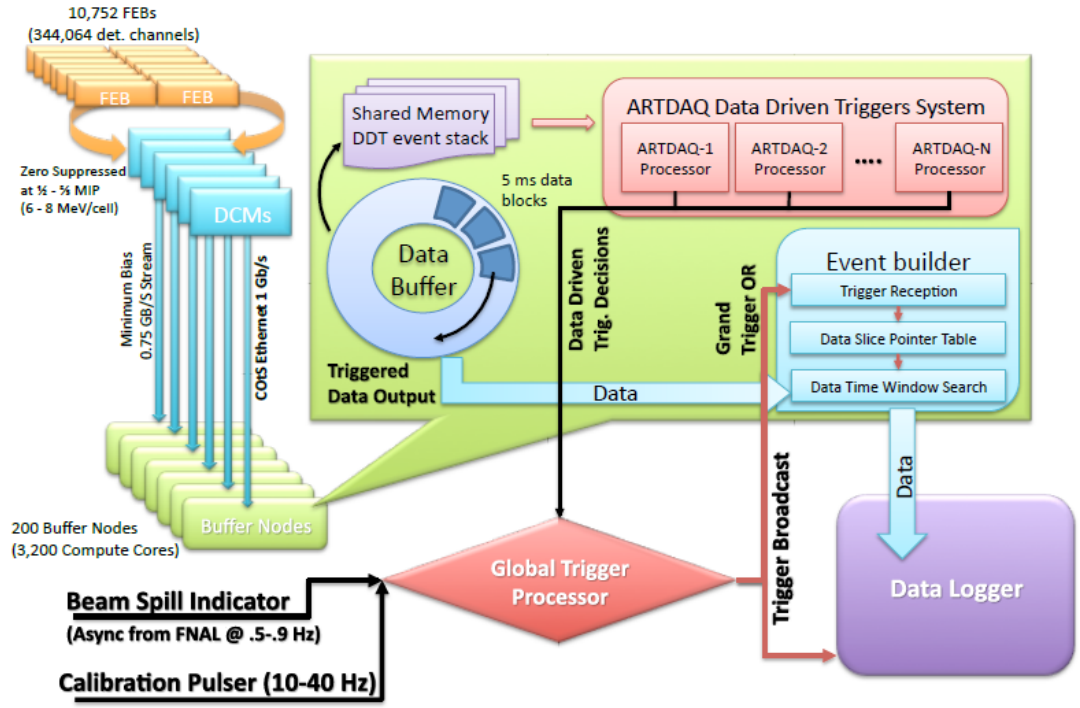

Figure 18: The NOvA DAQ structure schematic (170).

3.2.7 Detector Control Systems

The systems which handle the electronics voltages, the cooling, dry air, the environmental and status monitoring and overall care of suitable conditions for APD to take data, are grouped to the Detector Control System (DCS) sometimes also titled “slow controls”.

The DCS can be divided into two branches – the active detector control, i.e. APD voltage settings and cooling enabling, and strict monitoring of overall status of any subsystem or part of the detector. Similar to DAQ, the sensors, readout, and the backend of the system run locally at each detector and the handling and settings is done from computers at NOvA Control Room using the EPICS communication application (designed originally at the Argonne laboratory)

controlled by the CSS SW (Control Systems Studio designed by Oak Ridge Laboratory) or Fermilab's custom Acceleratior Controls NETwork (ACNET) systems Synoptic SW, reading data from Fermilab-proprietary ACNET network.

The environmental monitoring (temperature, humidity, dew point, rack interlock status, air flow) and the underground surveillance camera system were among my service tasks (tasks with marginal scientific potential) and the description of the subsystems is summarized in my thesis study report (1).

3.3 Monte Carlo Simulation

Monte Carlo simulation (MC) is a crucial part of modern particle experiments. Here I describe the parts of the simulation chain for the main NOvA ν_e analysis and the LDM generator architecture and how it interconnects with the general simulation train. The usual simulation sequence is FLUGG – GENIE – GEANT. My LDM analysis uses PYTHIA to skip the NuMI beam processes and the transportation code, and plugs directly into the GEANT simulation inside the detector.

3.3.1 Neutrino Beam MC

The Monte Carlo simulation for the NOvA experiment starts with the hadron processes in the NuMI beamline. The beam simulation is carried out in FLUGG package, which is a combination of FLUKA (118) for simulating particle interactions and decays, and GEANT4 (119) to simulate the environment and geometry in which the particles interact. An alternative simulation for beam propagation is based done using only Geant4 (G4NuMI package), which then uses the same GEANT geometries. The GEANT geometry includes the carbon target (graphite) and relevant target hall elements, the focusing horns and decay pipe. FLUKA (or Geant4 alternatively) simulates hadron production in the NuMI target and tracks them until they decay into neutrinos or are absorbed downstream in the hadron monitors (120).

The resulting flux files consist of neutrinos and their flavor, energy and momentum at the point of occurrence (from a parent particle). The kinetic properties of the neutrino parents are also stored in the flux files and can later be used for generating the neutrinos interacting in a detector. The availability of the parent information is useful for reweighting and assessing beam related

systematic errors (see further in Chapter 5.2). Both neutrino and antineutrino flux files are created using this method.

3.3.2 Detector interactions MC

The FLUKA generated flux files are read by the GENIE event generator, which simulates the neutrino beam interactions in the detector environment (121), using modified Bodek and Ritchie version of the Relativistic Fermi Gas. GENIE uses the flux and the total cross-section model to calculate the energies of the neutrinos that will interact and categorizes the interaction type, based on the interaction-specific cross-section models (quasi-elastic, deep inelastic etc.) and then the differential cross-section models to produce the final state kinematics. The type and properties of the final state particles are determined by the hadronization model. GENIE also uses an INTRANUKE package to simulate the interactions of final state hadrons inside the nucleus. The final state interaction (FSI) rates are derived from the free hadron cross-sections and the nucleon density. The measurements of those parameters are very challenging and there are large uncertainties in the models, which directly impact the observed neutrino energy in experiments.

The geometry of the detectors, detector hall, cavern and the surrounding earth is encoded in GDML (CERN Geometry Description Markup Language). After the secondary particles are created by a generator, their propagation, energy loss or decays in the NOvA detector are treated again by GEANT4 (119), simulating particle propagation step-by-step. The physics processes and models are decided based on the Physics List. NOvA uses the QGSP_BERT_HP list. This list consists of quark-gluon string model for high-energy hadrons with Bertini cascade model for hadrons with energy bellow 10 GeV. Thermal neutrons (<20 MeV) are accurately tracked with high-precision (HP) neutron model.

Cosmic ray background in NOvA is simulated separately, using the CRY (Cosmic RaY generator) package (122). It generates cosmic ray particles mainly between 1 GeV and 100 TeV and secondary cosmics between 1 MeV to 100 TeV and produces separate flux files (which can be overlaid with neutrino files) at the detector. These flux files are then fed into GEANT for tracking and readout simulation.

3.3.3 Readout simulation

GEANT yields energy depositions that must be transformed into photons that scatter, reflect and are absorbed in the optical fiber. A custom tracing algorithm has been developed to compute the expected light collection rate a priori (PhotonTransport package). It uses the measured scintillator response, the reflectivity of the PVC and the measured absorption spectrum of the optical fiber. All cells in a detector are treated equally at this stage, since all cell to cell variations in scintillator and fiber response are considered evened out during calibration.

Each end of the fiber loop gets half the captured light. The light loss in the fiber is simulated according to the average light attenuation measured in the fiber during detector construction. At this step, different cells in each module are treated differently, as the length of the fiber in the manifold is dependent on the cell position along the module.

Another custom package (ReadoutSim) models the APD to have a flat 85% quantum efficiency and a gain of 100 with 5% variation. The photo-electron (PE) pulse is shaped and smeared in time. The shaped pulse is distorted to simulate current and voltage variations (123) and converted in ADC based on a pre-determined PE to ADC conversion factor from charge-injection studies.

The baseline is determined from pedestal runs data and clock-ticks simulated to finally arrive at the ADC. A hit is registered if the ADC value is above the threshold for given cell. Threshold distribution is obtained from data from both Far and Near detectors and randomly sampled for simulation. For cells that have physics hits in them, the ADC trace is simulated for the full 500 μs window. We also insert noise in cells with no physics hits in them. The noise rate and ADC distribution are derived from pedestal scan data from both NOvA Far and Near detectors.

There is a number of additional improvements to the simulation chain, i.e. correction on the scintillator degradation, the APD sag, the mass variation, diblock and channel masking etc. They are important for an optimization of prediction of the background events in the detector, their detailed description is given in Chapter 55. There are also some precise simulation techniques developed, which were not implemented in the earlier main analysis runs and we omit them here (i.e. Čerenkov light simulation). The final output of the whole simulation is a ROOT

file of format identical to that of recorded data, with additional truth parameters to be used in downstream reconstruction (123).

3.3.4 Dark Matter generator

In case of Lightweight Dark Matter simulation, the first two tiers of NOvA Monte Carlo are bypassed. Instead, I use PYTHIA simulation framework (112) for generating a simple LDM beam, resulting in χ particles scattering of electrons inside the NOvA near detector. A text file of these very forward-going electrons in HEPEVT format can then be manually fed into the detector GEANT tier directly to create raw signal files. These files can be treated regularly with the mainstream NOvA reconstruction and analysis tools described in following chapter. More details on the LDM simulation in NOvA ND are given in Chapter 5.

4 Reconstruction

To reconstruct tracks and events from hits (a signal above threshold in a cell) in our detector, a sophisticated chain of methods is implemented in NOvA software. From the charge deposit in the cells, we can reconstruct the energy and clusters and trajectories of the particles.

Different types of interactions use special reconstruction methods. The difference can be demonstrated on the presence or absence of a muon in the event (2) (3). The LDM search focuses on the χ particle mimicking neutrino scattering on an electron, which has the same signature for any flavor neutrino NC scattering and ν_e CC scattering – forward going single EM shower.

4.1 Detector calibration

NOvA detectors are calorimetric and many reconstruction tools in NOvA software rely on information about *dE/dx*, so for correct reconstruction to be performed, the light signal from the detector must be translated to energy deposition. We first calibrate the hits relatively (time and position) and then perform absolute energy calibration. As an input, the output from DAQ or Monte Carlo simulation (MC) is used – which are hits above threshold in a detector cell (charge collected in an APD pixel).

The energy calibration of the NOvA detectors treats mainly the attenuation and aging of the detector and the absolute conversion of energy deposition recorded by the APDs into physical units of GeV (124) (125). Both relative and absolute energy calibration phases are done using muons – a selection of cosmic ray muons for FD and rock-muons (muons created in interactions of muon-neutrinos in rock surrounding the underground detector) for ND, which can provide a source of uniform energy deposition across the detector for the relative calibration and with stopping muons the Bethe-Bloch formula can be applied to precisely calculate the energy deposited in a cell.

4.1.1 Attenuation and relative calibration

The goal of relative calibration is to ensure uniform detector response in time and space - any two "calibrated hits" of same intensity anywhere in the detector occurring at any time must represent same energy deposition. Differences of the

recorded signal come mostly from the attenuation of light in the wavelength shifting (WLS) fiber, threshold effect and self-shielding.

First, the correction for threshold and self-shielding is evaluated. To record a hit, the APDs have a threshold (43 ADC hits), and also, in some cases, the energy deposition is so low that it doesn't create enough photons to reach the APD, therefore the final distribution of photoelectrons in the APD is shifted to higher values. Furthermore, when the muons travel through the detector, their energy distribution change in different depth of the detector and thus further affect the number of hits below the APD threshold. These effects are growing with the detector size, so for ND its less crucial, but up to 30% correction due to hits below threshold must be applied in FD calibration. Threshold and shielding effects are corrected based on the comparison with the MC bias (simulation-based calibration).

Since path-length calculation on a cell-by-cell basis can be difficult due to reconstruction effects, the calibration uses tri-cells, when the neighbor cells on both sides in the same plane also have energy depositions. These criteria allow for more precise calculation of the path length W inside a cell and thus dE/dx. The APD signal (photoelectrons PE) is created after the photons created in particle interactions in the scintillator are collected and transferred through the WLS fiber. The fiber creates a loop (30 meters for FD and 8m for ND) in a cell and photons may scatter or be absorbed before reaching the APD pixel at the ends of the fiber. To correct the effect of light attenuation in the WLS fiber, a non-parametric algorithm LOWESS (Locally weighted scatter plot smoothing) is applied for every cell (126). Statistics are accumulated for each cell in a calibration period and an attenuation curve is fit, shown for a FD example in Figure 19, such that an energy deposition at any location in any cell can be expressed in a consistent metric of calibrated photoelectrons (127).

4.1.2 Drift

NOvA detectors are running continuously for many years and their light output is not constant and drifts over time. Aging effects are corrected for by monitoring the mean response in a cell over time and correcting back to the calibration period. This may include aging of the scintillator, variations of temperatures, changes in the APD gain settings and other changes in the electronics. Similar to

the attenuation, the "standard candle" for drift calibration is through-going muon. The resulting drift correction is applied at the FEB level. This calibration component is currently very small, but it has been developed to be applied for long run analyses.

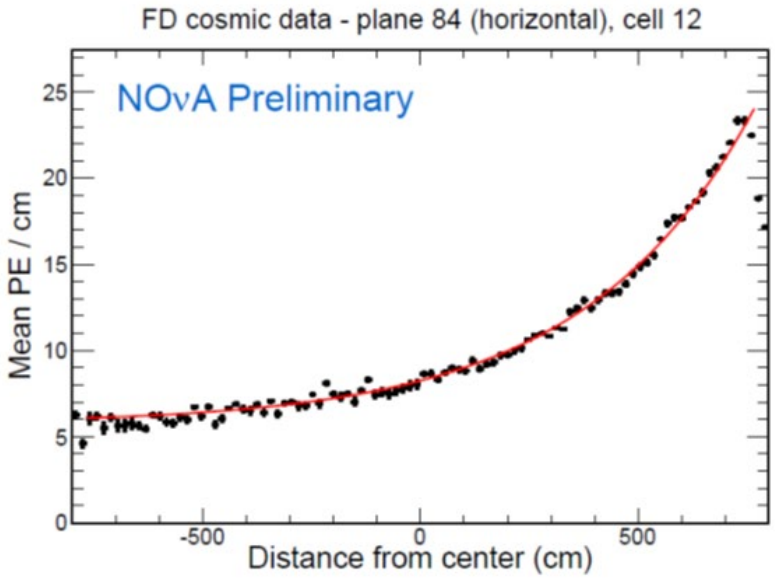

Figure 19: NOvA cell distance attenuation with a calibration curve fitted.

4.1.3 Absolute energy calibration

After the relative corrections have been applied, muons stopping inside of the detectors are selected to perform the absolute energy calibration (Figure 20). Tri-cell hits between 100 and 200 cm away from the well-defined (with Michel electron) end of a muon track, where the *dE/dx* is relatively constant, are selected and the average charge per centimeter is calculated for that region. This measurement is done in data and Monte Carlo that has been tuned to match the data in units of calibrated photoelectrons, further scaled to GeV units using the *dE/dx* MC truth for both detectors. That concludes the energy calibration procedure (128).

4.1.4 Timing

Because NOvA uses a pulsed beam (10 us every ~1.33s), the hits recorded in the detectors must be well synchronized. So, besides the energy calibration stack, the reconstruction also needs correct timing calibration, which also consists of relative and absolute parts and is mainly done in two steps – the DCM timing offset and the timing resolution determination. Again, through-going muons are

used for this purpose and a DCM offset matrix is used to correctly center the hits. The ND timing resolution is 5 ns and the FD resolution is 10 ns. More information about the timing system and its calibration can be found in (129) (130).

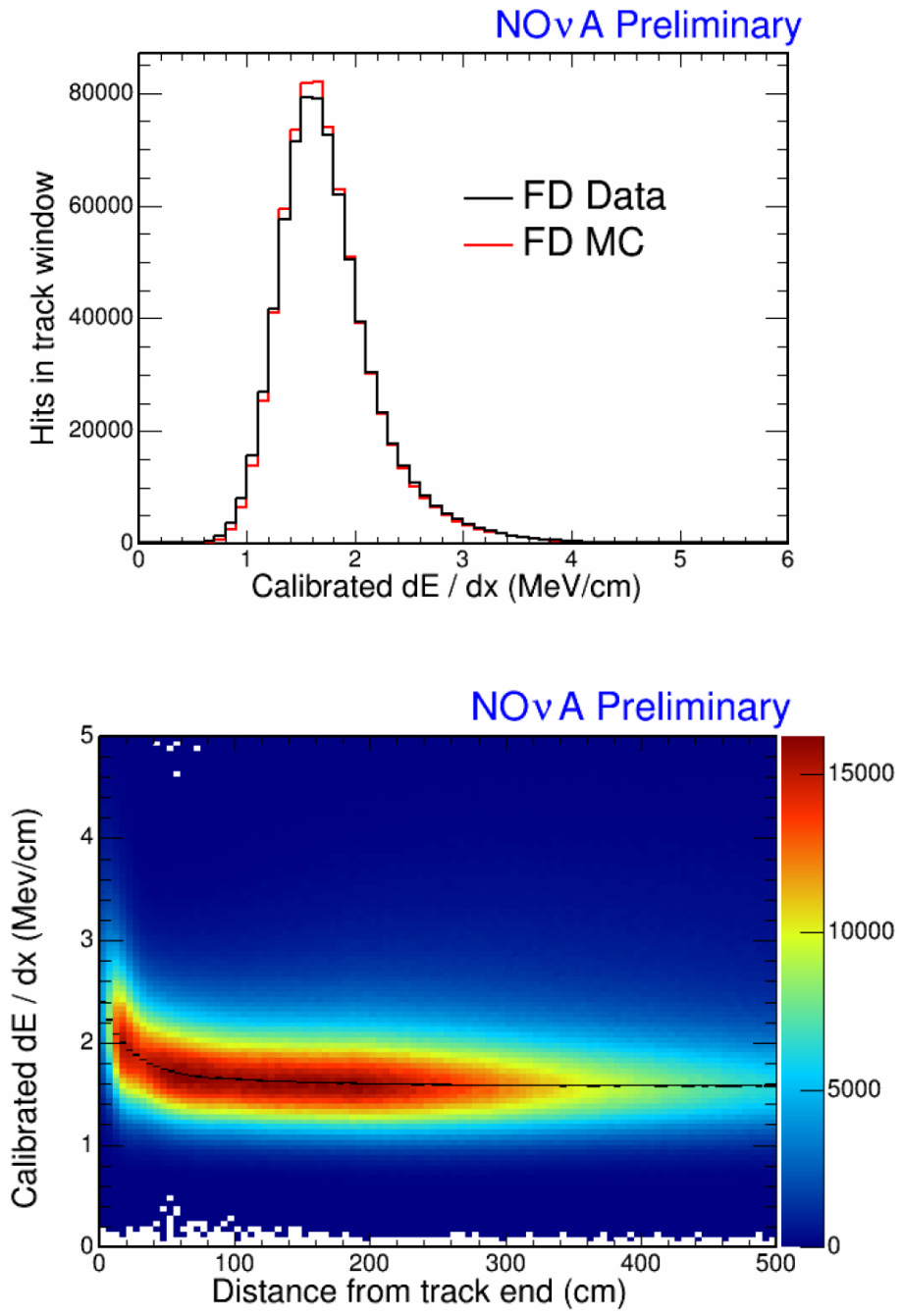

Figure 20: (Top) Calibrated *dE/dx* distributions of tricell hits. (Bottom) Distance to the end of the muon track vs. calibrated *dE/dx* with mean fit in black.

4.2 Event reconstruction tools

The goal of our reconstruction sequence is to find an electromagnetic shower caused by neutral particle (neutrino or LDM candidate) from the beam, therefore, here I focus on the methods used in NC and *ν+e* reconstruction chains (with some marginal and specific methods omitted). The reconstruction progress is outline in Figure 21.

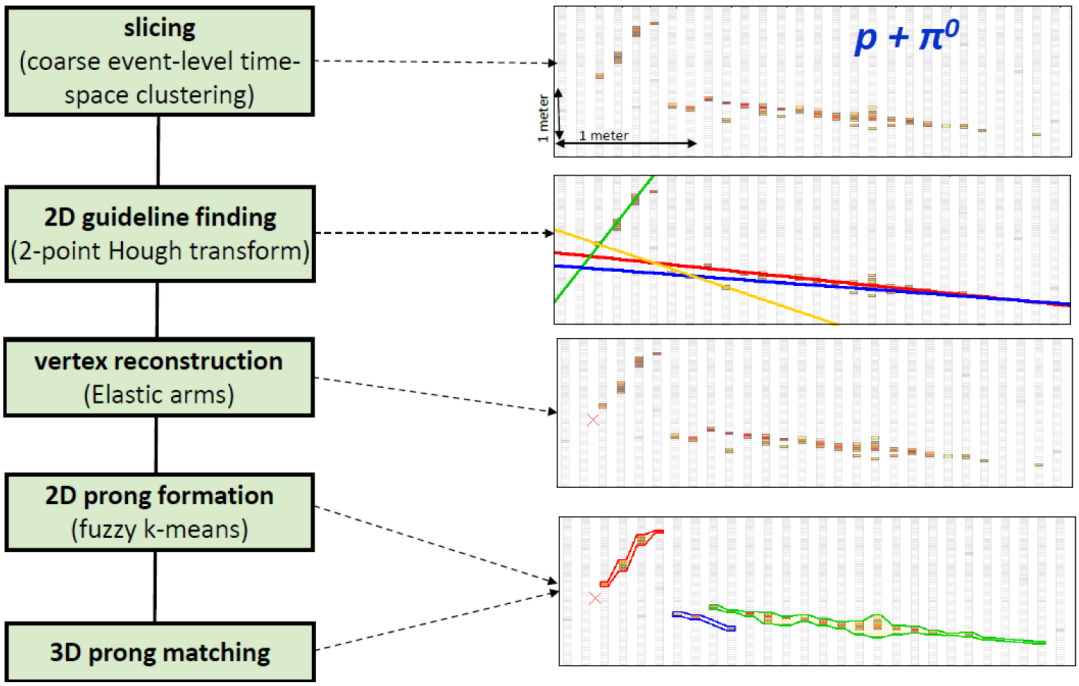

Figure 21: NOvA event reconstruction chain.

4.2.1 Slicing

The slicing method is based on the DBSCAN (Density-Based Spatial Clustering of Application with Noise) algorithm (131) which groups together points that are closely packed in some parameter space, marking points that stand in low density regions as noise. In the DBSCAN algorithm, if a point sees more than a certain minimum number of points within a set distance from itself, it is considered to be a core-point; the points within its neighborhood are its neighbors and are said to be directly reachable from core point. The points on the edges of clusters do not have the minimum number of hits in their neighborhood but are neighbors of core-points and are known as border points. A border point is reachable from a core point if all the points that connect cores with neighbors are directly reachable

from core (so they are core-points themselves). Points that belong to neither of these categories are loners and are treated as noise.

Clustering begins by scanning all points and calculating the number of points in their neighborhoods. If a core-point is found, a cluster is formed by finding all the points that are directly reachable from the seed point. The expansion of the cluster terminates when all the branches end in a border point. The algorithm then returns to the original list of points and finds the next core-point that is not yet assigned to a cluster. The requirement from the slicer is that each slice should contain a single interaction and it should contain it as a whole.

4.2.2 Hough transformation

The next step in the reconstruction chain is to identify guidelines that represent features in a slice for which a modified Hough Transform is used (132). In this algorithm, lines are parameterized in a polar space to also treat vertical lines. The lines are fit separately in the XZ and YZ views, storing the results in separate Hough space for each view. The line passing through each pair of points in the slice is recorded with a Gaussian smear vote with some restriction on minimum distance. The algorithm is iterative, removing the selected hits and recalculating the Hough map (133).

4.2.3 Vertexing

At this stage, we assume that the signals in each slice come from one interaction vertex (134). In NOvA, the vertex is not known a priori, so a modified version of the Elastic Arms method was used (135), favoring vertices in the beam direction, which also works well for LDM from beam on target.

Hits without a neighbor within 60 centimeters in a view are assumed to be noise and removed from the fit. The remaining hits are sorted in beam direction limited to the fifth percentile from the upstream end. The algorithm then tries to fit M lines of N hits to a common vertex while minimizing the energy function (reflecting the goodness of fit, exclusion of hits and large gaps from the vertex). To converge on a vertex, the Elastic Arms algorithm uses seeds obtained from Hough lines coordinates comparison and treated with the MINUIT ROOT class (136). This method results in efficient vertex reconstruction but has poor performance in terms of prong fitting (how many arms in the event there were).

4.2.4 Fuzzy-K prongs

To overcome the limitation of the prong reconstruction with Elastic Arms method, a custom form of Fuzzy-K Means algorithm was developed. It still treats each detector view separately and assumes that all hits in the slice come from the vertex. This tool fits K arms to the vertex with different hits having "fuzzy" membership in those arms and prongs (the number of arms is not known at NOvA). The algorithm is again probabilistic and is run iteratively. Finally, both views are matched to form a reconstructed 3D prong, comparing the reconstructed energy profiles along the prong in each view.

4.2.5 Kalman filter tracking

The use of a Kalman filter is specific for the ν_μ reconstruction chain, which begins with identifying track-like features in every slice. It uses an iterative process in which it predicts the positions of the next hit from "seeds" (hits closer than 4 planes apart) and using the linear character of muon tracks in 2D. The merged 3D reconstructed output of this filter is called "Kalman tracks" (137).

4.3 Particle Identification

After the reconstruction, we have the best fit of tracks caused by some particle interacting in our detector. These events need to be sorted out to separate signal from background. We do this by determining what was the interacting particle, how exactly it interacted, and where did it come from, using sophisticated particle identification (PID) algorithms (examples in Figure 22). NOvA mainly uses Convolutional Visual Network (CVN), Reconstructed Muon Identification (ReMId) and other algorithms like LID, LEM, MID, BDT...

My LDM analysis follows the ν_e and NC reconstruction chains and takes advantage of two existing algorithms for tuned ν-e selection and π^0 rejection. Since my conservative approach uses the official analysis ND dataset, I only briefly describe the methods here with more focus on additional custom cuts for LDM listed in the next chapters.

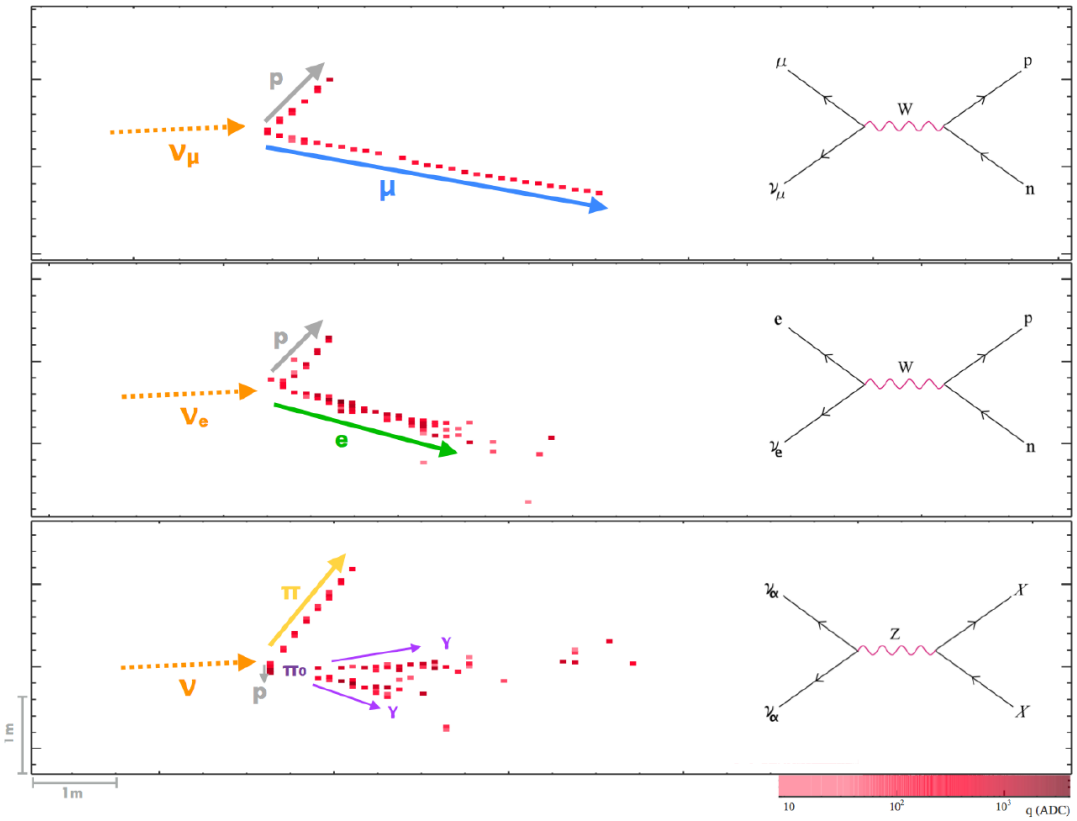

Figure 22: NOvA event displays for ν_μ CC, ν_e CC and ν NC scatterings.

4.3.1 Reconstructed Muon Identification

For ν_μ charged current events, the Reconstructed Muon Identification algorithm (ReMId) was developed, which identifies a 3D muon track through a k-Nearest Neighbors algorithm (kNN) (138). As an input, the ReMId uses the track length, the log likelihoods of the track energy deposition and the scattering, and the number of planes passed by the reconstructed track without hadronic activity. There is also a standalone filter for distinguishing cosmic induced events from ν_μ CC events in the FD, the Cosmic Rejection PID, which uses a boosted decision tree (BDT) trained on a large FD sample (139).

4.3.2 Convolutional Visual Network

Most of the mainstream NOvA analyses use a multi-purpose event classifier which employs a deep convolutional network in "image recognition style", called Convolutional Visual Network (CVN) particle identifier (140). The homogenous nature of neutrino detector such as NOvA made it an ideal candidate for heavy duty use in particle identification. The network is trained on two 2D views of the

event's calibrated hits, as the events in both views are essentially snapshots of physics processes, and we train it separately for the neutrino and anti-neutrino runs. The information of each view is combined in last layers of the network to assign a PID for each interaction.

As an input, we use slices (see section 4.2.1) without any additional reconstruction, the CVN finds and trains on all necessary features by itself. Each convolutional layer uses a stack of kernels to transform the image (in form of a pixel map, with single pixels representing individual cells with 256 possible values of encoded energy) and extract abstract image features. The output of the kernel applied to the whole image in given layer is called feature map.

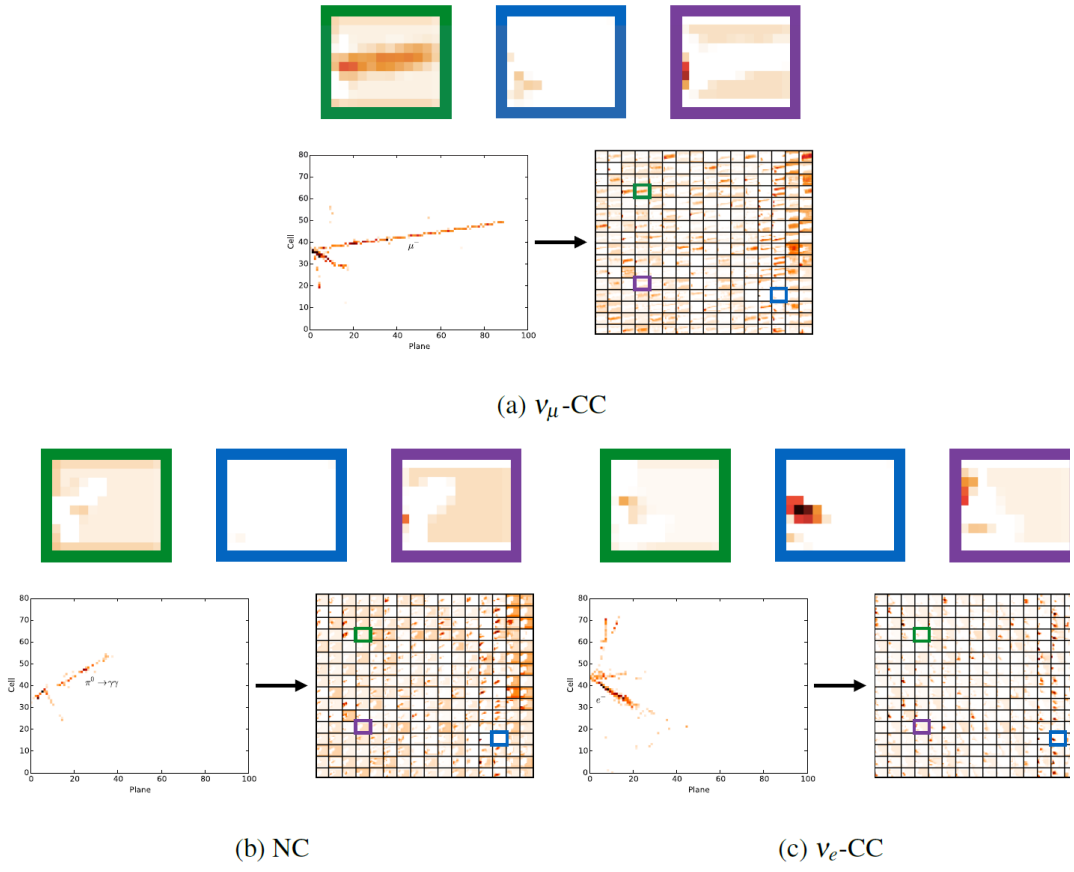

(a) ν_μ-CC

(b) NC

(c) ν_e-CC

Figure 23: Y-view examples of a simulated CC interaction in the cell-plane space and the extracted feature maps (end of the first inception module in the CVN network), with highlighted feature maps sensitive to muons (green), electromagnetic showers (blue) and hadronic activity (purple square). Respectively (140).

The first-generation NOvA CVN was built on the basis of the GoogLeNet image classifier, using the Caffe framework (141) (142). The output of the first layers of the network exaggerate found features, while deeper layers are more topological. The inception module extracts features in parallell at different scales and merges into a single layer. The pooling technique replaces subsets of pixels either with maximum value or with average value of pixels. The Local response normalization (LRN) removes local minima via pixel normalization across the feature maps. The two independent branches are joined at the end of the chain, the output is classified and normalized as a PID probability. The outline of the network can be seen in Figure 23.

The network is trained on MC images with known classification and also on FD cosmic data. The events are split into 13 categories: one for NC and four (QE, RES, DIS, Other) for CC of each neutrino flavor (ν_μ CC, ν_e CC, ν_τ CC).

The initial CVN implementation, increasing signal and reducing background, was equivalent to a 30% exposure increase for NOvA compared to traditional methods when first used. NOvA was the first physics experiment using convolutional networks to extract published results (in 2016, (4)).

These kinds of tools will become even more vital in high resolution liquid argon experiments like DUNE where traditional reconstruction techniques become very challenging. DUNE is now using its own variant of CVN, developed with the help of NOvA collaborators, to identify simulated neutrino interactions for sensitivity studies. These studies, for the first time, have reached the anticipated design performance given in the Conceptual Design Report using full simulation and reconstruction. The two experiments are in regular communication about the application of computer vision to physics problems, and new ideas often move between experiments; both informally through overlapping personnel, as well as through Machine Learning-focused activities at Fermilab like a Journal Club and User's Forum (143).

Current NOvA CVN moved to a MobileNet architecture, implementing widely used TensorFlow/Keras machine learning libraries (Figure 25). We also now produce training pixel maps in a form of highly structured .h5 files (in HDF5 format) on which the training time requirements drop by an order of magnitude.

For a custom LDM network, I have produced ND pixel maps from my MC signal samples in this HDF5 format on which an LDM identifying network could be trained in timely manner. However, new generation of unbiased networks was commenced in parallel by NOvA machine learning experts for i.e. electron showers and pion showers with flat energy distributions and much higher statistics, so I could eventually take advantage of their superior performance.

For this kind of single particle classification, a standalone ProngCVN network was also developed. This method classifies single particles, which were separated using geometric reconstruction methods. The architecture has four parallel branches – top and side views of the single particle and of the entire event to add context (144), which improves the PID efficiency by 10% (see Figure 24).

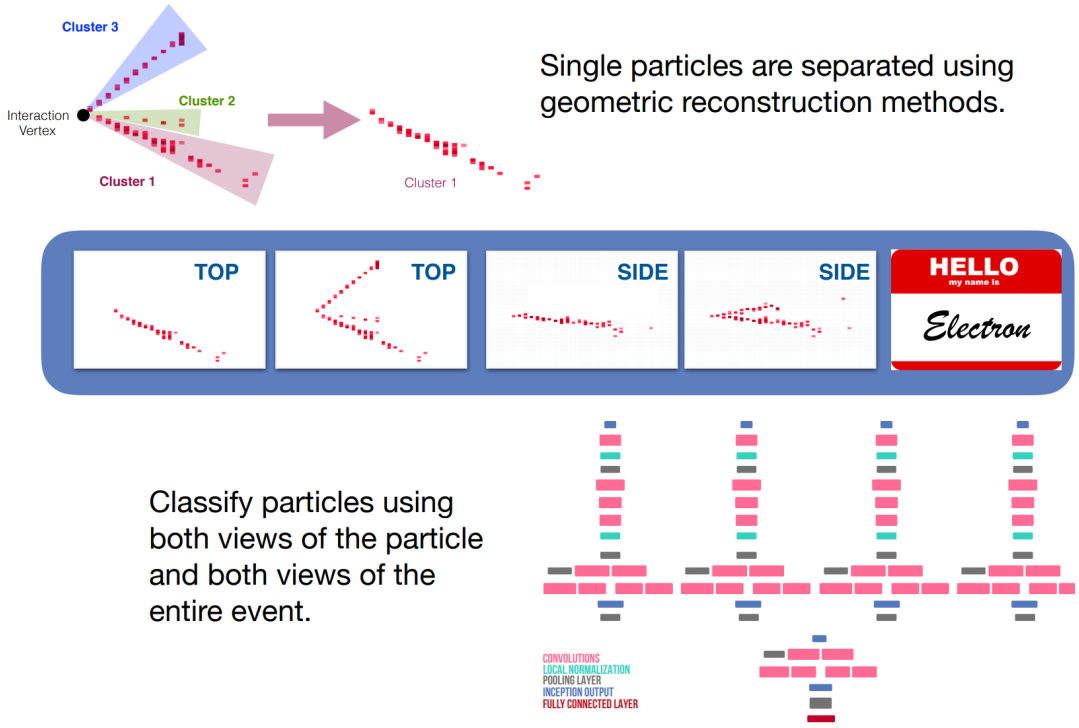

Figure 24: ProngCVN with the modified 4-view architecture with context (144).

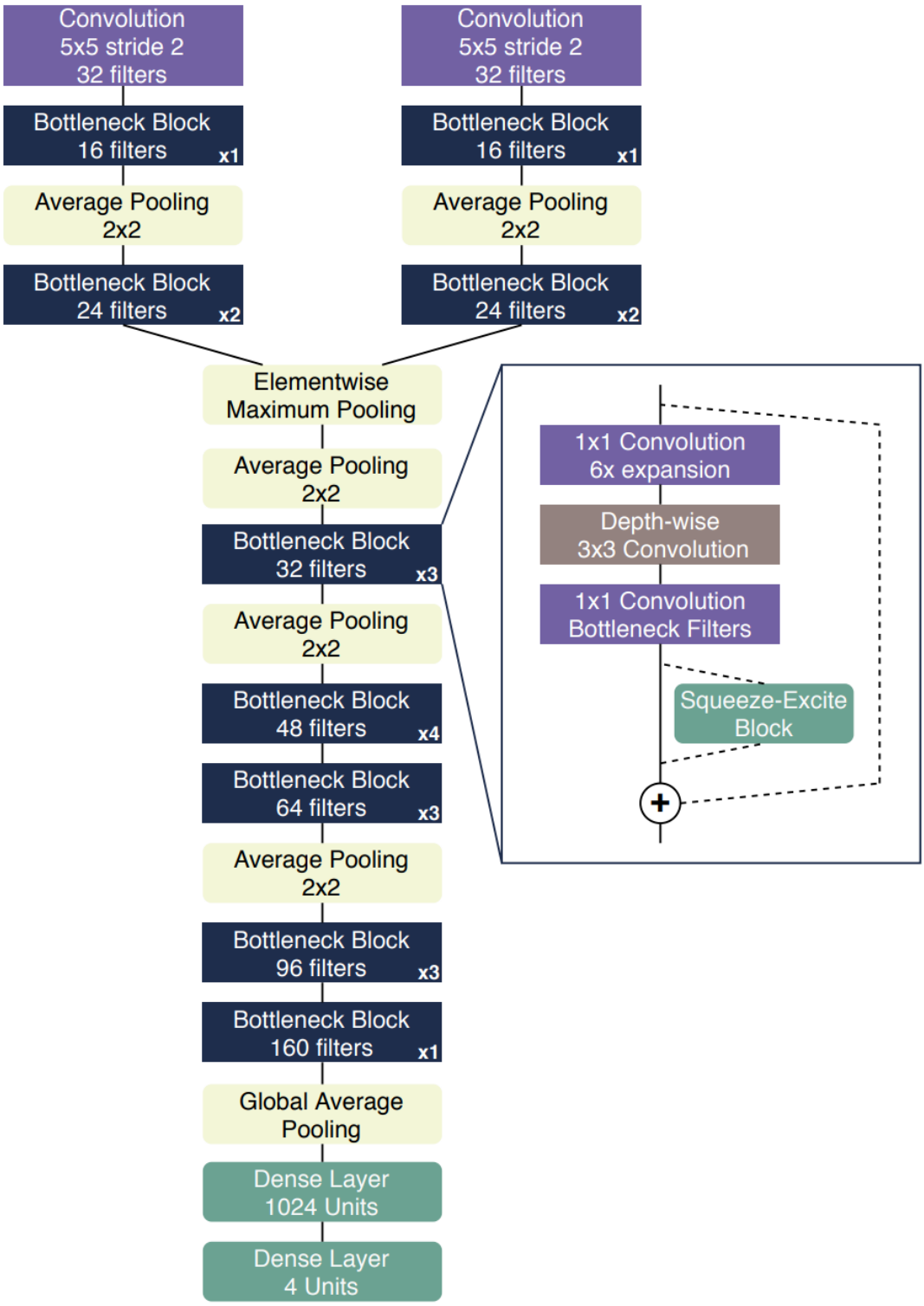

Figure 25: Example of simple NOvA CVN architecture – two separate branches start at the bottom, moving upwards. Output is a particle score as shown in Figure 26.

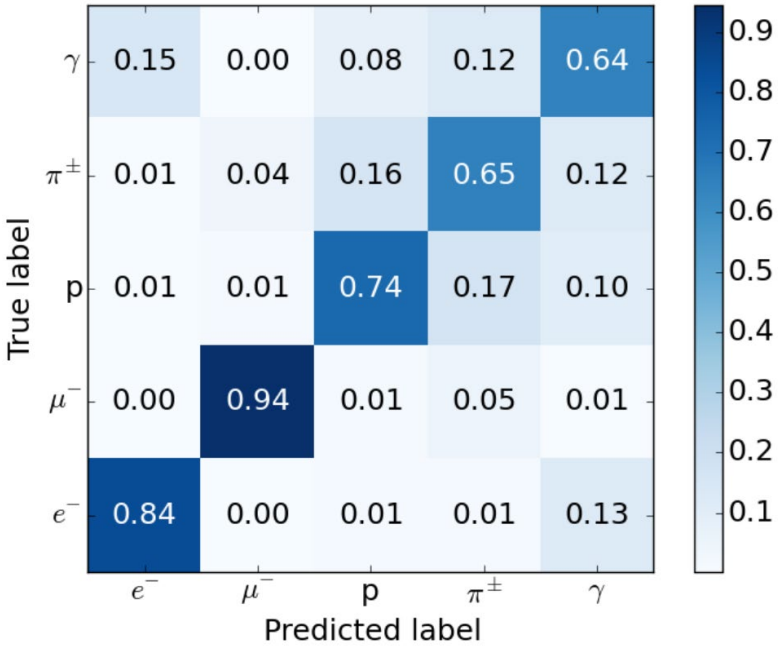

Figure 26: Normalized CVN output matrix of true (simulated) vs. predicted (reconstructed) labels.

4.3.3 Likelihood based PID

The Likelihood-based PID (LID), processes the fuzzy-K prong parameters with an artificial neural network (ANN) (145). First, the method redistributes hits and energy in the 3D prongs, creates shower candidates and derives the longitudinal and transverse *dE/dx* profiles. It also considers the angle of the shower to the direction of the beam and other parameters like fraction of energy in primary shower, invariant mass of all showers reconstructed in the event, energy deposited around the vertex (within 8 planes distance from the reconstructed vertex), and the gap between the vertex and shower start point. These distributions have the potential to differentiate particle type (e, γ, μ, π^0, p, n, π) (146).

The shower candidates are then fed to the ANN, trained on the Far detector MC. The overall performance is not exceeding signal selection efficiency of 48 %, background rejection efficiency 97 % and its performance is tuned to work best in regions bellow 3.5 GeV.

In the first years of neutrino analysis, before the rise of the machine learning with CVN, the ν_e appearance analysis also relied on the Library event matching (LEM) PID (147). This method takes a reconstructed event and compares it with a large library of well-known simulated events, matching on 5 physical variables (signal matches, mean hadronic *y*, mean charge fraction, energy difference and enriched fraction). Along with reconstructed event energy, these variables are fed into a decision tree to obtain the PID value.

The ANN technique is used in a method developed in (148) and (149) to constrain the neutrino beam flux through NOvA ND. It studies the elastic scattering of beam neutrinos off atomic electrons in the NOvA ND because it is a well understood interaction with a clean signal. Another study using this method in (148) searches for the existence of a magnetic moment in the neutrino. Both consider the beam neutrinos as the incident particle. As it was discussed above, the energy range around the peak rate in this beam is within 1 to 3 GeV and that is where the peak efficiency is as well.

Employing this technology to create the neutrino backgrounds for the LDM high recoil energy range of interest above the main neutrino focus band forces it to operate beyond its main design considerations and near the limits of its validity. Consequently, the efficiency of PID is the major limiting factor in this analysis and any future extensions. Another concern is that the PID efficiency is integrated in the overall detector response function, which includes other efficiencies and energy corrections, from deposited to reconstructed, and selections cannot be quoted as a single value or a simple function of shower energy.

Despite these limitations, at first stages this method was able to generate an approximation to the neutrino-induced spectra for a comparison with the LDM simulated signals. In order to estimate the PID efficiency and its validity extent, I considered several mass-model LDM simulated events from my signal files. I found that up to 10 GeV the efficiency is still viable although it vanishes beyond 20 GeV. Consequently, the search area for LDM signal for this work extends only to 15 GeV (also see in 6.3.6).

4.3.4 Energy estimation

To estimate the energy of the incoming particle, we sum the hadronic and leptonic activity in a fully reconstructed event. For the ν_μ events, it's a sum of muon energy

and reconstructed hadronic energy. We determine muon energy based on the length of the 3D Kalman track with best ReMId score. The hadronic energy is a sum of calorimetric energy from all hits in the slice, which do not belong to the reconstructed muon track and the vertex hits above the minimal ionizing threshold. Both these energies are fit with a spline function to improve the energy resolution.

The ν_e energy estimator also is a sum of two components – a quadratic sum of the hadronic calorimetric energy and the electron shower. Unlike the distinctively long muon tracks with low dE/dx, the shower size and E distribution are complicated to parametrize, therefore the shower energy is also determined calorimetrically (150).

5 Lightweight Dark matter in NOvA ND

In previous chapters, I have thoroughly described the NOvA apparatus and proposed its reinterpretation as a Dark Matter beam dump experiment. Following the motivation from Chapter 3.1.4 and in order to showcase the signal from $\chi - e$ scattering in the NOvA ND, I have simulated a subcategory of the vector portal mediator decay scenario of LDM production. I used the PYTHIA 8.244 simulation framework (112) and defined new particle *V* decaying into a pair of new particles χ. Here I describe a simple PYTHIA LDM beam simulation and the detector response to electrons, off which the LDM χ particles scatter.

5.1 Model example of NuMI LDM production

Based on the reasoning and examples in the theoretical introduction (Chapters 2.3, 3.1.4 and ref. (12) (11) (98) (99)), the various astrophysical and cosmological constraints predict the mediator production rate at about 40 μb for the proton on proton collisions. The experimental constrains narrow the mass region of interest to range of $6.9\ \mathrm{MeV} < m_\chi < 500\ \mathrm{MeV}$ (14). In combination with the NuMI beam intensity of ~6×10^{20} POT per year hitting the 1.2m long carbon NuMI target, the expected LDM production rate from direct Dark photon production and meson on-shell decays at NuMI is estimated to $\mathcal{O}(10^{12})$ LDM particle candidates per nominal year. They leave the target area in the forward direction boosted into few degrees (<10°) around the beam direction as described in Figure 27 and Figure 28.

To simulate the flux of LDM from these two production channels of Dark Photon mediator *V*, I used the standalone PYTHIA framework (151) for relativistic Breit-Wigner approximation of direct quark-on-quark production of higher masses, and boosted π^0 decay in the lower mass region. To improve the performance of the MC simulation, I simulate a forced *V* decay in both production cases into 2π forward geometry and further compress the decay region to obtain more LDM χ paths overlapping with ND geometry. Although I can set a softer condition for the masses of both the vector and scalar dark particles to follow just $m_V > 2m_\chi$ to obtain on-shell processes described in 2.3.2, in the final choice for MC simulation, I only consider a fixed masses combination of $m_V = 3m_\chi$.

The input to the simulation is a simple case of the Vector Portal HS model along with the case of creation of a vector mediator particle *V* of mass ranging from 30

MeV to 1 GeV decaying to a scalar LDM pair ($\chi,\chi^{\dagger}$) with mass cases of 10, 20, 30, 50, 100, 300, and 450 MeV. The simulation requires the mediator to decay instantly, and that the product masses add up to no more than the mediator mass. It also neglects any spin dependence in the distribution of the LDM pair and any tendency for Dark matter self-interaction. The LDM products leave the target interaction area boosted forward by the incident proton/meson momenta.

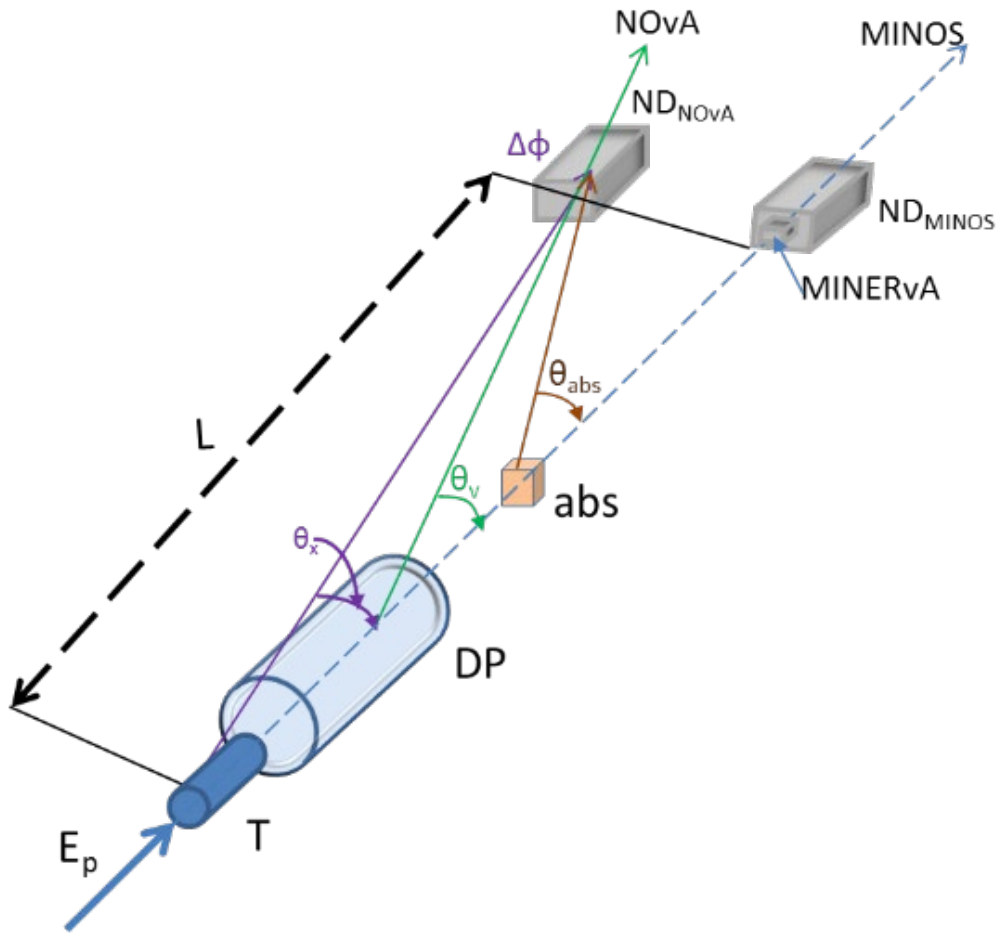

Figure 27: Schematic of the NOvA ND geometry and angular acceptance with the NuMI beam cascade. E_p – incoming protons, T – NuMI target, DP – decay pipe, abs – absorber, and L is the baseline of 990 m (courtesy of A. Hatzikoutelis).

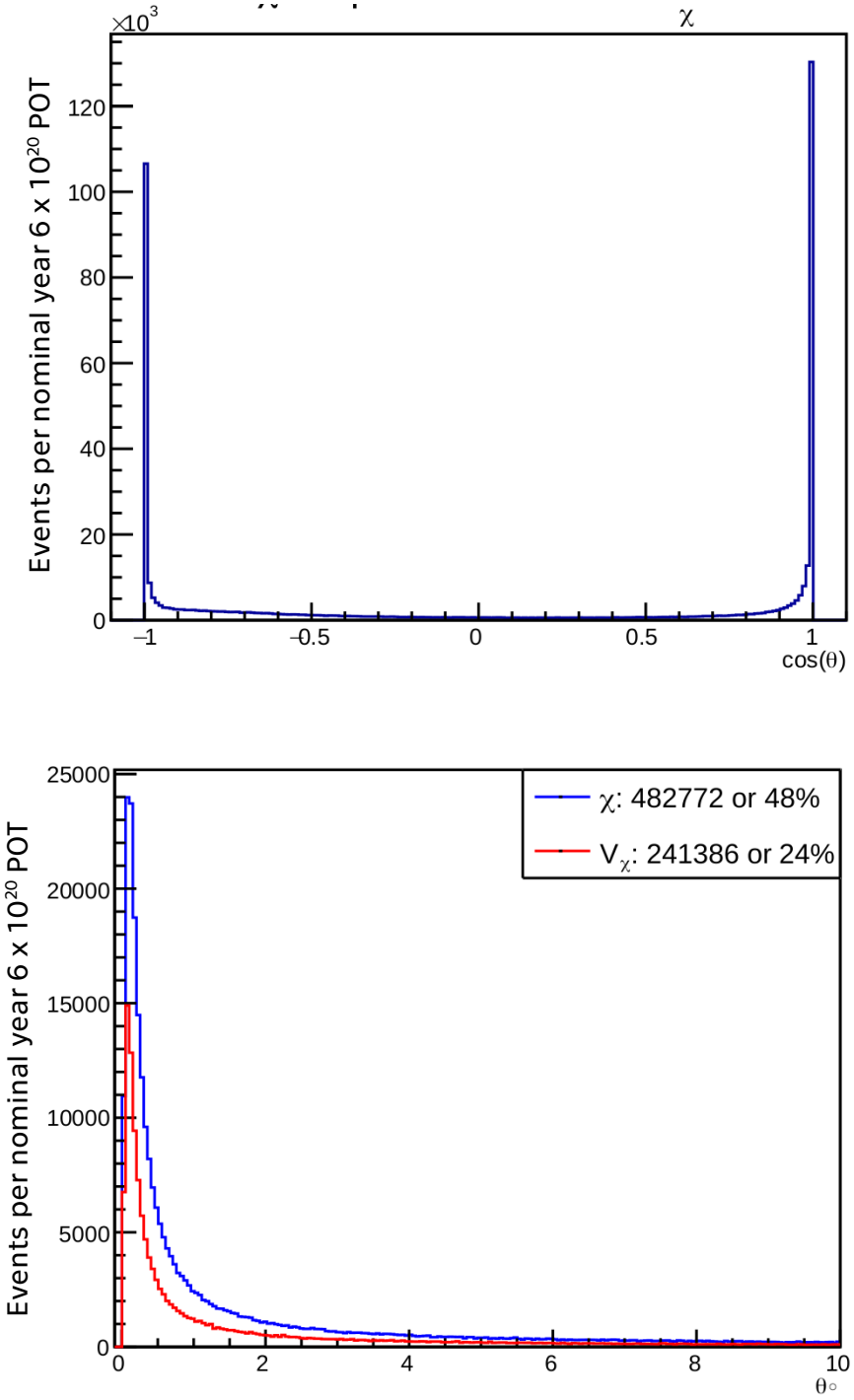

Figure 28: The decay angles of χ in the CM of V (top) and Angular distribution of the LDM particles leaving the target area (bottom).

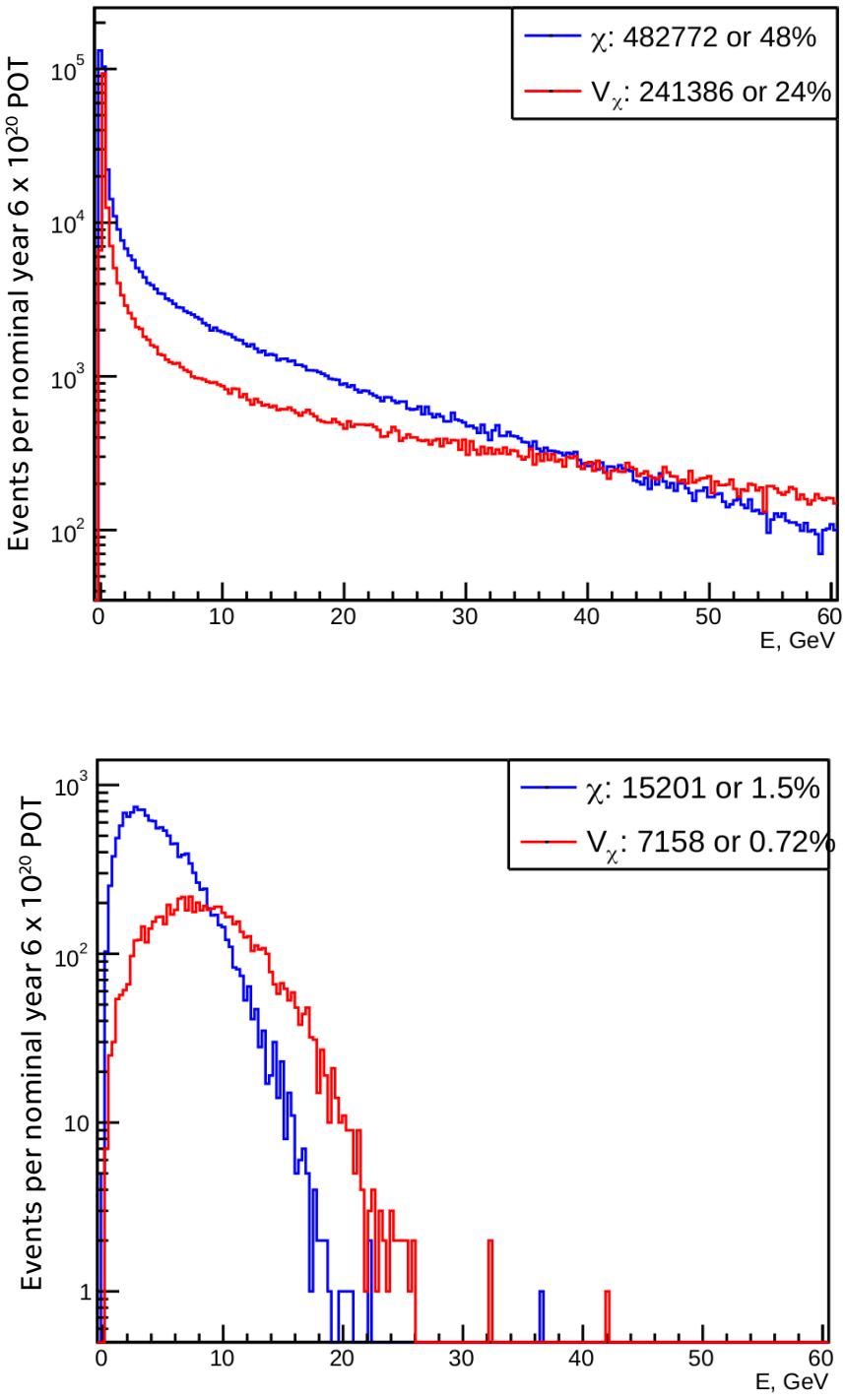

Figure 29: Energy spectra of the LDM particles leaving the target area (top) and their distribution within NOvA ND acceptance range of 0.2° (bottom).

5.2 LDM within the NOvA ND

The advantage of this standalone approach is that the initial beam simulation is very straightforward and I can avoid difficult hadronization models, which normally need to be dealt with in main NOvA MC chain. Expected signal event rate then can be scaled depending on the coupling parameters I choose.

5.2.1 LDM flux in NOvA ND

The LDM MC output from previous step can be translated into a HEPEVT text format (for this, I had to work with PYTHIA developers to update current SW version to be able to have such functionality). The stored text file contains full information about scattered electrons in two lines of text for each event.

The HEPEVT file can be then fed into a custom "TextFileGen" generator module from the NOvA SW EventGenerator package. This module translates stored electron information into a detector hits in "artdaq" format (art is Fermilab's Event Processing Framework (152)). The output is a set of raw signal ROOT files with electron events in the NOvA ND.

These raw files can be treated same as standard NOvA simulation samples or measured data and they are reconstructed and classified using tools described in Chapter 4. The highly structured result of the simulation production cascade is a set of PID file, a "Common Analysis File" (CAF), and a .h5 file (hierarchical HDF5 format for pixel maps, serving as an input for CVN training). Examples of event displays from reconstructed LDM PID files are shown in Figures 30 and 31.

The simulated energy spectra of the LDM (Figure 29) are produced by imposing the angular acceptance of NOvA ND (1,6 mrad) which covers the ranges of $0.60° < \theta < 0.79°$ (see also the "acceptance" band at Figure 11) as well as a cut on the azimuthal angle of $\Delta\varphi = 23{,}7°$ (Figure 26). The overall geometric acceptance efficiency of the NOvA ND can be estimated as $\Delta\varphi \cdot \Delta\theta \approx 10^{-4}$ of 2π, assuming that all LDM particles are boosted in the forward direction and depends on kinematics of each mass scenario.

For high-energetic LDM particles, $E_\chi \gg m_V$, the LDM scattering cross section on electron can be approximated as

$$\sigma(\chi - e) \backsim 10^{-27} \alpha \epsilon^2 \left(\frac{100\ \mathrm{MeV}}{m_V}\right)^2 \mathrm{cm}^{-2}. \qquad (15)$$

For my analysis, I choose a baseline example representing the sub-pion masses and I consider $\alpha = 0.5, \epsilon = 2 \times 10^{-5}$ and $m_V = 90\ \mathrm{MeV}, m_\chi = 30\ \mathrm{MeV}$.

5.2.2 Spectra from LDM scattering off atomic electrons.

The χ on e event distributions extend from few to 60 GeV of kinetic energy T and peak around 5-10 GeV with a peak rate of $\mathcal{O}(10^6)$ LDM per GeV bin for the baseline example 30 MeV LDM model. These mean kinetic energies are higher than the neutrino spectrum peak of 2 GeV, albeit, at 6 orders of magnitude lower event-rate. Nonetheless, this suggests that the mean interaction rate should be marginally higher than that of the neutrino or to put it differently, the drop of interaction rate with energy is slower for the LDM interactions than that of the neutrino induced interaction spectra. Therefore, the ratio of the LDM signature-signal to the neutrino background should improve with energy. This motivates extending the energy region of interest and is further validated in selection criteria optimization in Chapter 6.3.

The interaction example for this work is the cleanest of the channels discussed in Chapter 2.3. It is the elastic scattering of χ on atomic electrons, a neutral current event dependent exclusively on the kinematics of the involved particles. This channel is relatively weak for neutrinos compared to the scattering off nucleons, and it has a clean, well-understood, leptonic process, with an easily identifiable single EM-shower along the beam direction pointing directly back to the target, and without any nuclear or hadronic effects in the final state.

The spectrum of the arising EM-shower signatures depends on kinetic distributions of each model of LDM. The resultant spectra for 30 MeV χ are shown in Figure 29. The LDM kinetic energy peak moves to higher values for heavier cases having similar kinetic distributions cause similar distributions of the scattered electrons energies.

The finite size of the NOvA ND compared to these higher energy showers adds to the intricacy of the particle reconstruction challenges (153). As a result, the success rate of identification and exclusion of the neutrino events declines for high energies. Even though at the range of interest of 0.5-15 GeV the efficiency of identification of the produced EM-showers should still be viable, towards 15-20 GeV it may drop as low as few percent of the maximum achieved at the 1 to 3

GeV range where the NOvA experiment searches for events for its primary oscillation measurement. Above 15 GeV, the processes are mainly coming from deep inelastic scattering (DIS), for which the GENIE models are now under rapid development. Improving the reconstruction and particle ID efficiency for the higher energy showers is a high priority for any future analysis of a potential LDM signal in neutrino detectors.

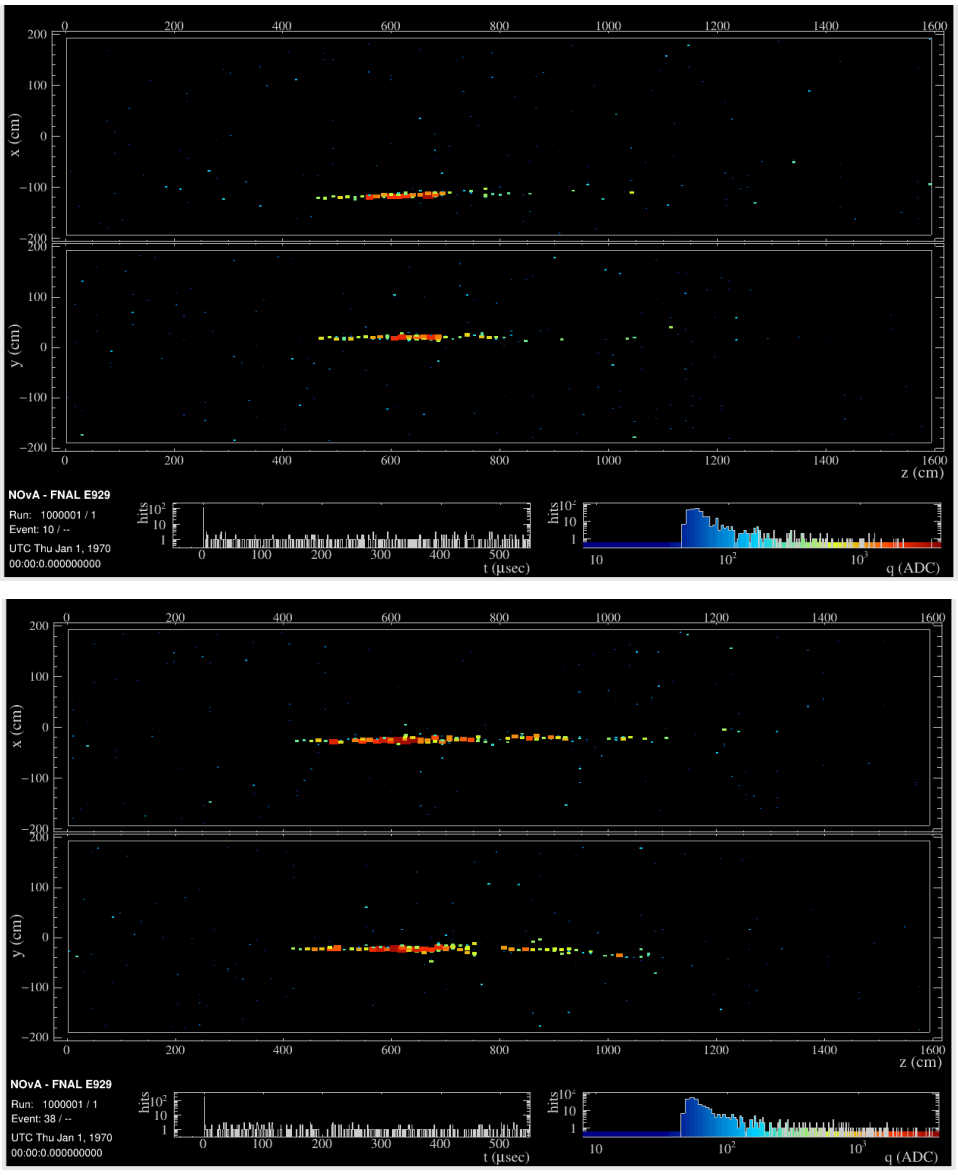

Figure 30: Event display of reconstructed single EM showers coming from χ in the NOvA ND

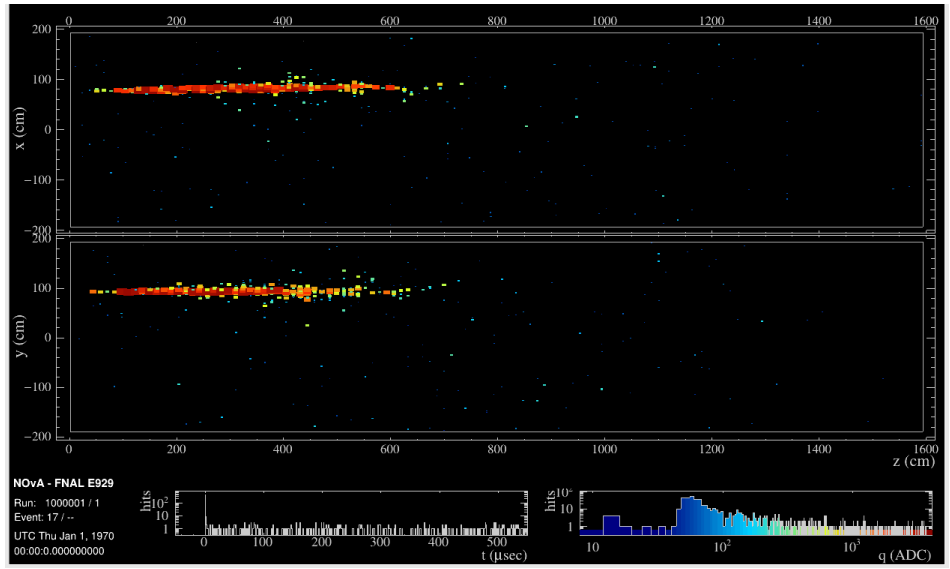

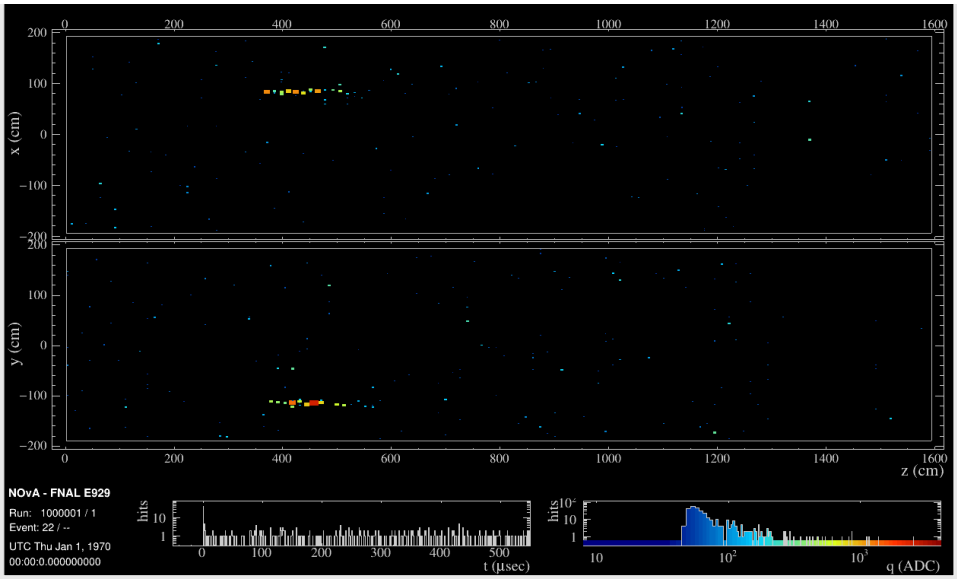

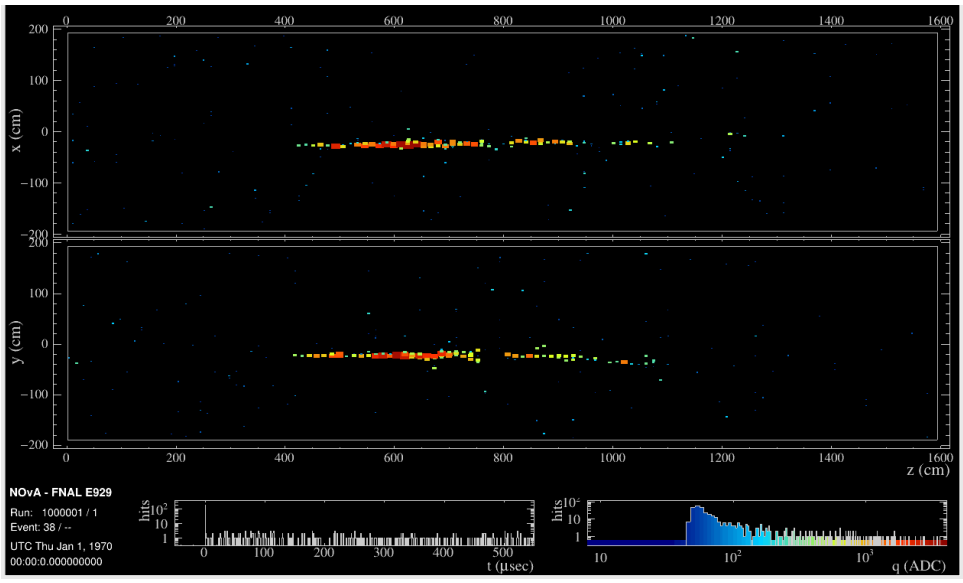

Figure 31: More examples of LDM event displays.

6 LDM analysis

On a simple LDM model example simulated in previous chapter, we define a given set of parameters, and calculate a hypothetical LDM flux, which should generate a significant signal in the detector. The scattering cross section and the interaction parameters can be calculated from the LDM observed signal (number of excess events) in NOvA ND. Using standardized NOvA analysis tools, I first tune and normalize the selection criteria on a control region, predict the number of events in the signal region and eventually compare the simulation to measured data for the NOvA FHC (neutrino mode) dataset.

6.1 Analysis strategy

As described in the Introduction and in Chapter 2.3, to estimate the LDM mixing parameter, I look for excess of single electron shower events in shower energy region 0.5-15 GeV, contained in the ND. In following section, I will describe the specific tools and techniques used for LDM analysis.

6.1.1 NOvA software

NOvA uses a standardized offline analysis software based on Fermilab's *art* framework (154), NOvAsoft, which is a sophisticated SVN-managed SW repository of distributed C++ code with a large library of feature branches and releases. For the LDM analysis, I used the official "Production 5.1" tagged release *R20-11-25-prod5.1reco.a*.

Working with large datasets and complicated SW requires a lot of overhead for both the analyzers and the computing division, so NOvA collaboration introduced a state-of-the-art architecture of CAF – Common Analysis Files, a condensed and structured set of high-level reconstructed .root files containing all variables needed for most of physics analyses in mainstream NOvA program. This approach was very successfully introduced into the HEP field and is now rapidly implemented by many large collaborations and experiments, both already operating or currently under construction.

6.1.2 Dataset

The data used in my LDM analysis are following the official NOvA Production 5.1 period dataset definitions for the ND in FHC (neutrino) mode (155), which are data taken between 16th of August 2014 and 26th of February 2019. The total ND

exposure in the FHC (neutrino mode) is 11×10^{20} POT. The GENIE Monte Carlo simulations are scaled down to match the data from 5.54×10^{21} POT. The datafiles for validation were produced with "stride 10" parameter by the NOvA production group in "Mini-production 5.1" batch (MP5.1) and are available in above mentioned common analysis file format (CAF). The data and MC SAM definitions are:

- *prod_caf_R20-11-25-prod5.1reco.a_nd_genie_N1810j0211a_nonswap_fhc_nova_v08_full_v1*
- *prod_caf_R20-10-06-miniprod5.1reco.b_nd_numi_fhc_full_v1_mpv2validation_10stride;*
- *prod_caf_R20-11-25-prod5.1reco.d_nd_numi_fhc_full_v1*
- *jediny_caf_R20-11-25-prod5.1reco.d_ldm_chi30-10k*

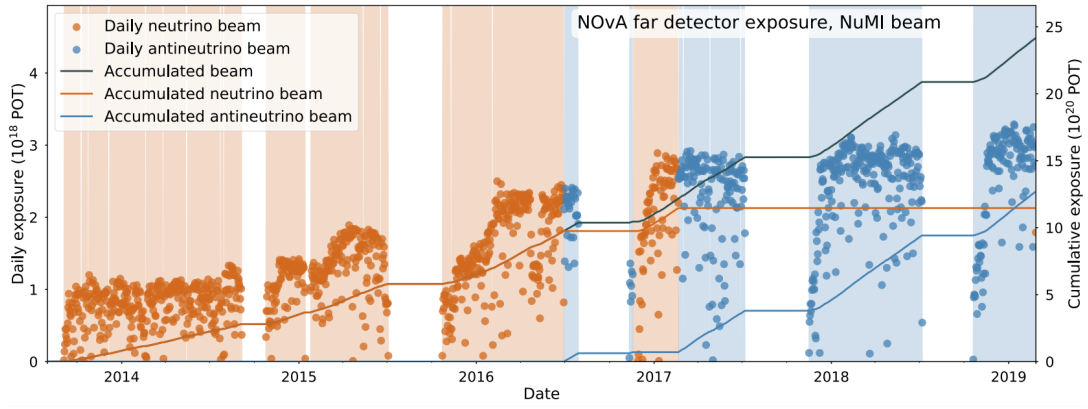

Figure 32: NOvA POT collected, running at >700 kW beam power since 2017.

6.1.3 Blinding

To prevent bias when analyzing measured data, so called "blind analysis" became mainstream in particle physics. Fundamentally, the data in signal region have to stay "blinded" and the analyzer performs all simulation and selection tuning and development on a sideband or other control region. This is a standard procedure in all NOvA analyses.

In my case, the very forward-going kinematics of events of interest provide a good candidate to create an angular sideband. It can be created in the final step of signal selection progression (cutting), when I choose only events with $T\theta^2$

between 0.005 and 0.03 GeV×rad^2 as signal and normalize all plots based on sideband region of 0.05 and 0.10 GeV×rad^2. The signal and sideband regions are conservatively matched to previous ν-e analyses, since a strong target-aiming can be assumed because of a prompt decay of the vector mediator and the incoming LDM particle aiming directly to the target area (with less angular smearing due to travel into the decay pipe). An important question arises of the DM contamination in the neutrino beam. It is possible other models of DM add to the actual beam flux, but here I only consider SM beam with one possible LDM model, which allows me to separate and normalize the background in the sideband $T\theta^2$ between 0.05 and 0.10 GeV×rad^2.

6.1.4 Sensitivity

The LDM analysis can be evaluated as a counting experiment, in which I verify the LDM test hypothesis against null hypothesis. In case of excess events observed, the traditional frequentist p-value and significance can be calculated (with 3σ limit for observation and 5σ for discovery), when no events are observed, the upper limit of LDM cross section with 90% confidence level is calculated via χ^2 quantile method. The result can be also rescaled to the self-annihilation parameter Y (defined in Eq. 1). The model independent character of my analysis then enables the result to be generalized over a larger area of so far un-probed parameter space.

6.2 Background

The signature of the LDM interacting in ND is a single EM shower from recoiling electron. Therefore, the background for my analysis consist of events leaving or mimicking same signature from neutrino interactions from the beam (i.e. in Figure 34). In general, I treat the neutrino interactions, which are signal for most NOvA analyses, as LDM background. Primarily, the background consists of true EM showers, mainly from ν_μ NC scattering on e and ν_e NC and CC events. Although the beam delivers mostly ν_μ (and anti-ν_μ), the cross section for ν_e CC is much larger than NC which makes also the ν_e channel significant (Figure 36).

Secondarily, decay of high energy π^0 from neutrino NC interactions, for which the two product photons merge into one shower (or only a shower from one photon is reconstructed), can be misidentified as a single electron shower (8). An event display of such event can be seen in Figure 33. This can be overcome by looking

at the profiles of energy depositions in first planes of the shower, which are different for two photons (146).

6.2.1 Neutrino flux prediction

Extensive study on the beam neutrino flux prediction and its uncertainties was carried out (156) (157), to account for a MC/Data discrepancy (mostly due to poor meson production modelling in the "thick target" and insufficient secondary hadronization models). Table 1 summarizes possible sources of beam neutrinos.

Although the two-detector setup eliminates a large portion of the simulation uncertainty, an accurate knowledge of neutrino flux is needed for precision measurements and cross-section studies and any ND-beam analysis including LDM scattering. Only 55% of NuMI neutrino flux originates from direct *p*-*p* interactions, 45% percent of mesons come from secondary interactions which cannot be constrained by data from thin target experiments (like NA49, MIPP).

Also, for higher energy events, more neutrinos originate from emerging kaons, for which we also lack sufficient flux data and which get focused by the NuMI magnetic horns (Figure 36). Based on discrepancies between the model prediction and detector measurements (taken from MINOS experiment), the kaon production rate can be therefore tuned by up to 30% as is illustrated in Figure 35.

Decay	Chanel	Branching ratio (%)
1	$\pi^{\pm} \rightarrow \mu^{\pm} + \ \nu_{\mu}(\ \bar{\nu}_{\mu})$	99.9877
2	$\pi^{\pm} \rightarrow e^{\pm} + \ \nu_{e}(\ \bar{\nu}_{e})$	0.0123
3	$K^{\pm} \rightarrow \mu^{\pm} + \ \nu_{\mu}(\ \bar{\nu}_{\mu})$	63.55
4	$K^{\pm} \rightarrow \pi^{0} + e^{\pm} + \ \nu_{e}(\ \bar{\nu}_{e})$	5.07
5	$K^{\pm} \rightarrow \pi^{0} + \mu^{\pm} + \ \nu_{\mu}(\ \bar{\nu}_{\mu})$	3.353
6	$K^{0}_{L} \rightarrow \pi^{\pm} + e^{\mp} + \ \nu_{e}$	40.55
7	$K^{0}_{L} \rightarrow \pi^{\pm} + \mu^{\mp} + \ \nu_{\mu}$	27.04
8	$\mu^{\pm} \rightarrow e^{\pm} + \ \nu_{e}(\ \bar{\nu}_{e}) + \ \bar{\nu}_{\mu}(\ \nu_{\mu})$	100.0

Table 1: Charged meson branching ratios for decay modes into neutrinos.

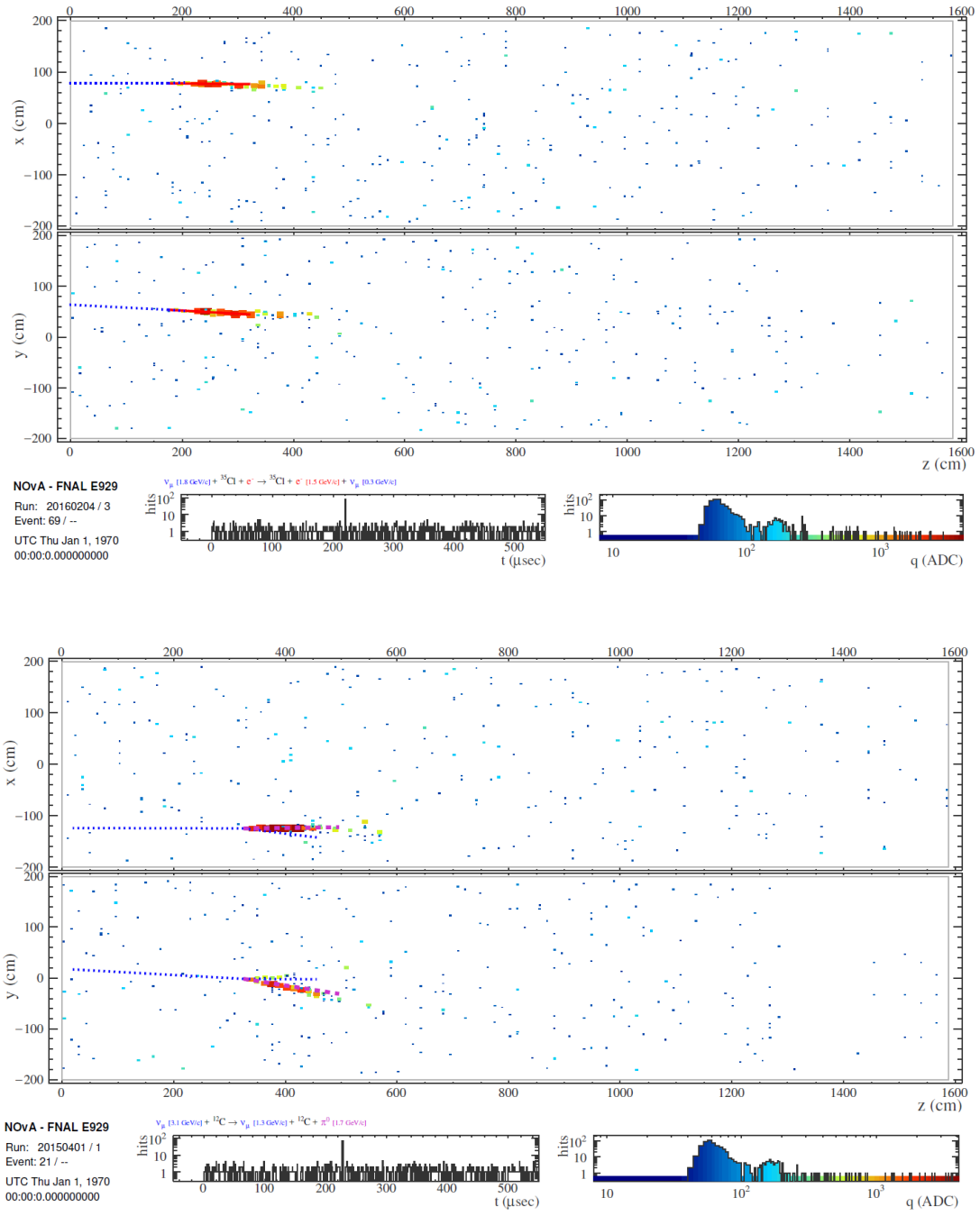

Figure 33: Example of an EM shower from ν-e scattering (top) compared to a π^0 decay (bottom) "shower" produced by two forward boosted merged photons.

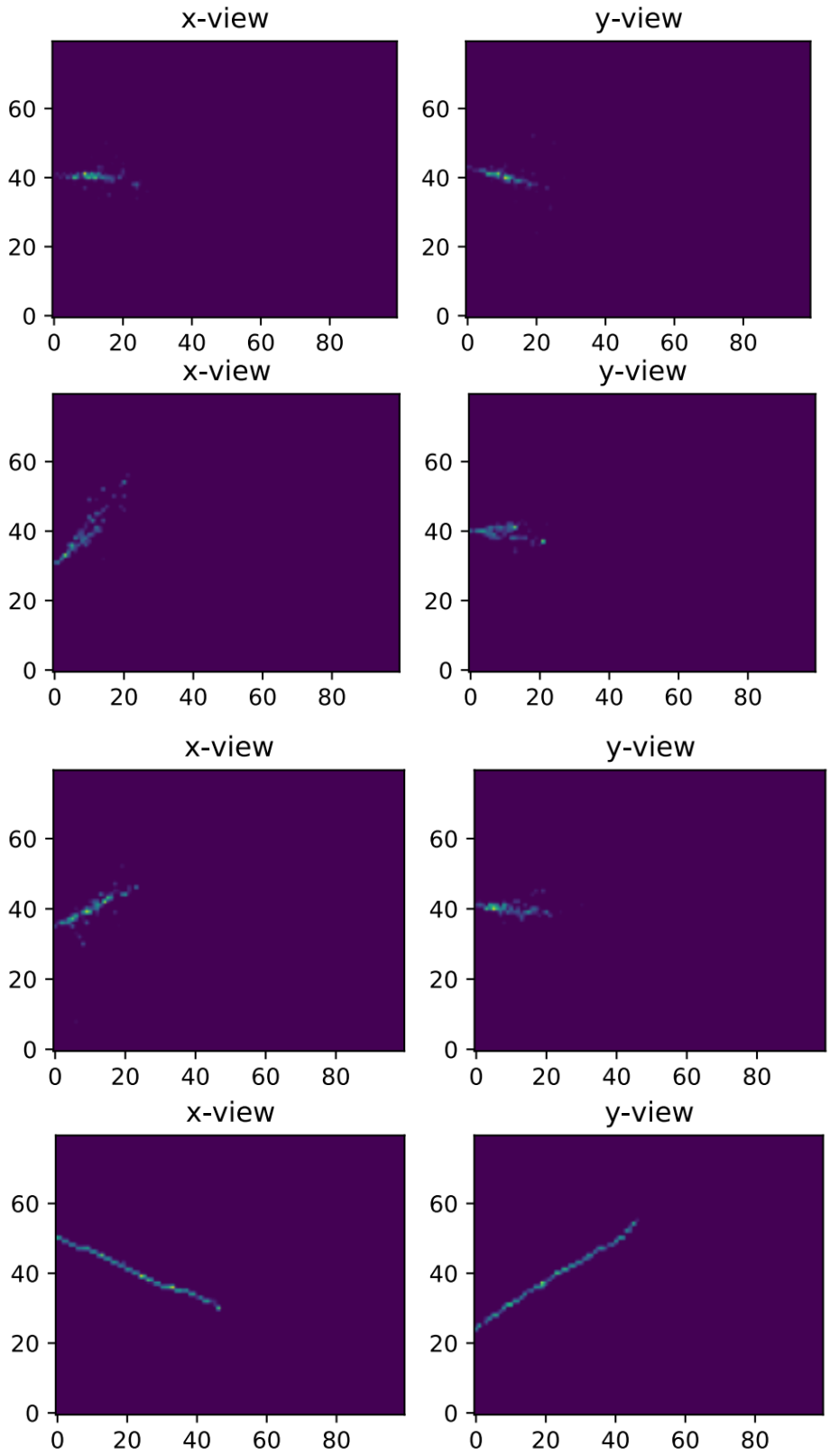

Figure 34: Examples of pixel maps used to train various CVN networks. From top: *v* elastic scattering on e^-, π^0, ν_e CC, ν_μ CC.

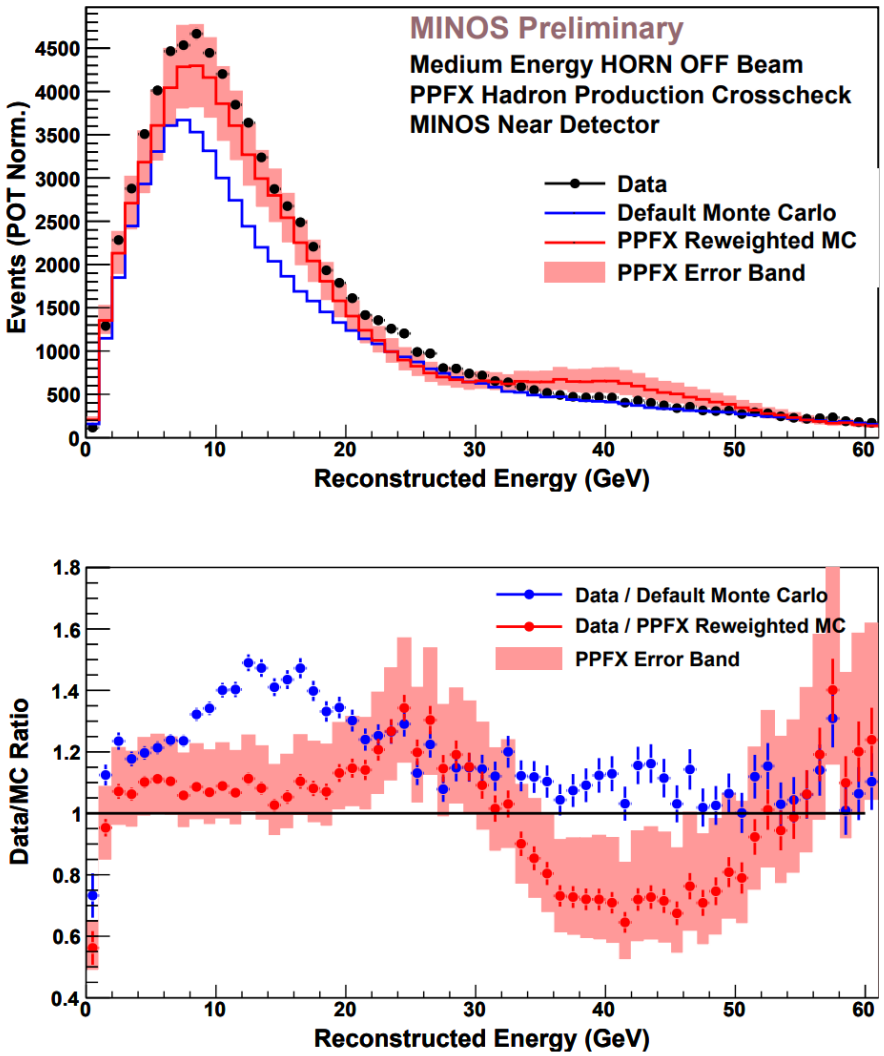

Figure 35: Kaon production uncertainty (at 30%) coming from experiment MINOS crosscheck of PPFX predictions (159). The crosscheck was done on a dedicated run with magnetic horns turned off (no focusing).

Besides collisions with the carbon target, the proton beam also collides with other elements in the beamline downstream the carbon stack (mostly Fe and Al, but also N, He, O, Be, H, Cr and Si are considered). The NuMI beam is simulated in NuMI-X Black Bird framework using FLUGG (version 2009-3d) and Fluka (2011.2b.6).

To determine the neutrino flux from the NuMI beam, the PPFX (Package to Predict the Flux (158) (159)), customized for NOvA conditions, is used. This package corrects the hadron production rates based on data from external data sources and predicts the systematic uncertainties in the neutrino beam flux (see Figure 35). The data used for these corrections come from experiments NA49 (using thin

target and 158 GeV beam production of pions, kaons, protons and neutrons), NA61 (pions and kaons at 31 GeV) and MIPP (for kaons and protons at 120 GeV). The MIPP also produced measurements using a spare target for NuMI at 120 GeV (pions up to 80 GeV and the pion/kaon ration above 20 GeV).

All the neutrino interaction spectra in their relative strengths are added up in Figure 37. The simulation sample corresponds to events collected analyzed for the most recent NOvA oscillation analysis result (160). The main component of the neutrino background is the interactions ("Beam ν_e") from high energy electron-neutrinos coming from the decay of kaons in the secondary beam as described in Chapter 3.1. The number of these K mesons compared to pions is not well known from beam measurements on thick targets and currently would comprise a significant source of systematic uncertainty in analyzed energy range (see further in section 5.2.2). This issue has increasing significance with growing energy, as can be seen from Figure 39 and Figure 40.

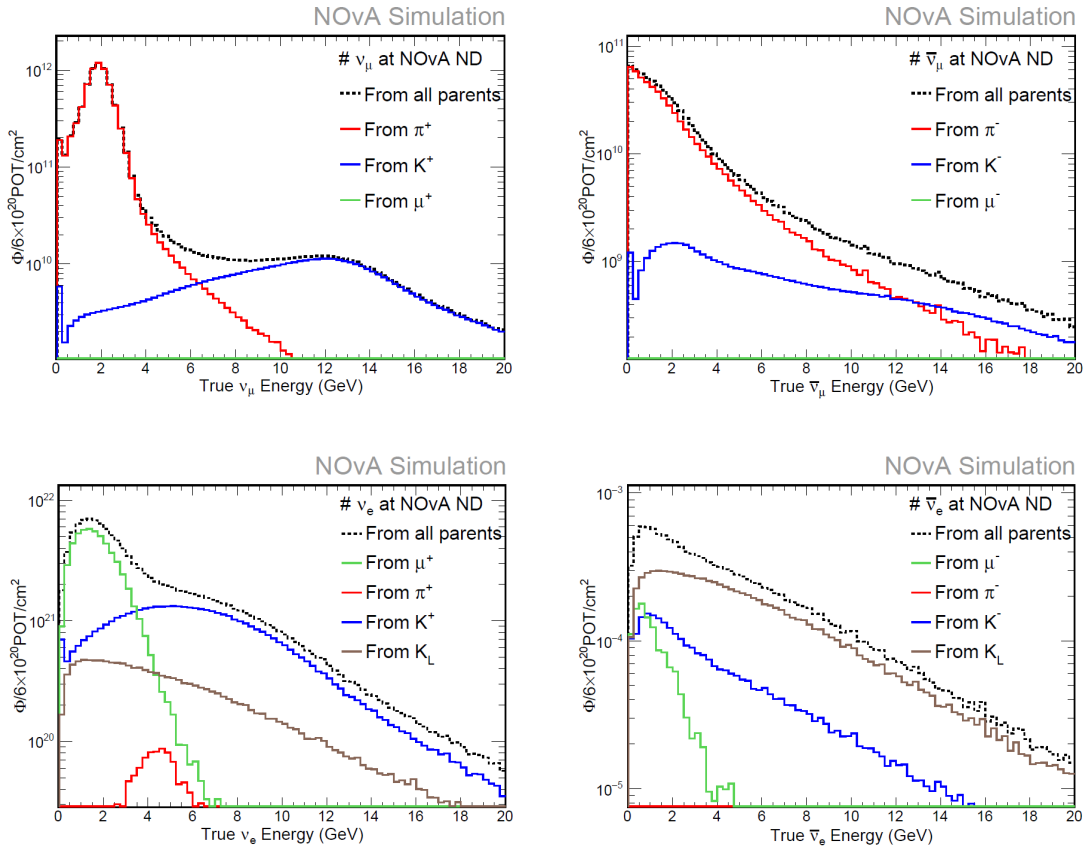

Figure 36: Neutrino (left) and antineutrino spectra at NOvA ND (160).

In an attempt to estimate a general profile of the detector response to LDM signal, a number of simulated LDM signal events corresponding to the 30 MeV mass case were put through the identification method of (148) in order to follow the same path as did the neutrino events that produced the background spectra.

The resulting events were single EM-showers with an energy spectrum vanishing around 10 GeV (see Figure 50). The reconstructed $T\theta^2$ distribution shows strong "forwardness" of simulated signal events as well as significant background bellow 0.005 GeV×rad^2, coming mostly from elastic scattering of neutrinos on electrons. This is consistent with current efforts to use bellow 0.005 GeV×rad^2 region for constraining the NuMI beam flux.

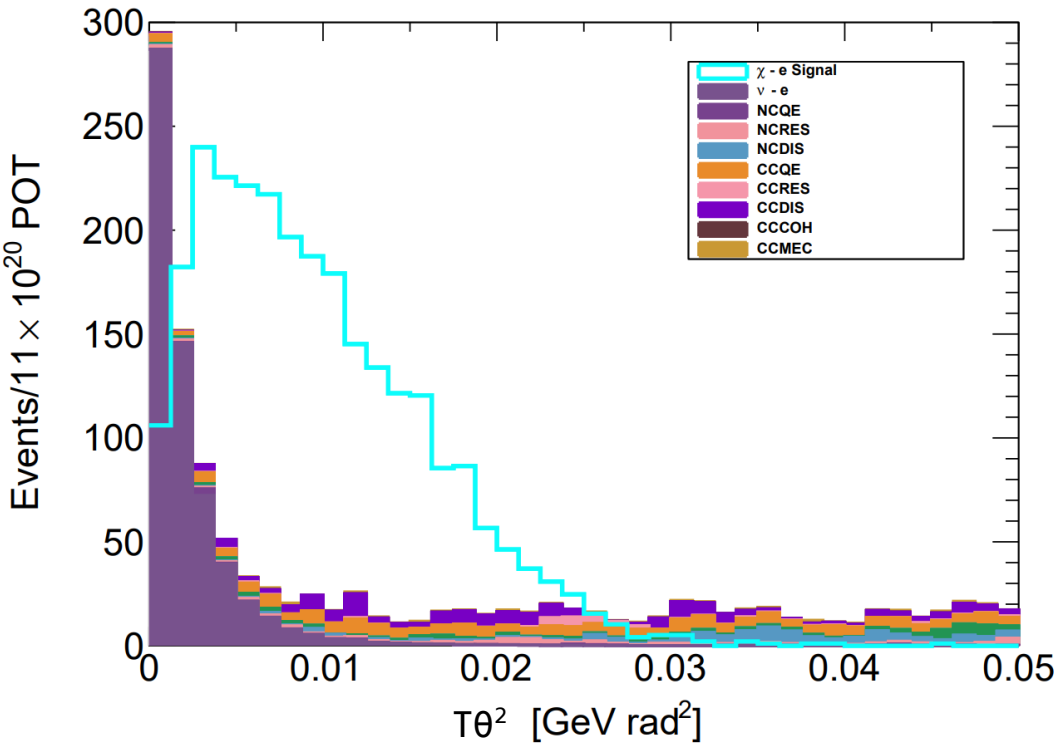

Figure 37: Single EM-showers in the NOvA ND background analysis. All of the expected neutrino interaction channels that have similar signatures are simulated here as the background. Imposed on this background is the simulated EM-showers coming from χ scattering on e. This motivates to use the $T\theta^2$ reconstructed variable for my signal and sideband region definition.

6.2.2 Background flux uncertainties

The uncertainties in neutrino flux prediction come from two principal sources – the beam transport and the hadron production (cross section uncertainty).

The main components of the beam transport systematics come from the maximal shift of range of thickness of the cooling water layer (see in Figure 6 and Figure 38), the size of the beam spot and the focusing horn and target position. Smaller additions come also from the horn current instabilities, beam aiming and the shape of the magnetic field in the horns. The values (totaled at 6.67%) are summarized in Table 2 and further details can be found in (157).

For hadron production uncertainties, which mainly manifest themselves in unknown π and K^+ production rates, I take the conservative 8.78% value from (161), (5), although a thick target tuning capable of lowering this large value by up to a factor of 2 is currently under review (162) (163).

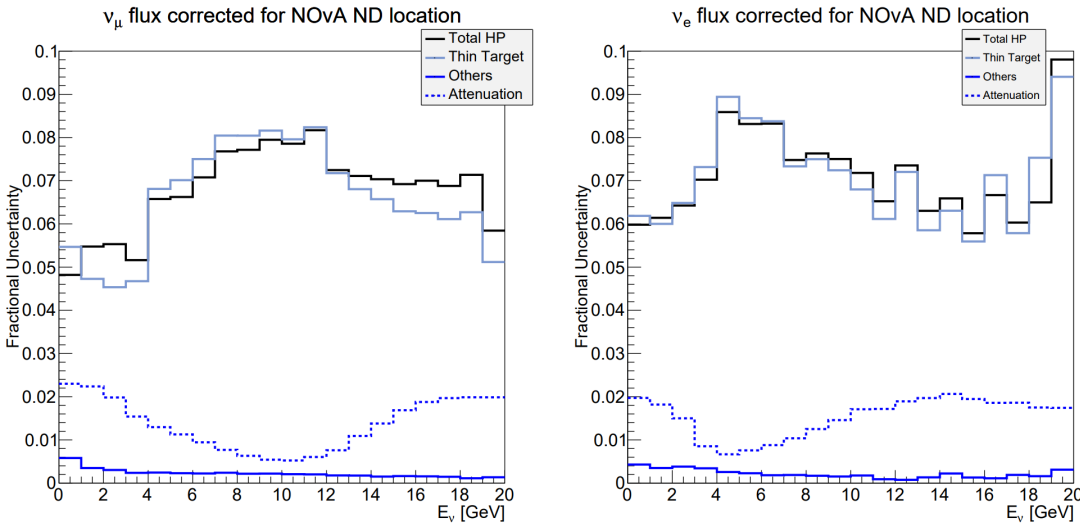

Figure 38: Fractional beam flux uncertainties (163).

Systematic shift	Value [%]
Horn current ±1kA	0.08
Horn 1 X, Y position ±2mm	2.34
Horn 2 X, Y position ±2mm	0.51
Beam on target X position ±0.5mm	0.68
Beam on target Y position ±0.5mm	0.43
Target Z position ±7mm	1.19
Beam spot size 0.9 – 1.5 mm	2.64
Cooling water layer thickness 1±0.5mm	4.60
Quadrature sum	**6.67**

Table 2: Systematic uncertainties in beam transport prediction.

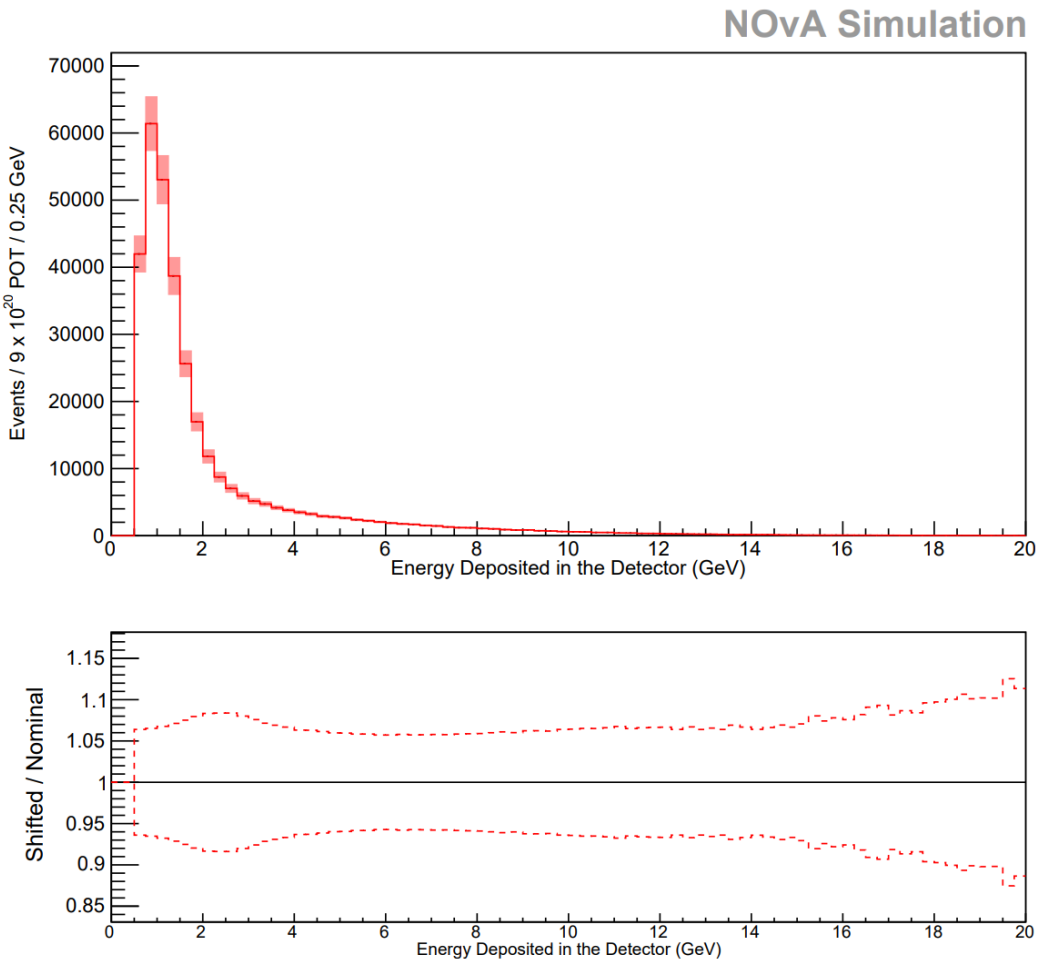

Figure 39: Total beam transport ND systematic uncertainties (161).

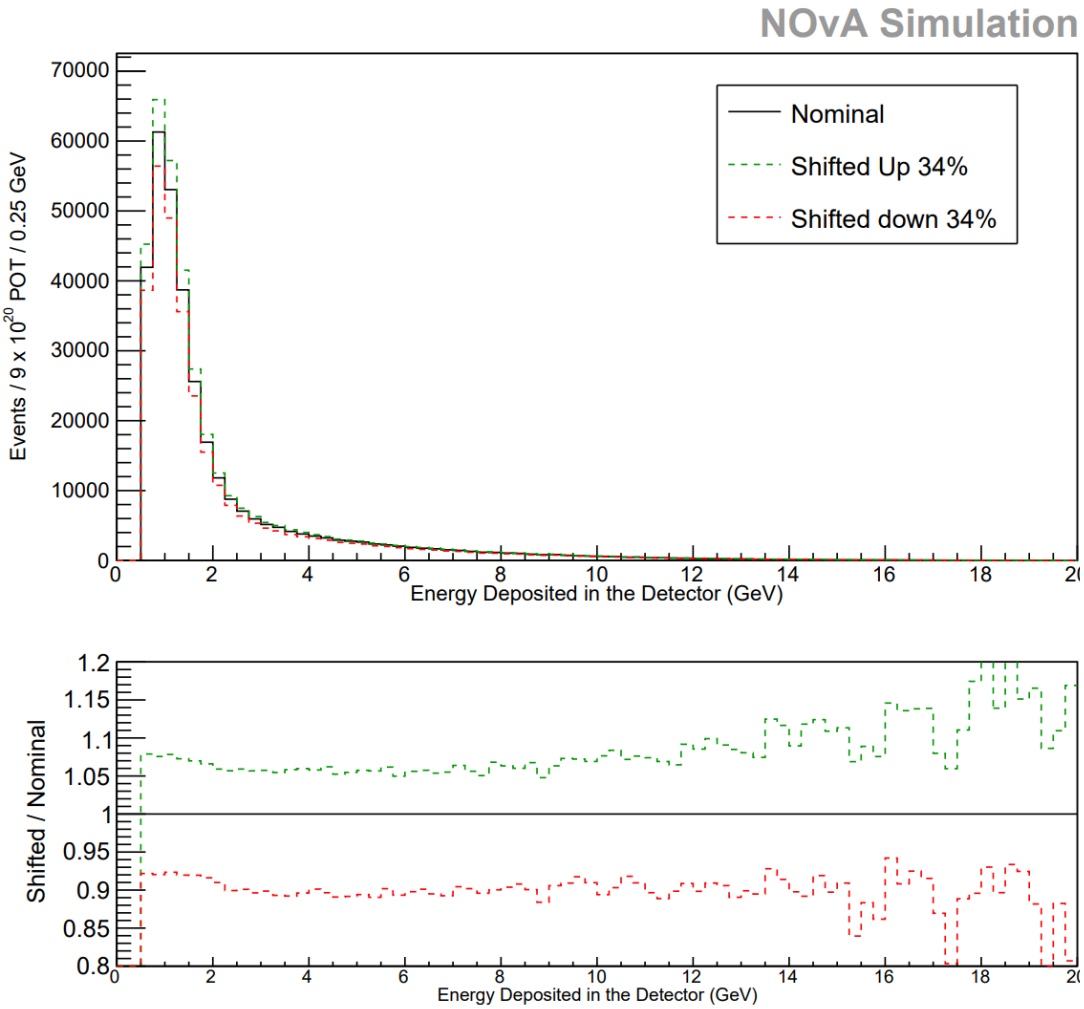

Figure 40: Total ND PPFX beam flux systematic uncertainties (163).

6.3 Signal selection

Section 2.3.2 and ref. (106) show that the probability of neutrinos scattering on nuclei is 10^4 higher than scattering on electrons. The goal of event selection procedure is to maximize the number of signal events and suppress the background (Figure 41). I start with picking only reconstructed events with single EM showers and optimize a set of further criteria to maximize Figure of Merit.

Unlike the FD, the ND is underground, shielded heavily from the cosmic background, so no Cosmic rejection cuts are required. Here I describe the progression of cuts to isolate the signal events of interest. The optimization of each cut was done recursively on a (N-1) cut sample (sample with all cuts applied except the one which is being optimized)

6.3.1 Data quality cut

To minimize the chance of using corrupted data, there is a sequence of strict data-quality cuts applied on the state of the detectors, beam and data. These or similar cuts are used by all NOvA analysis groups and are applied on a per-spill basis.

The beam running conditions are required to have at least 2×10^{12} POT in each spill and timing difference to the nearest beam spill to be 0.5 ns at most. The current in the focusing Horns must be within -202 and -198 kA and the beam has to aim 0.02 – 2.00 mm on target with 0.57 – 1.58 mm beam width in both X and Y coordinates. All spills also must have all DCMs present (0 missing DCM configuration) and the ambient noise metric (hit fraction from "Lights-on Effect" – noise coming from ambient light photons) can be max. 0.45.

To ensure good reconstruction, individual events must have at least one vertex and one prong reconstructed, at least three contiguous planes included and a maximum activity of 8 hits per plane.

6.3.2 Preselection

There is also a pre-selection cut present in majority of ND analyses to trim the data and increase the computing efficiency. It is safe to use a cut similar to ν_e appearance analysis (2), (7) pre-selection (or even looser) to remove obvious muon events. The preselection cut makes sure at least one 3D track has been reconstructed. It only picks tracks shorter than 800 cm (Figure 51), reconstructed from hits in less than 600 cells across less than 120 planes (Figure 42).

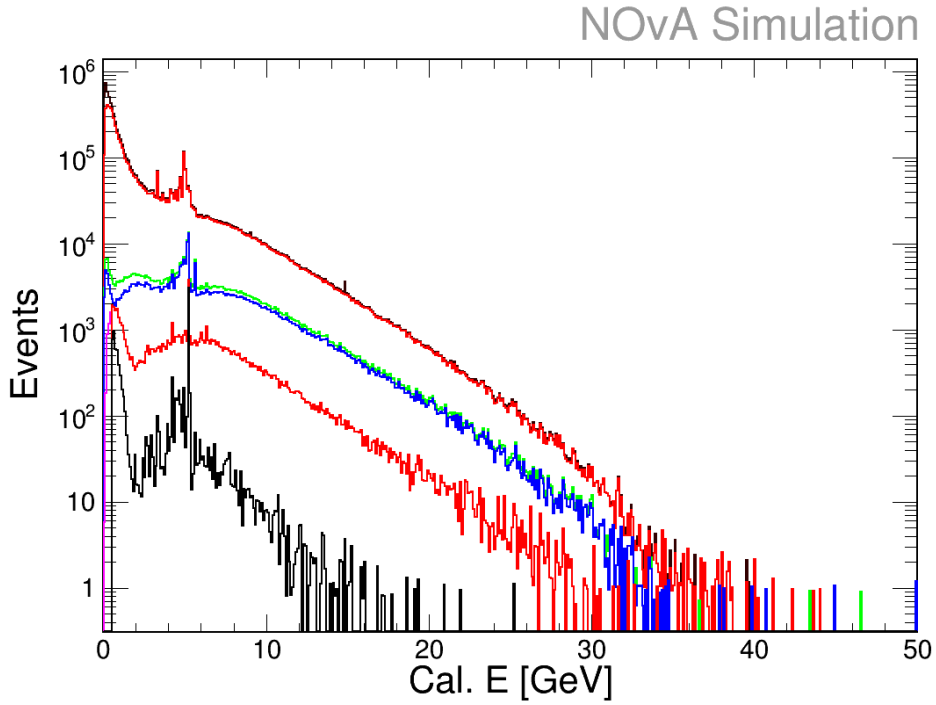

Figure 41: LDM cut flow progression without energy cut.

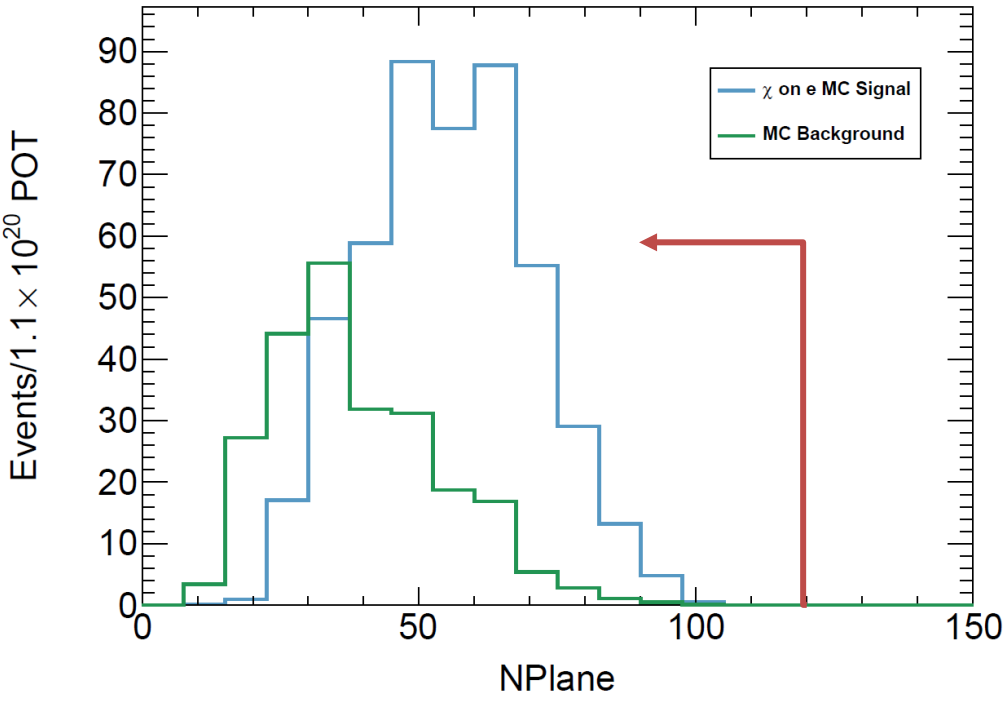

Figure 42: Distribution of number of planes included in reconstructed shower.

6.3.3 Fiducial volume

The fiducial cut (examples in Figure 43, 44, 45) ensures that the showers are induced by particles inside the detector, removing activity resulting from interactions in material surrounding the ND (mostly rock). This cut requires the reconstructed vertex to be:

- Min X > -180 cm, Max X < 180 cm
- Min Y > -180 cm, Max Y < 180 cm
- min Z > 50 cm, max Z < 1250cm

6.3.4 Containment

The containment cut only selects events, which are fully contained in the detector volume with no activity escaping the detector. It filters events which have any hits in any reconstructed prong 50cm or closer to front, back, east or west face of the ND, 10cm from bottom and 100cm from the top of the detector:

- Min. distance from all prong start/stop distances to ND Top > 100 cm
- Min. distance from all prong start/stop distances to ND Bottom > 10 cm
- Min. distance from all prong start/stop distances to ND East > 50 cm
- Min. distance from all prong start/stop distances to ND West > 50 cm
- Min. distance from all prong start/stop distances to ND Front > 50 cm
- Min. distance from all prong start/stop distances to ND Back. > 50 cm

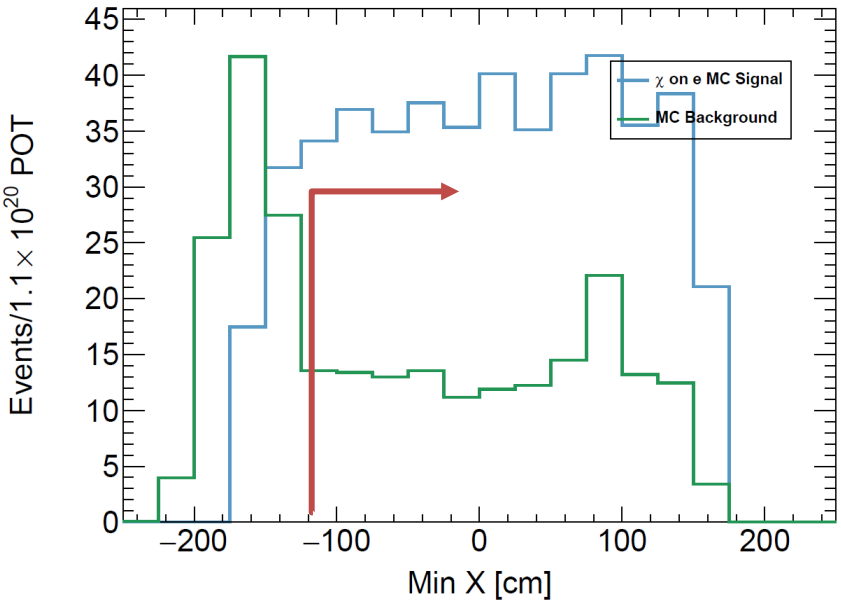

Figure 43: Distribution of minimum hits in X coordinate.

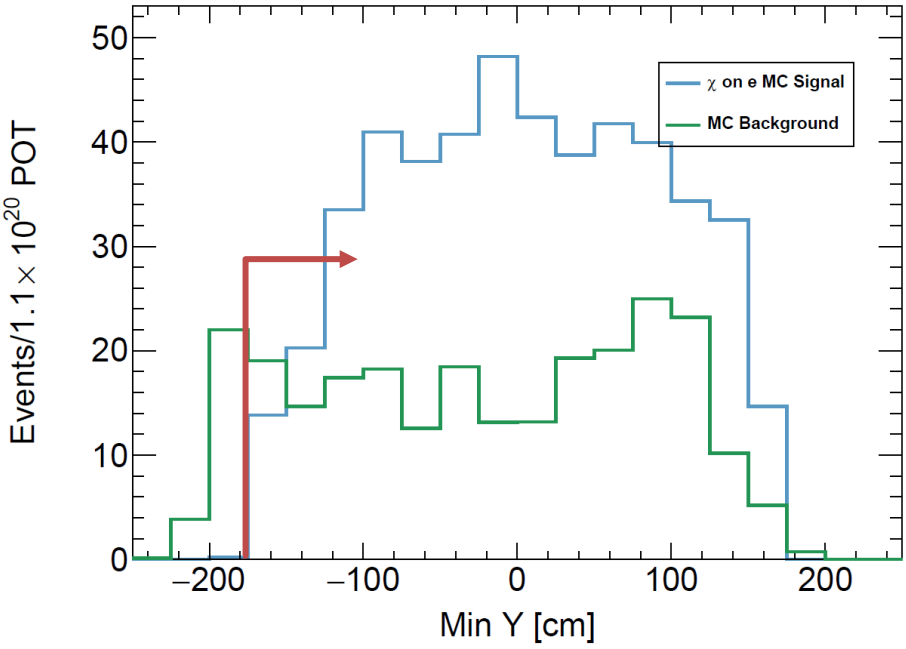

Figure 44: Distribution of minimum hits in Y coordinate.

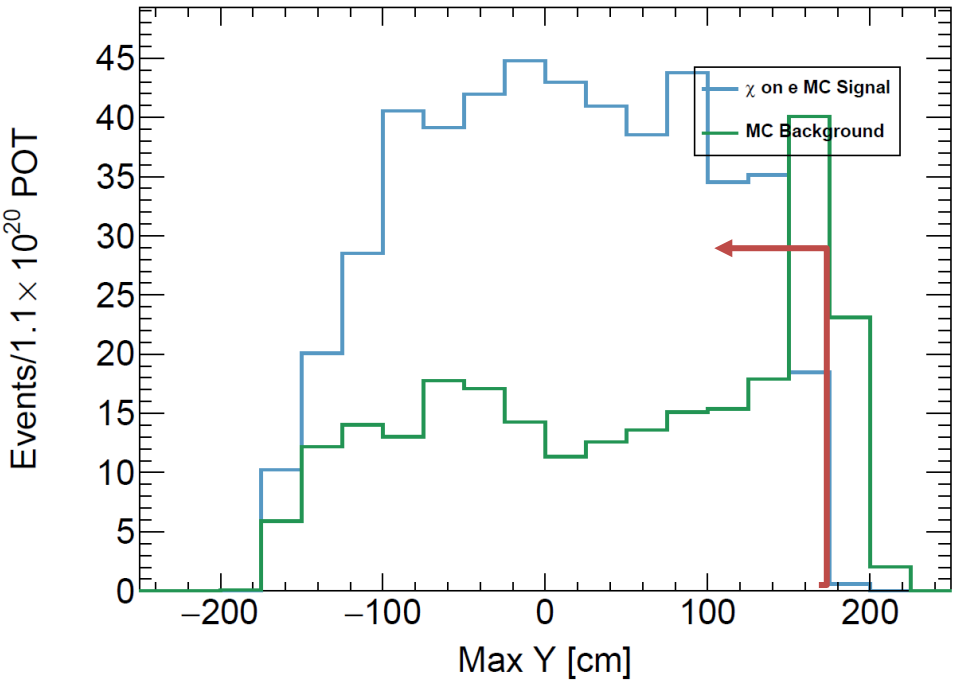

Figure 45: Distribution of maximum hits in Y coordinate.

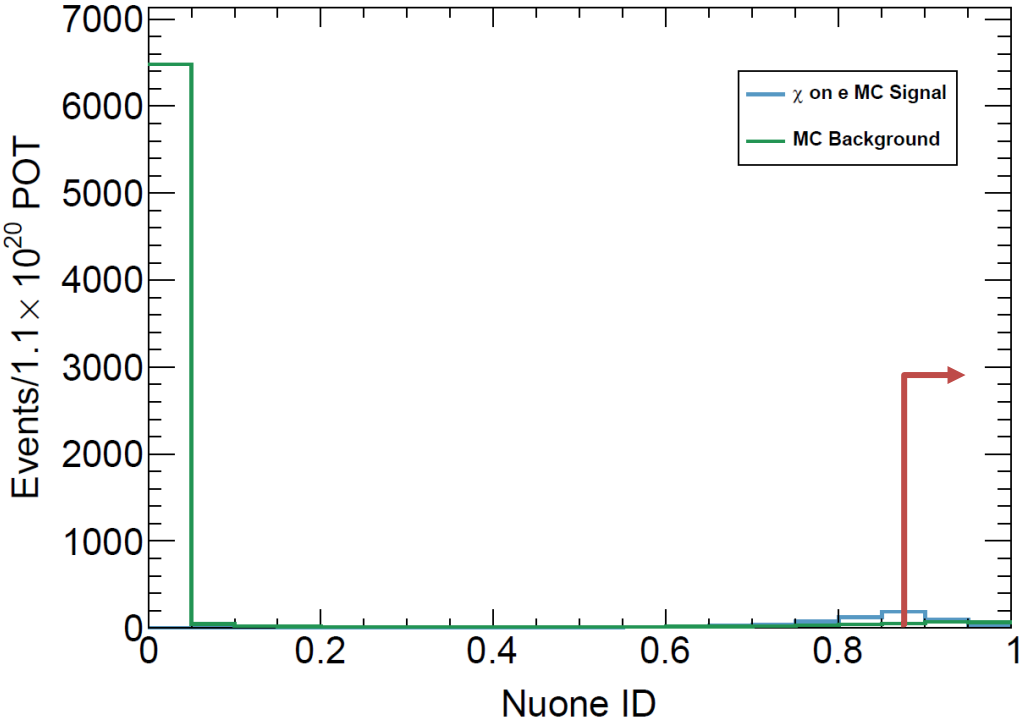

Figure 46: Nu-on-e PID CVN scoring.

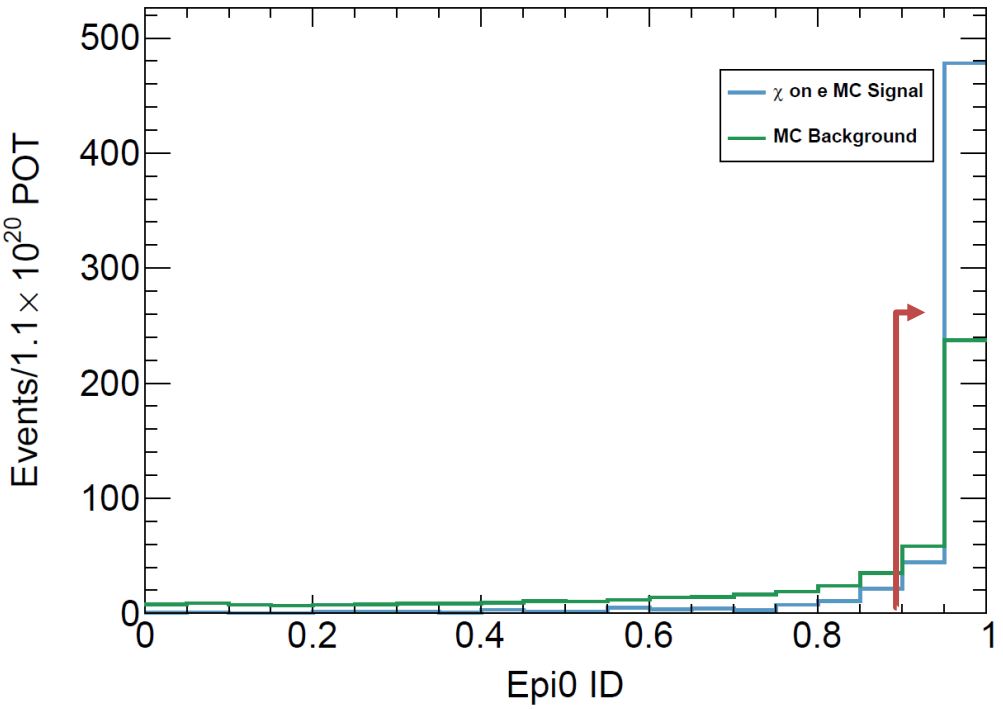

Figure 47: e/π^0 PID CVN scoring.

6.3.5 PID score

To select single electron EM showers, the v-e CVN described in section 624.3.2 is used with 0.9 threshold out of a score of 1 (Figure 46). To remove as much of dominant π^0 coherent interaction background as possible, an additional PID cut for e/π^0 scoring above 0.8 out of 1 is implemented (Figure 47).

6.3.6 Shower energy

To select single EM shower events, the energy requirement on a single shower (primary) is 90 percent of the total deposition ($E_{shower}/E_{tot} > 0.9$ GeV) and it must have started with zero vertex energy (no deposition up to 8 planes from vertex). The gap between the shower start and the vertex must be shorter than 20 cm, and the low energy electrons (bellow 0.5 GeV) as well as events above 15 GeV are discarded to ensure optimal PID scoring (Figure 50). The simulated signal and background distributions with cuts are plotted in Figure 48 and Figure 49.

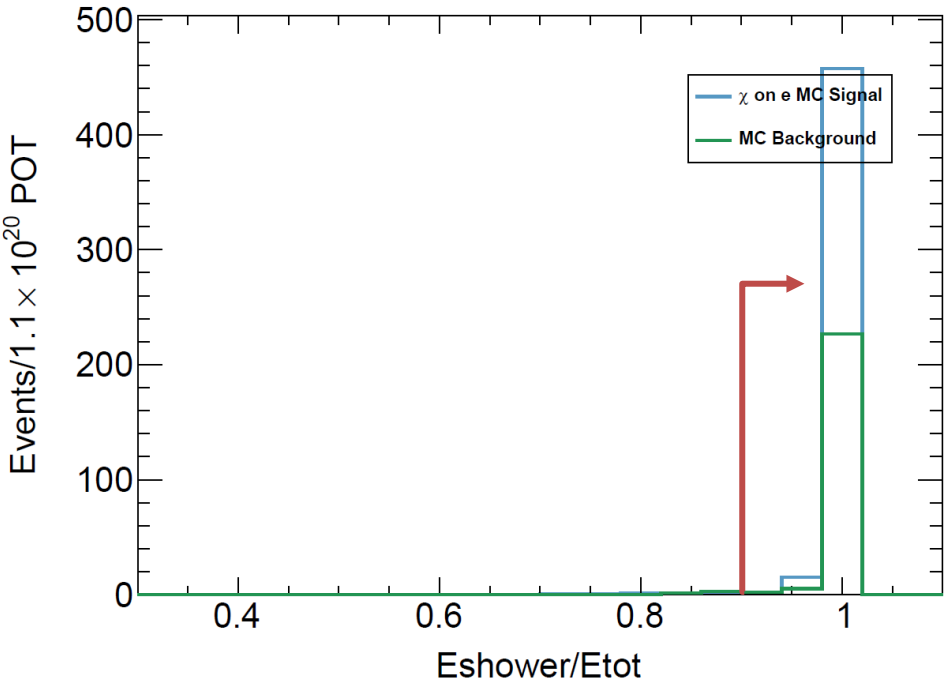

Figure 48: The distribution of E_{shw} to E_{tot} ratio.

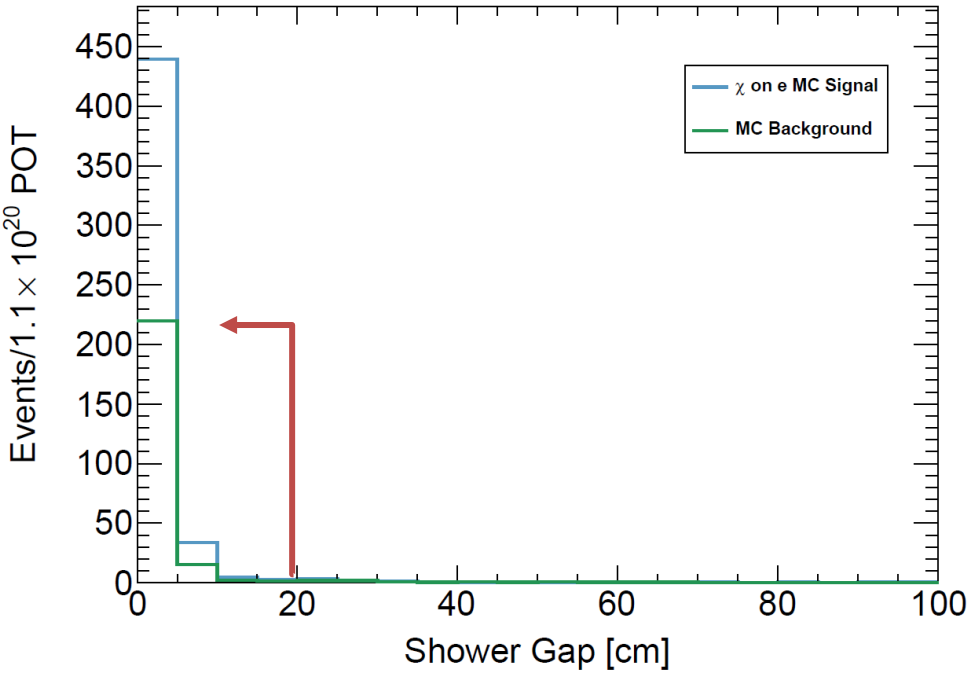

Figure 49: The distribution of the gap size between the reconstructed vertex and first hit included in the shower.

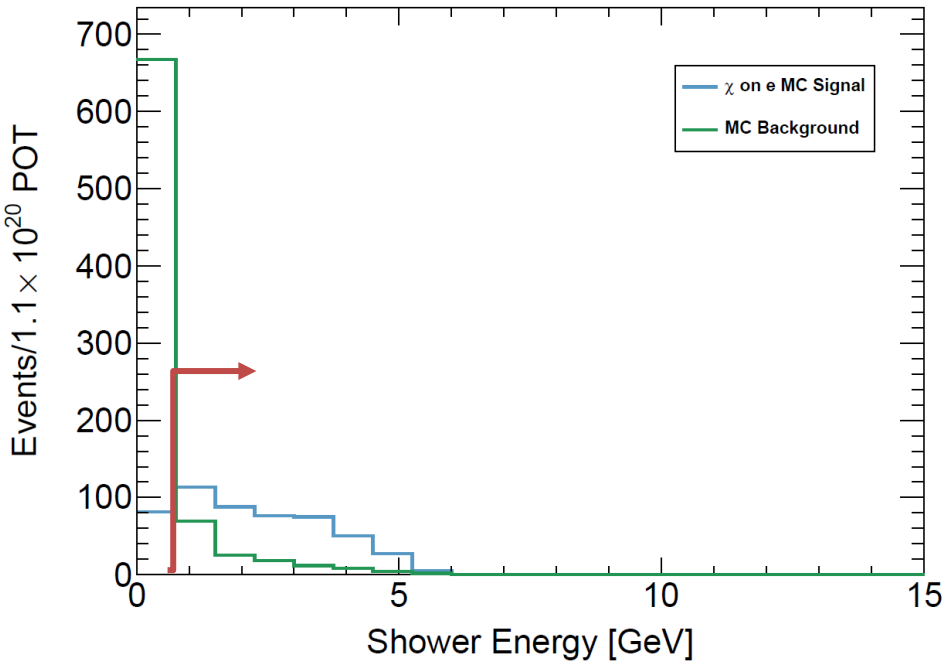

Figure 50: The spectrum of reconstructed shower energy.

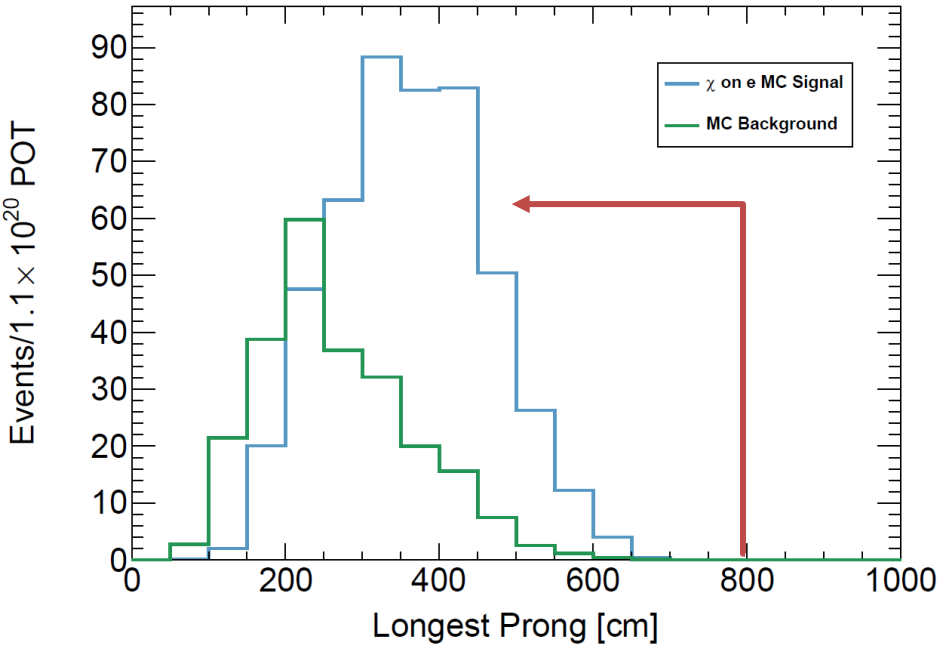

Figure 51: The maximal length of reconstructed prong.

6.3.7 Angular cut

The last step of the signal selection procedure splits the analysis in the sideband region and the blinded signal region. This is achieved by imposing a $T\theta^2$ cut on selected single EM showers (see Chapter 2.3.2). For the sideband analysis, we only consider events with $0.05 < T\theta^2 < 0.10$.

For "opening the box" (unblinding the signal region) and looking at the data, I eventually rerun the same analysis cut sequence with $0.005 < T\theta^2 < 0.03$ GeV×rad^2 final cut. Both region cuts are marked in Figure 52.

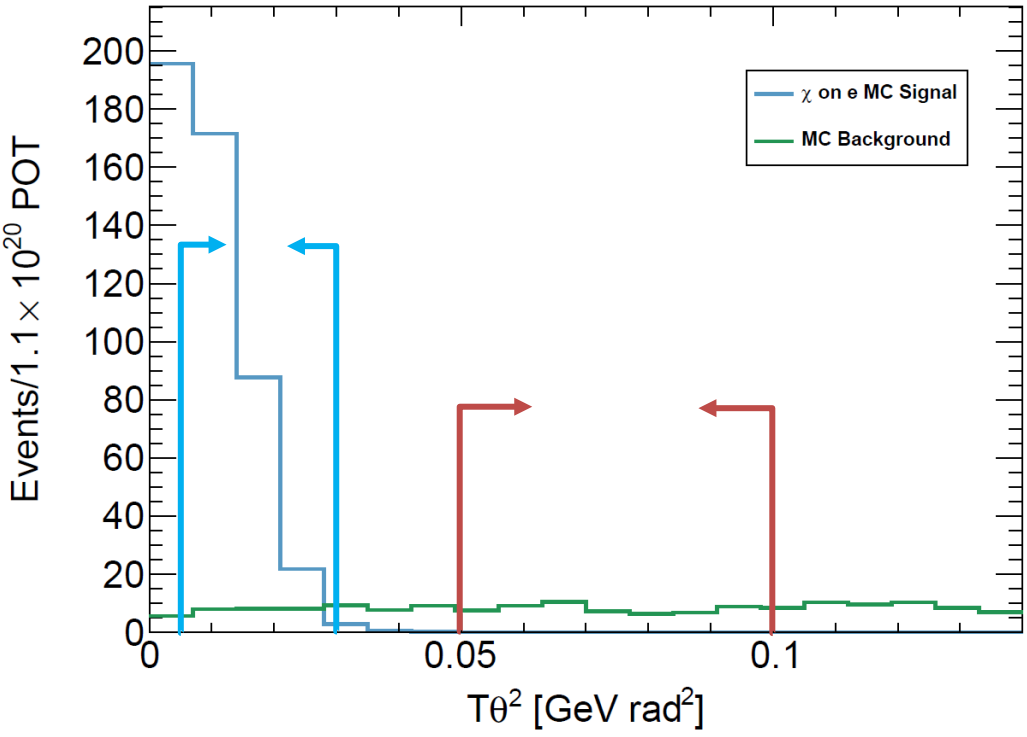

Figure 52: $T\theta^2$ cut describes the forward-going feature of the shower (electrons are boosted among the beam direction in very small angles). The background dominated sideband region is marked with red arrows, signal region for event counting with cyan arrows between 0.005 and 0.03 03 GeV×rad^2. More detailed background composition breakdown is in Figure 37.

6.4 Sideband validation

In the region of $0.05 < T\theta^2 < 0.10$, I can compare the MC to Data to verify the signal selection criteria and constrain the background flux. Due to mismodelling and systematic uncertainties, a background normalization is regularly done on the Data/MC difference. This correction can be then potentially applied in the signal region or further investigated for flux prediction tuning.

Using the MP5.1 dataset of 1.1×10^{20} POT, the observed data in sideband region are in good agreement with total simulated background (plotted in Figure 53).

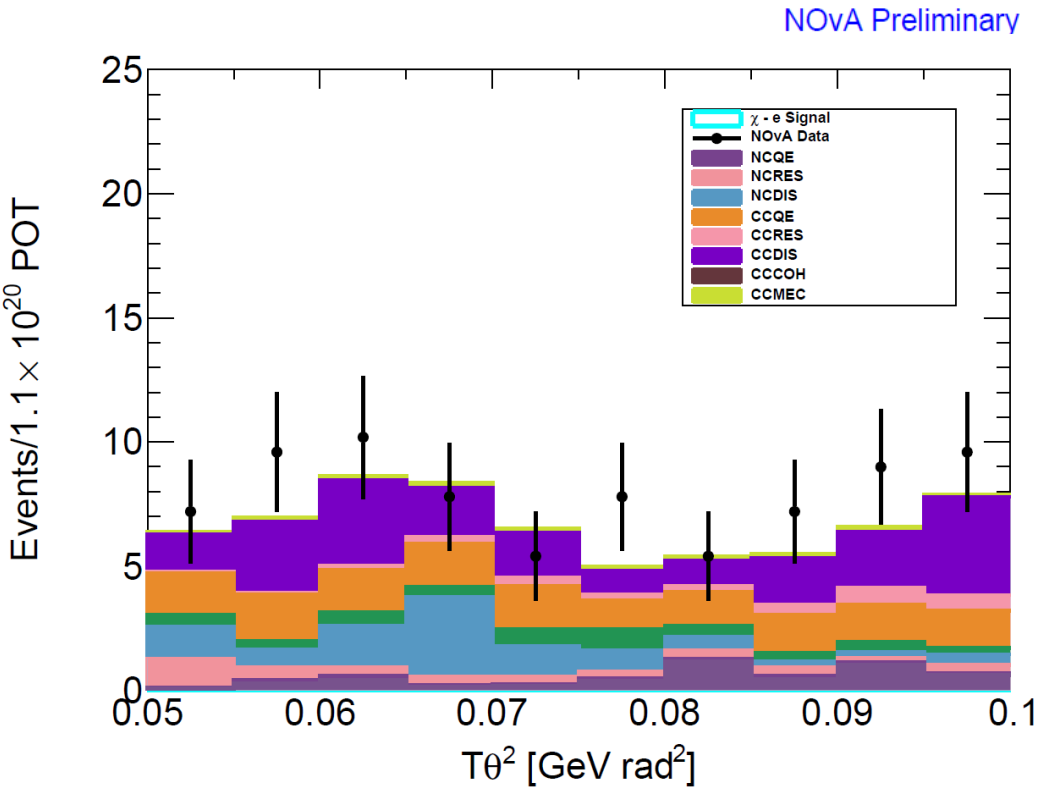

Figure 53: Scattered electron angular energy distribution in the sideband region is in good agreement with 1.1×10^{20} POT data sample.

6.5 Event counting

After validating the analysis on the sideband region and freezing the code, I can now look at the signal region (so called unblinding or box opening). The total number of expected events in $0.005 < T\theta^2 < 0.03$ GeV×rad^2 range is 431, with 269 events coming from hypothetical χ scattering on e and 162 events from various background.

With all selection criteria, I observed $182 \pm 19.79^{(syst.)} \pm 12.56^{(stat.)}$ events in the signal region. The resulting $T\theta^2$ distribution is plotted in Figure 54 together with breakdown of various background MC and expected LDM signal overlay. I found no evidence of LDM in the NOvA Near Detector.

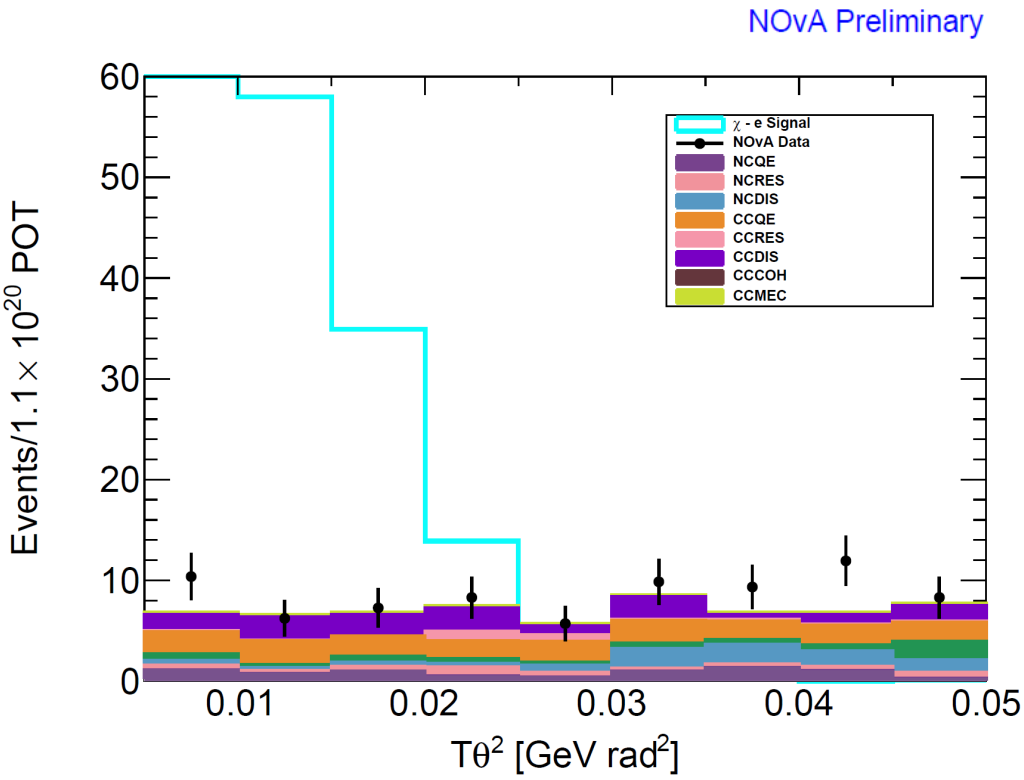

Figure 54: Scattered electron $T\theta^2$ distribution in signal region. The integral of observed events in measured data is $182 \pm 19.79^{(syst.)} \pm 12.56^{(stat.)}$. The data points are plotted against a sum of 169 background events in solid colors and cyan outline of hypothetical LDM events prediction. I found no evidence of LDM signal in analyzed data of 1.1×10^{20} POT.

6.6 Uncertainties

There are more than 80 different sources of systematic uncertainty in NOvA mainstream analysis suite (164). They can be categorized into 5 major groups with significant additions to total uncertainty of LDM analysis: detector calibration, detector response, cross section, beam flux, and other uncertainties.

To evaluate effect from each uncertainty source, a set of standardized MC simulation samples were made by NOvA production group in Production 5 campaign with values shifted up and down to their maximum and minimum values. The simulation is normalized to 9×10^{20} POT. I use these files to evaluate the

up and down shifts in the LDM analysis and plot some examples in Figures 55, 56 and 57.

In this section, I analyze the systematic uncertainties, coming mainly from the limitations of calibration, selection criteria, and mismodelling in MC simulation. The beam flux uncertainties were described in 5.2.2.

6.6.1 Calibration

The calibration systematic uncertainties come from the shifts of scale correction in transformation from collected amount of light to energy in MeV (PEcorr, shifted up or down by 5%), and from the shape variation of attenuation in the fiber. The attenuation correction is made cell by cell (from through going muons) and the shifts are applied both to relative and absolute uncertainties. The resulting total detector calibration uncertainty of 3.39% is plotted in Figure 55.

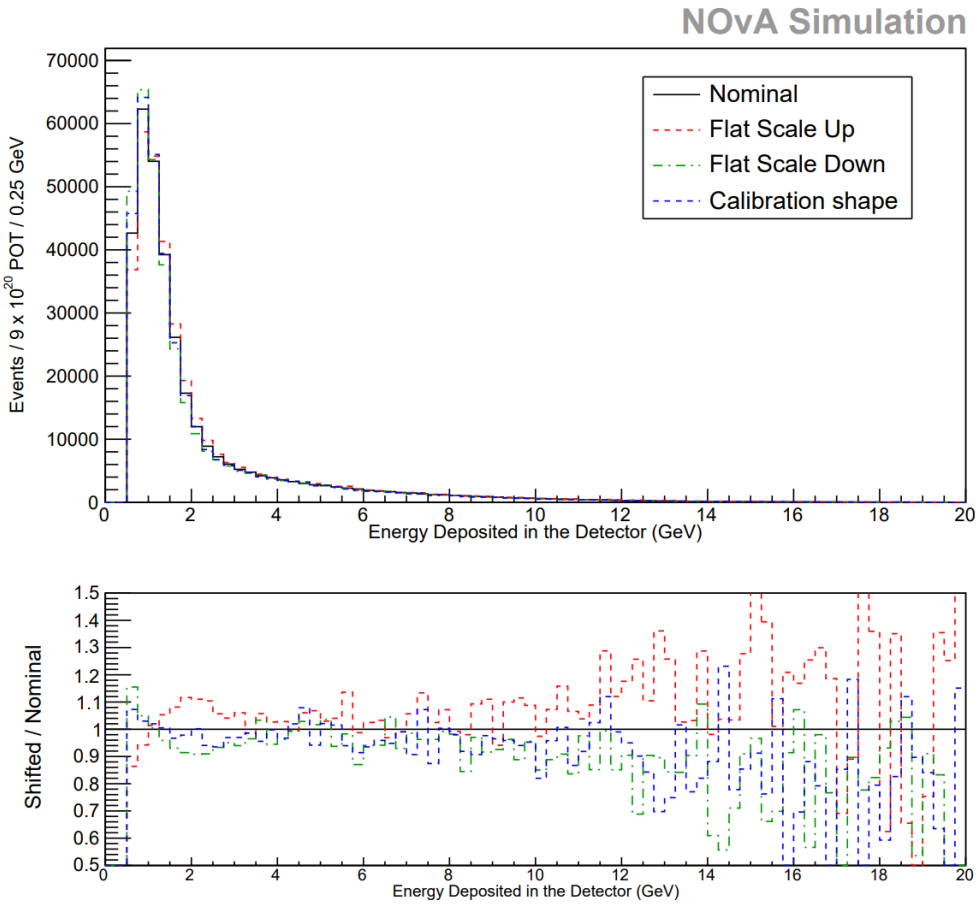

Figure 55: ND absolute scale and shape calibration systematic uncertainties.

6.6.2 Light level

There is a 3% downward difference observable in data/MC *dE/dx* matching of Čerenkov light. The corresponding uncertainty is 1.24% (Figure 56). The scintillation light attenuation is modelled using the regular Birks law first-order parametrization with 5% disagreement between the high and the low tail (0.45% uncertainty, Figure 57). Total detector response uncertainty is 1.68%.

6.6.3 GENIE simulation

The GENIE MC simulation uses more than 70 parameters to model the cross sections, hadronization and final state interactions. Although the GENIE simulation uncertainties are dominant in oscillation analysis (exceeding 10% uncertainty in some cases), by using the purely leptonic channel, I avoid using the models of hadronic and deep inelastic processes, which have limited accuracy and are now under rapid development. Total cross section uncertainty is 7.64%.

6.6.4 Other systematics

There are some other uncertainties with minor significance. The normalization uncertainty consists of 0.5% error in POT counting and 0.28% of ND mass uncertainty. There is also minor uncertainty from the beam flux monitor. Other effects like acceptance effect, intensity effect, time-dependency, GEANT physics lists, wrong sign mismodeling or neutron mismodeling are negligible and I sum them all into a total normalization uncertainty of 1%.

Uncertainty source	Value
Detector calibration	3,39%
Beam flux	6,67%
Detector response	1,68%
GENIE cross section simulation	7,64%
Normalization	1,00%
Quadrature sum	**10,87%**

Table 3: Breakdown of systematic uncertainties with their sum in quadrature

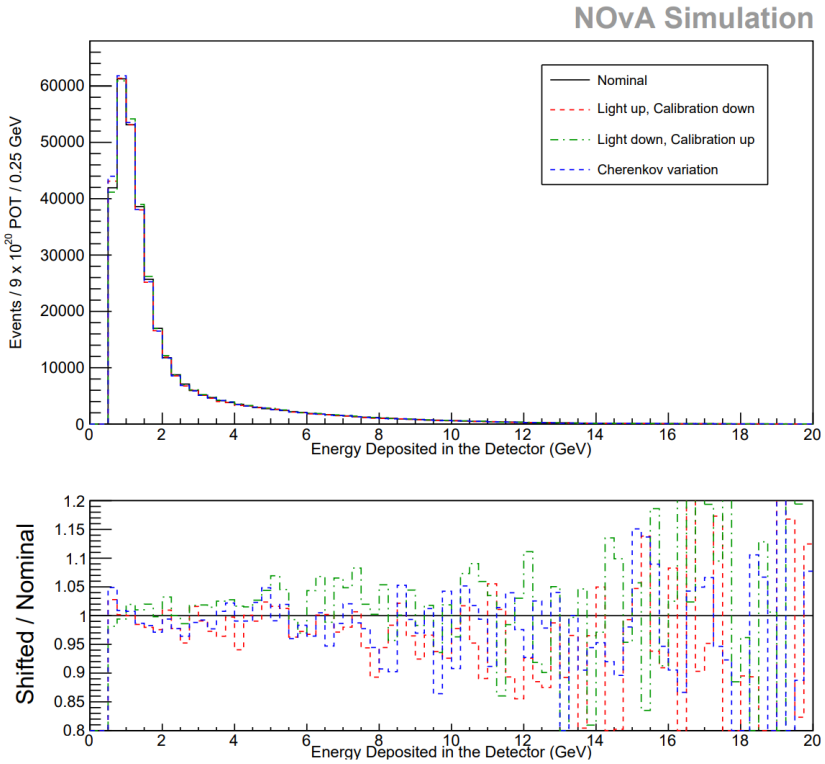

Figure 56: ND total light level systematic uncertainties.

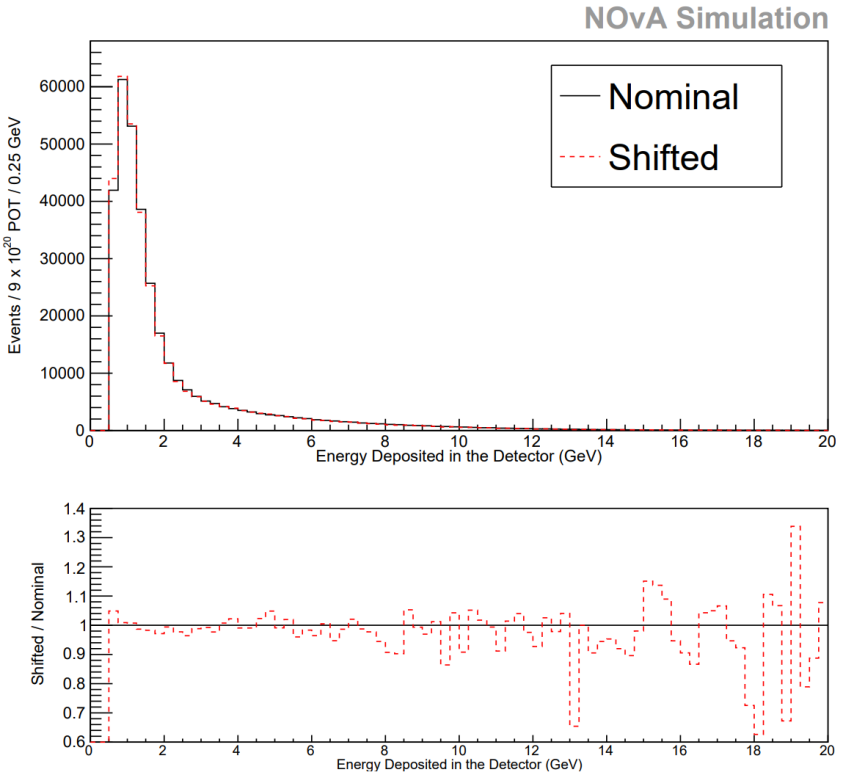

Figure 57: ND Čerenkov systematic uncertainties.

6.7 LDM upper limit

The experimental sensitivity (not dependent on a given model) is evaluated with the number of signal events excluded at a certain Confidence level (C.L.) limit, traditionally chosen to be 90%. The number of events expected to be observed in the detector:

$$N_{sig} = \sigma_{\chi e} \epsilon_{ND} \Phi_{\chi} N_e, \tag{16}$$

where $\sigma_{\chi e}$is the cross section for LDM particle scattering on an electron, ϵ_{ND} is the total acceptance of the ND (including efficiency), $\Phi_{\chi}$is the total flux of LDM particles and N_e is number of electrons present in the ND (here I take fiducial volume defined by signal selection criteria and average electron density of 4.13×10^{29} electrons in m^3).

Because the number of observed events is reasonably large and there are no other conditions or theoretical model assumptions about the variable, I can calculate the upper limit of the unknown measured variable. Using a relation between the Poisson and χ^2 distributions in frequentist approach from (165), we can say that an experiment is sensitive to signal if the number of events is greater than the 90% C.L. exclusion upper limit (166). In this approach, my LDM sensitivity threshold can be expressed as:

$$\sigma_{\chi e} \Phi_{\chi} \geq \frac{N_s^{90}}{\epsilon_{ND} N_e}, \tag{17}$$

where

$$N_s^{90} = \frac{1}{2} F_{\chi^2}^{-1}\big(90\%; 2(N_{obs} + 1)\big) - N_B, \tag{18}$$

for which we calculate a corresponding inverse cumulative distribution function (quantile $F_{\chi^2}^{-1}$ of the χ^2distribution) with single right tail (165).

With number of observed events $N_{obs} = 182$, background $N_B = 161{,}38$ and significance level α=0.1 (C.L. 90% is 1-α = 0.9), I get threshold event number:

$$N_s^{90} = 39.16$$

This upper limit of observed events can be then put to relation with the mixing parameter - using the equations 11 from 2.3.2 and 15 from 3.4.1 with my example set of $3m_\chi = m_V = 90\ \mathrm{MeV}$ and HS parameter $\alpha_D = 0.5$, such limit corresponds to

$$\epsilon = 1.6 \pm 0.28 \times 10^{-5}$$

6.7.1 Result generalization

To be able to compare between different models and experiment performances, the DM community is often using ϵ rescaled to the self-annihilation parameter *Y*, as mentioned in the introduction in 1.1:

$$Y = \epsilon^2 \alpha_D \left(\frac{m_\chi}{m_V}\right)^4 \quad (1)$$

This also allows us to compare results so various cosmological constraints, with aim on correct abundances of thermal relic DM (*Y* controls the DM annihilation cross section).

With above calculated upper limit of ϵ and using the values of my model example ($\alpha_D = 0.5$ and $3m_\chi = m_V = 90\ \mathrm{MeV}$) and calculated uncertainties, I get the upper limit for self-annihilation parameter

$$Y = \epsilon^2 \alpha_D \left(\frac{m_\chi}{m_V}\right)^4 = 1.6^2 \cdot 10^{-10} \cdot \left(\frac{30}{90}\right)^4 = \mathbf{1.59 \pm 0.28 \cdot 10^{-12}}$$

The choice of production channel, HS particles masses, and fine structure parameters allows me to generalize my result to wider range of masses, as both production and detection processes are the same for all these models.

Therefore, I can simply normalize the upper limit (exclusion) threshold to other parameters set of masses with fixed $\alpha_D = 0.5$ and $3m_\chi = m_V$. Although different values of α_D would also only change the scale (number of events) and maintain same signatures and kinematics behavior, the choice of $\alpha_D = 0.5$ offers direct comparisons with results from i.e. MiniBooNE (104) or future sensitivities of DAEdALUS (13) or other proposed facilities.

This choice also covers much more parameter space than much lower, already well covered values (i.e. 0.05), but because of linear dependence of total event rate, the results are easy to extend to these regions to cover more space.

The mass ratio between the parent vector Dark photon as a Neutral Vector mediator and a pair of scalar DM into which it decays, can be also changed within the condition of $2m_\chi < m_V$ with kinematics staying reasonably similar within a few percent as shown in the initial simulation in 3.1.4, but again, the choice of $3m_\chi = m_V$ is not random and allows us to compare with findings from various other measurements.

Using the rescaling from Eq. 1 and calculating with different masses m_χ, m_V, I can eventually draw the resulting upper limits of *Y* depending on the dark scalar mass m_χ. The resulting generalized upper limit contour is plotted in Figure 58 and is also the main outcome of this analysis.

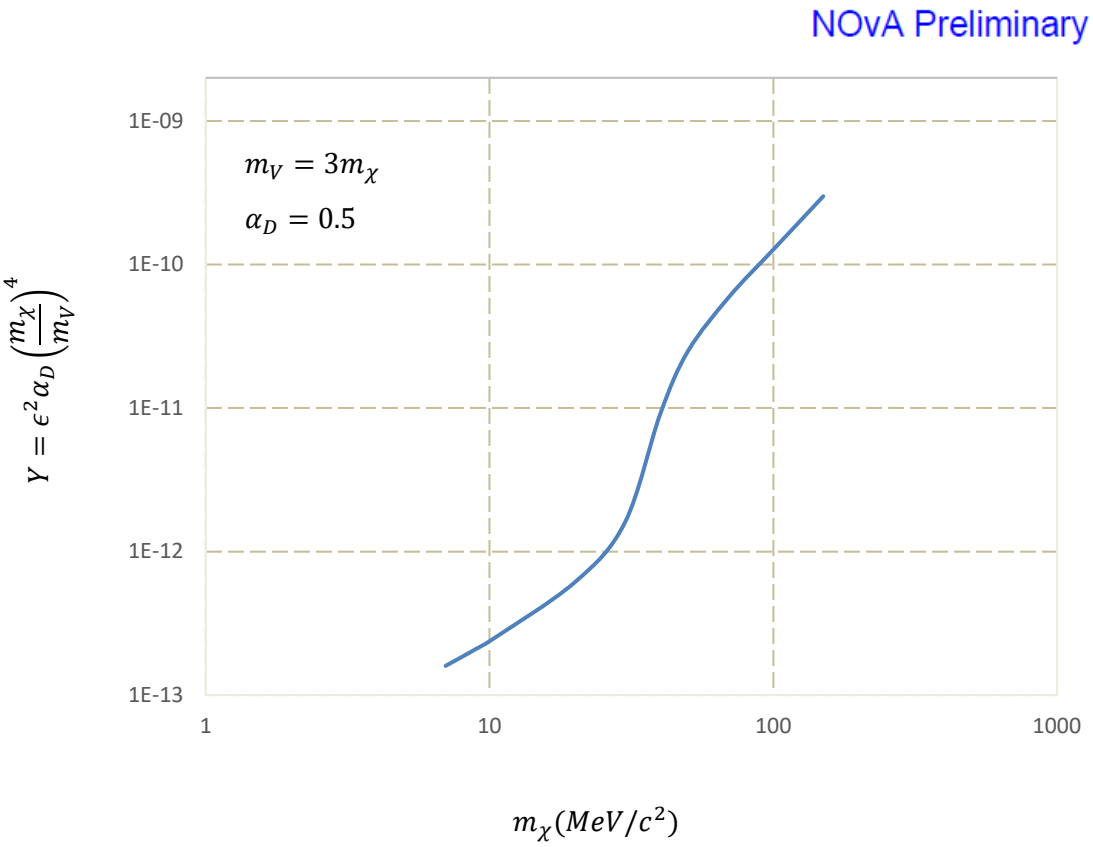

Figure 58: Extended result of maximal value (90% C.L. upper limit) of self-annihilation parameter *Y* with fixed parameters of $\alpha_D = 0.5$ and $3m_\chi = m_V$. The fitted sensitivity curve is based on observing no evidence of 30MeV LDM scattering inside the NOvA Near Detector.

7 Conclusions

I have presented a demonstration of a New Physics example of the Neutral Vector Portal model postulating the production of a vector mediator particle of mass 90 MeV in the proton on proton collisions at the NuMI neutrino source which feeds the NOvA long baseline neutrino experiment. I was able to show that re-interpreting the NuMI/NOvA complex at Fermilab as a proton beam-dump experiment can provide a thorough test of the postulated LDM produced in a high intensity proton beam with a mass range m_χ of few MeV up to ~7.5 GeV. The sensitivity of the detection system was discussed in respect to studies of Lightweight dark matter particles, created in pairs through the decay of the vector mediators into a neutral scalar and then scattered off atomic electrons in the NOvA ND.

At the projected NuMI beam delivery on target and current maturity of the NOvA software suite for particle reconstruction and identification at energy ranges above the main NOvA neutrino oscillation signal, I was able to demonstrate an initial upper limit of

$$\boldsymbol{Y \geq 1.59 \pm 0.28 \cdot 10^{-12}}$$

on a $3m_\chi = m_V = 90$ MeV model example at 90% confidence level, analyzing a 10% fraction of the total available data sample, clearly surpassing best currently published limits (from MiniBooNE measurements (103)). Generalizing the result for similar parameter sets, the upper limit of *Y* is order of magnitude lower (10^{-13} – 10^{-12}) than current results from world-leading experiments. Projecting to the full data sample, NOvA will be able to exclude the regions of sub-GeV candidates from this family of models alone utilizing the scattering on atomic electrons channel.

7.1 Discussion

Due to the model independent attitude of this study, the distributions of LDM and their interaction products have been normalized to themselves, even when they are estimated specifically for the NOvA ND. In order to compare them to the neutrino background level, they must be scaled to the assumptions of each model they are meant to constrain.

The production cross section of the mediator particles at the target was used above (section 3.4.1) to help constrain the flux of the LDM through the NOvA ND. A nominal yearly flux of i.e. $\mathcal{O}(10^{11})$ is enough to leave several thousands of events per year considering the scattering cross section of LDM on the atomic electrons of the organic material of the 290-ton NOvA ND fiducial volume within the same model.

The currently interesting range for this scattering cross section is within 10^{-36} and 10^{-45} cm^2. The former value has been reported as the detection limit by several collider experiments based on mono-jet measurements summarized in (101). The latter is where the "neutrino floor" is expected by direct detection experiments (111). This floor is where the detection sensitivity is such that the cosmic neutrino presence becomes the background for Dark Matter searches. At the cross section high end using an ideal detection efficiency, the signal size in NOvA ND is expected in the $\mathcal{O}(10^3)$ event range per year, dropping by 10 for each factor of 10 drop of the cross section. The sensitivity of NOvA to a given model is defined as the level of statistically significant presence of the expected LDM signal on top of the total, simulated, neutrino interaction background. The comparison with the simulated neutrinos comes from all potential interaction channels and for events that pass the selection cuts defines the detection limit for that given model and the sensitivity to the interaction coupling. For the exclusion and upper limit calculation, I used the χ^2 quantile method, although other frequentists approaches might also be considered (Monte Carlo method or Feldman-Cousins method in case of very low count yields of events).

The neutrino induced interaction spectra that I used for comparison to the LDM event rates was produced in the analysis framework developed by the NOvA experiment (153). The primary selection criteria define the containment of interaction vertices and energy deposition within the detector. The secondary involved the identification and rejection of the elastic scattering on electron signal among with the dominant neutral pion-induced backgrounds (148). The technology used to achieve this uses large simulated event libraries as input for training to artificial convolutional neural network (CNN) software (167), which calculates the likelihood level of the signature identification (particle identification or PID), described in Chapter 4.3.

The potential presence of LDM on top of the neutrino spectra can be an alternative model of filling the "gap" in the shape between the simulated neutrino interactions and the data in this range, if the flux (*i.e.* kaon contribution to beam ν_e) is constrained in a different channel. This is an important condition, which needs to be considered when any sideband normalization is performed.

7.2 Future analysis

This initial analysis of LDM in NOvA ND can be extended in several possible ways, which would push the upper limit of cross section even lower, excluding more of the theoretical phase space for various DM models. Alternatively, same technique can be deployed on different experiments, either already running or proposed, or also modified for searches of signatures of DM belonging to a family of different models, like the heavy neutral leptons.

7.2.1 Total sensitivity

As discussed above, the null observation of the LDM was done on a 1.1×10^{20} POT fraction of the total 63×10^{20} POT expected from the NuMI facility before shutdown planned for 2027. The most immediate extension is to redo the analysis on already measured and processed RHC dataset (the anti-neutrino run), which now corresponds to 12.5×10^{20} POT of processed and reconstructed ND data (total FD FHC exposure for prod5 era recorded until 26th of February 2019 is 14.23×10^{20} POT).

Although the reconstruction tools and the background PID and selection criteria perform differently for the RHC data, the flux of LDM would not be altered by horn configuration (FHC vs RHC), as I assume LDM production from immediate mediator decay at the target area, and particles involved in these scenarios are not affected by the magnetic horns (or rather their configurations). Given the linearity of formulas considered above, the upper limit is directly proportional to exposure, providing a path to reach order of magnitude lower values of upper limits on *Y*. Joint FHC+RHC analysis would be a natural next step in a pursuit to entertain as much data as possible in standalone LDM analysis.

7.2.2 Beam uncertainty improvements

Another possibility to increase the sensitivity is to improve the reconstruction and particle identification efficiencies.

A significant effort was made to modify the default GENIE v2.12.2 and v3.0.6 models to enhance the agreement between the NOvA ND data and simulation, mainly for selected muon-neutrino candidates. A correction model on quasi-elastic (QE) and non-resonant pion production predictions, improved nuclear models for QE scattering kinematics and suppression of low Q^2 resonant pion production were proposed and successfully implemented and a publication describing this tuning is currently under review (162). This improvement will aid any future NOvA analysis, including LDM scattering.

Looking into the future, this research with the anticipated capability extensions of the reconstruction and identification of electromagnetic showers, including the inclusion of the ND Muon Catcher into the chain, at the high end of the interactions in the NOvA ND, will improve the sensitivity of NOvA by a factor of ~2.

This effort is mainly driven by an extensive deployment of deep learning techniques, such as the neural networks we already use for classification in NOvA. A third generation of deep learning PID methods using TensorFlow was recently implemented into CVN for NOvAsoft. An investment in similar capabilities for the hadronic showers in the signals, combined with critical improvements from the community of neutrino interaction simulation generators, would validate these and other Dark matter models (discussed in Chapter 2.3) at a competitive sensitivity level, making it a leading search ahead of the future experiments like DUNE (9) and SHiP (10).

7.2.3 Other modifications

As I have mentioned at several sections above, tools like the LDM flux simulation or neural network PID are directly portable to other (or future) experiments, namely DUNE. The fact that DUNE uses same *art* analysis framework and deep-learning approaches makes the transition of LDM analysis straightforward. This is mainly driven by the overlap of DUNE and NOvA programs in terms of both the personnel and institutional membership, and the hosting laboratory.

A twin analysis of DM in NOvA ND could be done using similar techniques but looking for two EM showers instead of one. This channel searches for forward boosted products of a heavy neutral lepton (HNL) decaying inside the detector into a pair of SM leptons (e^++e^- in our case), so it is a natural extension of future work on DM search.

7.2.4 Outlook

The short baseline section of New Physics program of DUNE (Deep Underground Neutrino Experiment) (168) involves the use of DUNE Near Detector as a beam dump experimental setup. The higher beam intensity of projected 1.2 MW combined with the 60% shorter, on-axis, baseline, improves the acceptance efficiency by a factor of 10 from NOvA. The projected model constraints by the NOvA ND measurement could guide design requirements of the DUNE ND which is now being finalized. The PID efficiency, for example, needs to be several times better to compensate for the much higher neutrino background in DUNE's beam. The choice of interaction material in the central tracker of the DUNE ND will also be a factor of the achieved sensitivity and, in combination with the advances in PID software by the time of physics operations in "late 2020's", may take the lead by pushing its sensitivity one order of magnitude further (DUNE will possibly not start regular beam running before mid-2029).

Such level of sensitivity is expected as simply initial by the SHiP (Search for Hidden Particles) experiment (10) which is devoted to the search of New Physics candidates, among which the models of LDM discussed in this work are, with a time horizon comparable to that of DUNE. The low projected integral intensity, of $6{\cdot}10^{20}$ POT at 400 GeV beam energy on a heavy metal target is compensated by the very short on-axis baseline (10% of NOvA ND) and the proposals of the central tracking design bringing technology choices from the current state-of-the-art instruments. The low intensity may allow SHiP to be the first to use time techniques to identify LDM coming from the target, something the Fermilab source configuration cannot do with NOvA or DUNE.

To summarize, estimating the sensitivity and limits of current particle experiments on different models of New BSM Physics has a large scientific potential. The tools in place, the data being recorded and the possibility to shape future experiments yield a serious scientific impact.

References

1. **Jediný, F.** *NOvA Experiment.* s.l. : Study for Dissertation at FNSPE, Czech Technical University in Prague, 2016.

2. **Adamson, P. et al. (NOvA Collaboration).** First Measurement of Electron Neutrino Appearance in NOvA. *Phys. Rev. Lett. 116.* 2016, 151806.

3. —. First measurement of muon-neutrino disappearance in NOvA. *Phys. Rev. D.* 93, 2016, 051104(R).

4. —. Measurement of the Neutrino Mixing Angle theta23 in NOvA. *Phys. Rev. Lett.* 118, 2017, 151802.

5. —. Constraints on Oscillation Parameters from nue Appearance and numu Disappearance in NOvA. *Phys. Rev. Lett. .* 118, 2017, 231801.

6. —. Search for active-sterile neutrino mixing using neutral-current interactions in NOvA. *Phys. Rev. D.* 96, 2017, 072006.

7. **Acero, M. A. et al. (NOvA Collaboration).** New constraints on oscillation parameters from nue appearance and numu disappearance in the NOvA experiment. *Phys. Rev. D.* 98, 2018, 032012.

8. —. Measurement of Neutrino-Induced Neutral-Current Coherent pi0 Production in the NOvA Near Detector. *FERMILAB-PUB-19-047-ND.* 2019, arXiv:1902.00558.

9. **Acciarri, R. et al.** Long-Baseline neutrino Facility. *FERMILAB-DESIGN-2016-02.* 2015, Vol. Volume 2: The Physics Program for DUNE at LBNF, arXiv:1504.04956.

10. **Anelli, M. et al. (SHiP Collaboration).** A facility to Search for Hidden Particles (SHiP) at the CERN SPS. *CERN-SPSC-2015-016.* SPSC-P-350, 2015, arXiv:1504.04956.

11. **Lin, T., Yu, H., Zurek, K. M.** Symmetric and asymmetric light dark matter. *Phys. Rev. D.* 2012, Vol. 85, arXiv:1111.0293.

12. **de Niverville, P., Pospelov, M., Ritz, A.** Observing a light dark matter beam with neutrino experiments. *Phys. Rev. D.* 2011, Vol. 84, arXiv:1107.4580.

13. **Kahn, Y., et al.** DAEdALUS and Dark Matter Detection. *Phys. Rev. D.* 2015, Vol. 91.055006, arXiv:1411.1055.

14. **de Niverville, P. and Frudiuele, C.** Hunting sub-GeV dark matter with the NOvA near detector. *Phys.Rev.D.* 99, 2019, 051701, arXiv:1807.0650.

15. **Aghanim, N. et al.** Planck 2018 results. VI. Cosmological parameters. 2018, arXiv:1807.06209.

16. **Bertone, G., and D. Hooper.** A History of Dark Matter. *Rev. Mod. Phys. 90, 4500.* 2018, arXiv:1605.04909.

17. **Poincaré, H.** The Milky Way and the Theory of Gases. *Popular Astronomy 14.* 1906, 475.

18. **Oort, J. H.** The force exerted by the stellar system in the direction perpendicular to the galactic plane and some related problems. *Bulletin of the Astronomical Institutes of the Netherlands, Vol. 6, p.249.* 1932.

19. **Zwicky, F.** Die Rotverschiebung von extragalaktischen Nebeln. *Helvetica Physica Acta, Vol. 6, p. 110-127.* 1933.

20. —. On the Masses of Nebulae and of Clusters of Nebulae. *Astrophysical Journal, vol. 86, p.217.* 1937.

21. **Meekins, J. F., G. Fritz, T. A. Chubb, and H. Friedman.** The Hubble Constant and X-rays from Galaxy Clusters. *NAture 232, 393.* 1971.

22. **Rubin, V. C., and W. K. Ford, Jr.** Rotation of the Andromeda Nebula from a Spectroscopic Survey of Emission Regions. *Astrophysical Journal, vol. 159, p.379.* 1970.

23. **Alcock, C., C. W. Akerlof, R. A. Allsman, T. S. Axelrod, D. P. Bennett, S. Chan, K. H. Cook, K. C. Freeman, K. Griest, S. L. Marshall, H.-S. Park, S. Perlmutter, B. A. Peterson, M. R. Pratt, P. J. Quinn, A. W. Rodgers, C. W. Stubbs, and W. Sutherland.** Possible gravitational microlensing of a star in the Large Magellanic Cloud. *Nature, 365, 621.* 1993.

24. **Lasserre, T., et al (EROS Collaboration).** Not enough stellar Mass Machos in the Galactic Halo. *A&A 355, L39.* 2000, astro-ph/0002253.

25. **Lasserre, T., et al, (EROS-2 Collaboration).** Limits on the Macho Content of the Galactic Halo from the EROS-2 Survey of the Magellanic Clouds. *Astron.Astrophys.469, 387.* 2007, arXiv:astro-ph/0607207.

26. **Hinshaw, G, D. Larson, E. Komatsu, D. N. Spergel, C. L. Bennett, J. Dunkley, M. R. Nolta, M. Halpern, R. S. Hill, N. Odegard, L. Page, K. M. Smith, J. L. Weiland, B. Gold, N. Jarosik, A. Kogut, M. Limon, S. S. Meyer, G. S. Tucker, E. Wollack, E. L. Wright.** Nine-Year Wilkinson Microwave Anisotropy Probe (WMAP) Observations: Cosmological Parameter Results. *ApJS 208, 19.* 2013, arXiv:1212.5226.

27. **Planck Collaboration, , P. A. R. Ade, N. Aghanim, M. Arnaud, M. Ashdown, J. Aumont, C. Baccigalupi, A. J. Banday, R. B. Barreiro, J. G. Bartlett, and et al.** Planck 2015 results. XIII. Cosmological parameters. *A&A 594, A13.* 2015, arXiv:1502.01589.

28. **Milgrom, M.** A modification of the Newtonian dynamics as a possible alternative to the hidden mass hypothesis. *Astrophys.J. 270, 365.* 1983.

29. —. A modification of the Newtonian dynamics - Implications for galaxies. *Astrophys.J. 270, 371.* 1983.

30. —. A Modification of the Newtonian Dynamics - Implications for Galaxy Systems. *Astrophys.J. 270, 384.* 1983.

31. **Bekenstein, J. D.** Relativistic gravitation theory for the MOND paradigm. *Phys.Rev. D70, 083509.* 2004, arXiv:astro-ph/0403694.

32. **Clowe, D., M. Bradač, A. H. Gonzalez, M. Markevitch, S. W. Randall, C. Jones, and D. Zaritsky.** A direct empirical proof of the existence of dark matter. *Astrophys.J. 648, L109.* 2006, arXiv:astro-ph/0608407.

33. *Building for Discovery - Strategic Plan for U.S. Particle Physics in the Global Context.* **Ritz, S. et al. (HEPAP Subcommittee).** 2014. http://science.energy.gov/~/media/hep/hepap/pdf/May.

34. **Lee, B. W., and S. Weinberg.** Cosmological Lower Bound on Heavy-Neutrino Masses. *Phys.Rev.Lett. 39, 165.* 1977.

35. **Gunn, J., B. Lee, I. Lerche, D. Schramm, and G. Steigman.** Some astrophysical consequences of the existence of a heavy stable neutral lepton. *Astrophys.J. 223, 1015.* 1978.

36. **Pagels, H., and J. R. Primack.** Supersymmetry, Cosmology, and New Physics at Teraelectronvolt Energies. *Phys.Rev.Lett. 48, 223.* 1982.

37. **Dimopoulos, S., and H. Georgi.** Softly broken supersymmetry and SU(5). *Nucl.Phys. B193, 150.* 1981.

38. **Weinberg, S.** Upper Bound on Gauge-Fermion Masses. *Phys.Rev.Lett. 50, 387.* 1983.

39. **Peccei, R. D., and H. R. Quinn.** Constraints imposed by CP conservation in the presence of pseudoparticles. *Phys. Rev. D 16, 1791.* 1977.

40. —. CP Conservation in the Presence of Pseudoparticles. *Phys. Rev. Lett. 38, 1440.* 1977.

41. **Weinberg, S.** A New Light Boson? *Phys.Rev.Lett. 40, 223.* 1978.

42. **Dine, M., W. Fischler, and M. Srednicki.** A simple solution to the strong CP problem with a harmless axion. *Phys. Lett. B104, 199.* 1981.

43. **Kephart, T. W., and T. J. Weiler.** Luminous axion clusters. *Phys.Rev.Lett. 58, 171.* 1987.

44. **Abbott, L., and P. Sikivie.** A cosmological bound on the invisible axion. *Phys.Lett. B120, 133.* 1983.

45. **Linde, A. D.** Axions in inflationary cosmology. *Phys.Lett. B259, 38.* 1991.

46. **Tegmark, M., A. Aguirre, M. Rees, and F. Wilczek.** Dimensionless constants, cosmology, and other dark matters. *Phys.Rev. D73, 023505.* 2006.

47. **Wilczek, F.** A Model of Anthropic Reasoning, Addressing the Dark to Ordinary Matter Coincidence. [book auth.] B. Carr. *Universe or multiverse.* Cambridge : arXiv:hep-ph/0408167, 2004.

48. **Miller, J. P., Rafael, E., Roberts, B. L., Stöckinger, D.** Muon (g-2): Experiment and Theory. *Ann. Rev. Nucl. Part. Sci. 62.* 2012.

49. **Antognini, A. et al.** Proton Structure from the Measurement of 2S-2P; Transition Frequencies of Muonic Hydrogen. *Science.* 6118, 2013, Vol. 339.

50. **Krasznahorkay, A. J. et al.** Observation of Anomalous Internal Pair Creation in 8Be: A Possible Signature of a Light, Neutral Boson. *Phys. Rev. Lett. 116.* 2016, arXiv:1504.01527.

51. **Abbott, B. P. et al. (LIGO Scientific Collaboration and Virgo Collaboration).** Observation of Gravitational Waves from a Binary Black Hole Merger. *Phys. Rev. Lett. 116.* 2016, arXiv:1602.03837.

52. **Mount, B. J. et al.** LUX-ZEPLIN (LZ) Technical Design Report. 2017, arXiv:1703.09144.

53. **Ehret, K. et al.** New ALPS Results on Hidden-Sector Lightweights. *Phys.Lett. B689, 149.* 2010.

54. **Robilliard, C., R. Battesti, M. Fouche, J. Mauchain, A.-M. Sautivet, F Amiranoff, C. Rizzo.** No 'Light Shining through a Wall': Results from a Photoregeneration Experiment. *Physical Review Letters. 99,19.* 2007.

55. **Pugnat, P. et al.** Search for weakly interacting sub-eV particles with the OSQAR laser-based experiment: results and perspectives. *Eur. Phys. J. C, 74.* 2014, arXiv:1306.0443 .

56. **Zavattini, E. et al. (PVLAS Collaboration).** Experimental observation of optical rotation generated in vacuum by a magnetic field. *Physical Review Letters. 96 (11).* 2006, arXiv:hep-ex/0507107.

57. **Duffy, L. D. et al.** A High Resolution Search for Dark-Matter Axions. *Phys.Rev.D74.* 2006, arXiv:astro-ph/0603108.

58. **Anastassopoulos, V. et al. (CAST Collaboration).** New CAST limit on the axion-photon interaction. *Nature Phys. 13, 584.* 2017, arXiv:1705.02290.

59. **Brubaker, B. M. et al.** First results from a microwave cavity axion search at 24 micro-eV. *Phys. Rev. Lett. 118.* 2017, arXiv:1610.02580.

60. **McAllister, B. T. et al.** The ORGAN Experiment: An axion haloscope above 15 GHz. *Physics of the Dark Universe, 18, 67.* 2017, arXiv:1706.00209.

61. **Aprile, E. et al. (The XENON100 Collaboration).** First Axion Results from the XENON100 Experiment. *Phys. Rev. D. 90.* 2014, arXiv:1404.1455.

62. **Goodman, M. W., and E. Witten.** Detectability of certain dark-matter candidates. *Phys.Rev. D31.* 1985, 3059.

63. **Ahlen, S. P., F. T. Avignone, R. L. Brodzinski, A. K. Drukier, G. Gelmini, D. N. Spergel.** Limits on cold dark matter candidates from an ultralow background germanium spectrometer. *Phys.Lett. B195, 603.* 1987.

64. **Agnese, R., et al. (CDMS).** Silicon Detector Dark Matter Results from the Final Exposure of CDMS II. *Phys.Rev.Lett. 111 (25).* 2013, arXiv:1304.4279.

65. **Armengaud, E. et al. (EDELWEISS Collaboration).** A search for low-mass WIMPs with EDELWEISS-II heat-and-ionization detectors. *Phys. Rev. D 86.* 2012, arXiv:1207.1815.

66. **Angloher, G. et al. (CRESST Collaboration).** Results on low mass WIMPs using an upgraded CRESST-II detector. *Eur.Phys.J. C74 (12).* 2014, arXiv:1407.3146.

67. **Bernabei, R., et al. (DAMA/LIBRA).** New results from DAMA/LIBRA. *Eur.Phys.J. C67, 39.* 2010, arXiv:1002.1028.

68. **Aalseth, C. et al. (CoGeNT Collaboration).** Results from a Search for Light-Mass Dark Matter with a P-type Point Contact Germanium Detector. *Phys.Rev.Lett.106.* 2011, arXiv:1002.4703.

69. **Aalseth, C. E. et al.** Search for an Annual Modulation in a P-type Point Contact Germanium Dark Matter Detector. *Phys. Rev. Lett. 107.* 2011, arXiv:1106.0650.

70. **Kraus, H. et al.** EURECA – the European Future of Dark Matter Searches with Cryogenic Detectors. *Nuclear Physics B (Proc. Suppl.) 173, 168.* 2007.

71. **Aprile, E. et al. (the XENON collaboration).** Search for Electronic Recoil Event Rate Modulation with 4 Years of XENON100 Data. *Phys. Rev. Lett. 118.* 2017, arXiv:1701.00769.

72. **Amaudruz, P.-A. et al. (DEAP-3600 Collaboration).** First results from the DEAP-3600 dark matter search with argon at SNOLAB. *Phys. Rev. Lett. 121.* 2018, arXiv:1707.08042.

73. **Tan, A. et al. (PandaX Collaboration).** Dark Matter Search Results from the Commissioning Run of PandaX-II. *Phys. Rev. D 93.* 2016, arXiv:1602.06563.

74. **Agnes, P. et al. (DarkSide Collaboration).** Results from the first use of low radioactivity argon in a dark matter search. *Phys. Rev. D 93.* 2016, arXiv:1510.00702.

75. **Benetti, P. et al.** First results from a Dark Matter search with liquid Argon at 87 K in the Gran Sasso Underground Laboratory. *Astropart. Phys. 28.* 2008, arXiv:astro-ph/0701286.

76. **Gunn, J., B. Lee, I. Lerche, D. Schramm, and G. Steigman.** Astrophys.J. 1978, Vol. 223, 1015.

77. **Sreekumar, P., et al. (EGRET).** *Astrophys.J.* 1998, Vol. 494, 523.

78. **Ackermann, M., et al. (Fermi-LAT).** 2015, arXiv:1501.05464.

79. —. *Phys. Rev. Lett.* 2015, Vols. 115 (23), 231301, arXiv:1503.02641.

80. **Adriani, O., et al. (PAMELA).** *Phys.Rev.Lett. 105, 121101.* 2010, arXiv:1007.0821.

81. **Boezio, M., et al. (WiZard/CAPRICE).** The Cosmic-Ray antiproton flux between 3 and 49 GeV. *Astrophys.J. 561, 787.* 2001, arXiv:astro-ph/0103513.

82. **Abe, K., H. Fuke, S. Haino, T. Hams, A. Itazaki, et al.** Measurement of cosmic-ray low-energy antiproton spectrum with the first BESS-Polar Antarctic flight. *Phys.Lett. B670, 103.* 2008, arXiv:0805.1754.

83. **Hooper, D., P. Blasi, and P. D. Serpico.** Pulsars as the Sources of High Energy Cosmic Ray Positrons. *JCAP 0901, 025.* 2009, arXiv:0810.1527.

84. **Krauss, L. M., K. Freese, W. Press, and D. Spergel.** *Astrophys. J. .* 1985, Vol. 299, 1001.

85. **Silk, J., K. A. Olive, and M. Srednicki.** *Phys.Rev.Lett.* 1985, Vol. 55, 257.

86. **Krauss, L. M., M. Srednicki, and F. Wilczek.** *Phys.Rev.* 1986, Vol. D33, 2079.

87. **Ahrens, J., et al. (AMANDA).** Limits to the muon flux from WIMP annihilation in the center of the Earth with the AMANDA detector. *Phys.Rev. D66, 032006.* 2002, arXiv:astro-ph/0202370.

88. **Adrian-Martinez, S., et al. (ANTARES).** First Search for Dark Matter Annihilation in the Sun Using the ANTARES Neutrino Telescope. *JCAP 1311, 032.* 2013, arXiv:1302.6516.

89. *Progress in the Search for Dark Matter Using Upward-going Muons in NOvA.* **A. Tsaris, P. Ding, C. Group, S. Kurbanov, Y. Oksuzian, C. Principato, L. Aliaga, R. Mina, A. Norman.** ICHEP2016 : PoS vol. 282, 2017.

90. **Aaboud, M. et al. (ATLAS Collaboration).** Search for new phenomena in final states with an energetic jet and large missing transverse momentum in pp collisions at √s=13 TeV using the ATLAS detector. *Phys. Rev. D94.* 2016, arxiv:1604.07773.

91. **Khachatrzan, V. et al. (CMS Collaboration).** Search for dark matter in final states with an energetic jet, or a hadronically decaying W or Z boson using 12.9 fb−1 of data at √s= 13 TeV. *Phys. Rev. D 97.* 2017, arXiv:1712.02345.

92. **Essig, R. et al.** Dark Sectors and New, Light, Weakly-Coupled Particles. *hep-ph.* 2013, ArXiv:1311.0029.

93. **Batell, B. et al. (Project X).** New, light, weakly-coupled particles with Project X. *FERMILAB-TM.* 2013, Vol. chapter VII, 2557.

94. **Ayres, D. S. et al. (NOvA Collaboration).** The NOvA Technical Design Report. *FERMILAB-DESIGN.* 2007, 2007-01.

95. **Hatzikoutelis, A.** Neutrino oscillations at the intensity frontier: The NOvA experiment. *IOP Journal of Physics.* Conf. Series, 2013, 410 012146.

96. **NOvA, Collaboration.** The NOvA experiment. [Online] FERMILAB, 2010. [Cited: July 1, 2016.] http://www-nova.fnal.gov/.

97. **Fermilab, Fermi National Accelerator Laboratory.** NuMI Technical Design Handbook. *NuMI Technical Design Handbook.* [Online] http://www-numi.fnal.gov/numwork/tdh/tdh_index.html.

98. **de Niverville, P., McKeen, D., Ritz, A.** Signatures of sub-GeV dark matter beams at neutrino experiments. *Phys. Rev. D.* 2012, Vol. 86, arXiv:1205.3499.

99. **de Niverville, P.** Searching for Sub-Gev Dark Matter at Fixed Target Neutrino Experiments. *Physics Procedia.* 2014, Vol. 61.

100. **Holdom, B.** Two U(1)'s and Epsilon Charge Shifts. *Phys. Lett. B 166.* 1986, 196.

101. **Athanassopoulos, C. et al. (LSND Collaboration).** The Liquid Scintillator Neutrino Detector and LAMPF neutrino source. *Nucl. Instrum. Meth.* 1997, Vol. A388, 9605002.

102. **Auerbach, L. B. et al. (LSND Collaboration).** Measurement of electron - neutrino - electron elastic scattering. *Phys. Rev. D.* 2001, Vol. 63, 0101039.

103. **Aguilar-Arevalo, A. A. et al. (MiniBooNE Collaboration).** The Neutrino Flux prediction at MiniBooNE. *Phys.Rev. D.* 2009, Vol. 79, arXiv:0806.1449.

104. **Aguilar-Arevalo, A. A. et al. (MiniBooNE-DM Collaboration).** Dark matter search in nucleon, pion, and electron channels from a proton beam dump with MiniBooNE. *Phys. Rev. D.* 2018, Vol. 98, 112004.

105. **Abe, K. et al., (T2K Collaboration).** The T2K Experiment. *Nucl.Instrum.Meth.* 2011, Vol. A659, arXiv:1106.1238.

106. **Alexander, J. et al.** Dark Sectors 2016 Workshop: Community Report. 2016, arXiv:1608.08632.

107. **Adamson, P. et al. (The NOvA Collaboration).** The NuMI Neutrino Beam. *Nuclear Instruments and Methods in Physics Research Section A: Accelerators, Spectrometers, Detectors and Associated Equipment 806.* 2015, arXiv:1507.06690.

108. **Martens, J. H. M., Anderson, K.** Target and horn con. *Fermilab Technical Report.* 2009.

109. **Abramov, A. G. et al.** Beam optics and target conceptual designs for the NuMI project. *Nucl.Instrum.Meth.* 2002, Vol. A485.

110. **Aprile, E. et al. (XENON100 Collaboration).** Dark Matter Results from 225 Live Days of XENON100 Data. *Phys. Rev. Lett.* 2012, Vol. 109, arXiv:1207.5988.

111. **Kelso, Ch., Hooper, D. and Buckley, M. R.** Toward a consistent picture for CRESST, CoGeNT, and DAMA. *Phys. Rev. D.* 2012, Vol. 85, arXiv:1110.5338.

112. **Sjöstrand, T., Mrenna, S., Skands, P.** A Brief Introduction to PYTHIA 8.1. *Comput.Phys.Commun.* 2008, Vol. 178, arXiv:0710.3820.

113. **Hatzikoutelis, A., Kotelnikov, S., Bambah, B. A., and Kasetti S. P.** New light weakly-coupled particle searches in a neutrino. *Fermilab conf. ser.* 2013, FERMILAB-CONF-13-544-E.

114. **Mufson, S. et al.** Liquid scintillator production for the NOvA experiment. *NOvA internal docdb.* 2015. docdb-13014.

115. **Cooper, J.** NOvA Far detector mass. *NOvA internal docdb.* 2014. docdb-11905.

116. —. NOvA Near detector mass. *NOvA internal docdb.* 2014. docdb-13014.

117. **Norman, A.** The NOvA Data Acquisition System. *J.Phys.Conf.Ser.* 2012, Vol. 396, 396:012035.

118. **Battistoni, G. et al.** The fluka code: description and benchmarking. *AIP Conf.Proc.* 2007, Vol. 896.

119. **Agostinelli, S. et al.** GEANT4 - a simulation toolkit. *Nucl. Intrum. and Meth.* 2003, Vol. A506.

120. **Radovic, A.** *Measuring the Disappearance of Muon Neutrinos with the.* s.l. : University College London, 2013. FERMILAB-THESIS-2013-24.

121. **Andreopoulos, C. et al.** The GENIE Neutrino Monte Carlo Generator. *Nucl.Instrum.Meth.* 2007, Vol. A614, 0905.2517.

122. *Cosmic-ray Shower Library (CRY).* **Hagman, Ch. et al.** s.l. : Lawrence Livermore National Laboratory, 2012. UCRL-TM-229453.

123. **Aurisano, A. et al.** The NOvA simulation chain. *Journal of Physics.* Conf. Series, 2015, Vol. 664, 072005.

124. **Backhouse, Ch., Radovic, A.** The Attenuation and Threshold Correction of the NOvA Detectors. *NOvA internal docdb.* 2012. docdb-9069.

125. **Vinton, L.** Calorimetric Energy Scale Calibration of the NOvA Detectors. *NOvA internal docdb.* 2015. docdb-13579.

126. **Jacoby, W. G.** LOESS: a nonparametric, graphical tool for depicting relationships between variables. *Electoral Studies 19.* 2000, Vol. 577.

127. **Backhouse, C. et al.** The Attenuation and Threshold Calibration of the NOvA Detectors. *NOvA Collaboration Internal Document.* 2017, docdb 13579.

128. **Alion, T.** Third Analysis Calorimetric Energy Scale in the NOvA Detectors. *NOvA Collaboration Internal Document.* 2017, docdb 23372.

129. **Norman, A. et al.** The nova timing system: A system for synchronizing a long baseline neutrino. *Journal of Physics: Conf. series.* 396, 2012, 012034.

130. **Niner, E.** Timing Calibration Technical Note. *NOvA internal technote.* 2015, docdb-13579.

131. **Ester, M., Kriegel, H. P., Jrg, S. Xu, X.** A density-based algorithm for discovering clusters in large spatial databases with noise. *AAAI Press.* 1996.

132. **Fernandes, L., Oliviera, M.** Real-time line detection through an improved Hough transform voting scheme. *Pattern Recognition.* 2008, Vol. 41, 2007.04.003.

133. **Baird, M.** Tech Note for the Multi-Hough Transform. *NOvA internal docdb.* 2012. docdb-8241.

134. **Ohlsson, M.** Extensions and explorations of the elastic arms algorithm. *Computer Physics Communications.* 1993. Vol. 77, 1.

135. **Messier, M.** Vertex reconstruction based on elastic arms. *NOvA internal docdb.* 2012. docdb-7530.

136. **James, F., Winkler, M.** MINUIT User's Guide. [Online] http://seal.web.cern.ch/seal/documents/minuit/mnusersguide.pdf.

137. **Raddatz, N. J.** Kalman track technical note. *NOvA internal document.* 2015, NOvA-docdb 13545.

138. **Raddatz, N.** A technical note describing the numu pid algorithm ReMId. *NOvA Collaboration Internal document.* 2014, docdb-11206.

139. **Bays, K.** Cosmic rejection technical note. *NOvA Internal Document.* 2014, docdb-11205.

140. **Aurisano, A. et al.** A Convolutional Neural Network Neutrino Event Classifier. *JINST 11.* P09001, 2016, arXiv:1604.01444.

141. **Jia, Y. et al.** *Caffe: Convolutional architecture for fast feature embedding.* 2014. arXiv:1408.5093.

142. **Szegedy, C., et al.** *Going Deeper with Convolutions.* 2014. arXiv:1409.4842.

143. **Himmel, A.** NOvA to DUNE CVN Story. *NOvA Internal Document.* 2018, NOvA doc-db 33252.

144. **Psihas, F. et al.** Context-Enriched Identification of Particles with a Convolutional Network for Neutrino Events. *submitted to PRD, currently under review.* 2019, arXiv:1906.00713.

145. **Bian, J.** EID tech note. *NOvA internal docdb.* 2013, docdb-9923.

146. **Bian, J., Niner, E., Sachdev, K.** LID and e/pi0 identifier. *NOvA Collaboration internal document.* 2016, docdb-15344.

147. **Backhouse, C.** The library event matching nue PID technote. *NOvA Collaboration internal document.* 2015, docdb 13590.

148. *Numu-electron elastic scattering in the NOvA Near Detector and its applications beyond the SM.* **Bian, J. et al.** London : Neutrino2016, 2016.

149. **Wang, B.** *Muon-neutrino electron elastic scattering and a search for the muon-neutrino magnetic moment in the NOvA Near detector.* s.l. : Southern Methodist University, Dallas, TX, 2017. FERMILAB-THESIS-2017-24.

150. **Lein, S.** Numu charged current energy estimators. *NOvA Collaboration internal document.* 2016, docdb-15211.

151. **Petkov, V. and Zworksi, M.** Breit-Wigner Approximation and the Distribution of resonances. *Comm Math Phys.* 1999, Vol. 204, https://doi.org/10.1007/s002200050648.

152. **Green, C et al.** The Art Framework. *J.Phys.Conf.Ser. 396.* 2012, Vols. DOI: 10.1088/1742-6596/396/2/022020, FERMILAB-PUB-12-301-CD.

153. **Habig, A. et al.** Recent Evolution of the Offline Computing Model of the NOvA Experiment. *J.Phys.* Conf.Ser., 2015, Vol. 664, FERMILAB-CONF-15-198-CD-ND.

154. **Green, C. et al. (Fermilab).** The Art Framework. *J.Phys.Conf.Ser. 396.* 2012.

155. **Group, NOvA Production.** Fourth production datasets. [Online] 2019. http://nusoft.fnal.gov/nova/production/production4/index.html.

156. **Aliaga, L.** NuMI Beam Prediction for the NOvA 2017 analyses. *NOvA internal document.* 2017, docdb -23441.

157. **Aliaga, L. et al.** NuMI flux systematic uncertainties for the NOvA third analyses. *NOvA internal document.* 2017, docdb 17608.

158. **Aliaga Soplin, L.** *Neutrino Flux Prediciton for the NuMI Beamline.* Williamsburg, Virginia, USA : College of William and Mary, 2016.

159. **Aliaga Soplin, L., et al. (MINERvA Collaboration).** Neutrino flux predictions for the NuMI beam. *Phys. Rev. D.* 2016, Vol. 94, 092005.

160. **Acero, M. A. et al. (NOvA Collaboration).** First Measurement of Neutrino Oscillation Parameters using Neutrinos and Antineutrinos by NOvA. *Phys.Rev.Lett.* 2019, Vol. 123, 151803, arXiv:1906.04907.

161. **Edayath, S.** Technote: Systematics study for NC Disappearance Nus2018 FHC Analysis. *NOvA internal document.* 2018, docdb 28778.

162. **Acero, M. A. et al. (NOvA Collaboration).** Evaluating Uncertainties on Neutrino Interaction Models using NOvA Near Detector Data. *NOvA internal document, submmitted to Eur. Phys. J. C.* 2019, docdb-40101.

163. **Bostan, N.** PPFX implementation on neutrino flux at the On-Axis and Off-Axis NuMI neutrino detector locations. *Internal NOvA Document.* 2020, NOvA doc-db 45215.

164. **Nosek, T. (NOvA Collaboration).** Systematic Uncertainties of the NOvA Neutrino Oscillation Analysis. *Proceedings of Science.* 2020, Vols. 40th International Conference on High Energy physics - ICHEP2020.

165. **Cowan, G.** *Statistical Data Analysis.* Oxford : Oxford University Press, 1998. ISBN 0 19 850155 2.

166. **Read, A.L.** Modified frequentist analysis of search results (The CL(s) method). *CERN Open-2000-205.* Workshop on confidence limits - Proceedings, 2000.

167. *The RooFit toolkit for data modeling.* **Verkerke, W., Kirkby, D.** La Jolla : CHEP03, 2003. arXiv:physics/0306116.

168. **Billard, J., Figueroa-Feliciano, E., Strigari, L.** Implication of neutrino backgrounds on the reach of next generation dark matter direct detection experiments. *Phys. Rev. D.* 2014, Vol. 89, arXiv:1307.5458.

169. **Chandra.** Chandra :: Photo album :: 1E 0657-56. *Chandra X-ray observatory.* [Online] NASA by SAO, August 13, 2018. [Cited: December 29, 2018.] http://chandra.harvard.edu/photo/2006/1e0657/more.html.

170. **Baird, M. et al.** The NOvA DAQ Monitor System. *J. Phys. Conf. Ser. 664.* 2015, 082020.

171. **Picture Gallery - Planck - Cosmos.** *Planck image gallery.* **[Online] European space agency, 2019. https://www.cosmos.esa.int/web/planck/picture-gallery. .**

172. Kralik, R. Update on Horn-Off . *NOvA internal document.* **2020, NOvA doc-db 45218.**